SC5222.FR

Copy No. _____

LIFETIME PREDICTION OF ORGANIC COATING/METAL SYSTEMS

FINAL REPORT FOR THE PERIOD
July 1, 1979 through October 31, 1985

CONTRACT NO. N00014-79-C-0437
PROJECT NO. NR036-136 (471)

Prepared for

Metallurgy & Ceramics Program
Material Sciences Division
Office of Naval Research
800 North Quincy Street
Arlington, Virginia 22217

F. Mansfeld and M. Kendig
Principal Investigators

APRIL 1986

Rockwell International
Science Center

UNCLASSIFIED
SECURITY CLASSIFICATION OF THIS PAGE

AD-A167281

REPORT DOCUMENTATION PAGE

1a. REPORT SECURITY CLASSIFICATION Unclassified	1b. RESTRICTIVE MARKINGS
2a. SECURITY CLASSIFICATION AUTHORITY	3. DISTRIBUTION/AVAILABILITY OF REPORT Approved for public release; distribution unlimited.
2b. DECLASSIFICATION/DOWNGRADING SCHEDULE	
4. PERFORMING ORGANIZATION REPORT NUMBER(S) SC5222.FR	5. MONITORING ORGANIZATION REPORT NUMBER(S)
6a. NAME OF PERFORMING ORGANIZATION Rockwell International Science Center 6b. OFFICE SYMBOL (If applicable)	7a. NAME OF MONITORING ORGANIZATION
6c. ADDRESS (City, State and ZIP Code) 1049 Camino Dos Rios Thousand Oaks, CA 91360	7b. ADDRESS (City, State and ZIP Code)
8a. NAME OF FUNDING/SPONSORING ORGANIZATION Metallurgy & Ceramics Program Office of Naval Research, Material Sciences Div. 8b. OFFICE SYMBOL (If applicable)	9. PROCUREMENT INSTRUMENT IDENTIFICATION NUMBER Contract No. N00014-79-C-0437
8c. ADDRESS (City, State and ZIP Code) 800 North Quincy Street Arlington, Virginia 22217	10 SOURCE OF FUNDING NOS PROGRAM ELEMENT NO. / PROJECT NO. NR036-136 (471) / TASK NO. / WORK UNIT NO.
11. TITLE (Include Security Classification) LIFETIME PREDICTION OF ORGANIC COATING/METAL SYSTEMS (U)	
12. PERSONAL AUTHOR(S) Mansfeld, F. and Kendig, M	
13a. TYPE OF REPORT Final Report 13b. TIME COVERED FROM 07/01/79 TO 10/31/85	14. DATE OF REPORT (Yr., Mo., Day) APRIL 1986 15. PAGE COUNT 98
16. SUPPLEMENTARY NOTATION	
17 COSATI CODES FIELD / GROUP / SUB GR	18 SUBJECT TERMS (Continue on reverse if necessary and identify by block number)

19. ABSTRACT (Continue on reverse if necessary and identify by block number)

A lifetime prediction model has been developed for polymer coating/metal systems. The elements of the model fall into the category of system variables that describe the surface of the substrate, the coating or the environment, or the category of processes that determine the degradation of the coated metal. These processes include formation of defects in the coating and at the metal/coating interface, transport of corrosive species to the metal, loss of adhesion, corrosion and failure. The causal relationship between system variables and processes has been discussed.

The lifetime prediction model is based on a series of experimental studies which have been performed during the course of this project. A number of new techniques have been developed which can be used to determine the properties of the coating/metal compound and its changes during interaction with corrosive environments. Electrochemical impedance spectroscopy (EIS) has been found to be very valuable in providing information concerning the coating and the metal surface and degradation of the coating as corrosion proceeds. An acoustic pulse technique has been used to detect areas of delamination and corrosion. Acoustic emission from coated steel during straining of the sample has provided characteristic fingerprints for surface and coating properties and has demonstrated the importance of the mechanical properties of the coating. (over)

20 DISTRIBUTION/AVAILABILITY OF ABSTRACT UNCLASSIFIED/UNLIMITED ☒ SAME AS RPT. ☐ DTIC USERS ☐	21. ABSTRACT SECURITY CLASSIFICATION Unclassified
22a. NAME OF RESPONSIBLE INDIVIDUAL Dr. Philip A. Clarkin	22b TELEPHONE NUMBER (Include Area Code) 22c OFFICE SYMBOL

DD FORM 1473, 83 APR EDITION OF 1 JAN 73 IS OBSOLETE.

UNCLASSIFIED
SECURITY CLASSIFICATION OF THIS PAGE

(Block 19 Continued)

The experimental results have demonstrated convincingly the importance of proper surface preparation. It has been found by a comparison of coated metals and a free film that corrosion products of steel can cause stresses in the coating which produce defects. Surface preparation can also affect the structure of phosphate layers which in turn can change the nature of transport phenomena. Using EIS it has been shown that an anodized surface layer on Al produces better corrosion protection of the polyurethane coated surface than a conversion coating layer. New insight into reactions at the metal/coating interface has been obtained with the use of segmented electrodes which allow the recording of EIS data under the coating. This new technique has been applied to steel/steel, Cu/steel and Zn/steel electrodes. Analysis of the EIS data allows an estimate of the effective delaminated area under the coating and the corrosion rate of the surface. Cathodic protection was observed for steel in the Zn/steel couple. The role of pigments such as phosphates, chromates and Zn dust and the importance of transport phenomena has also been studied with EIS during exposure of coated steel to NaCl.

Keywords: Anodizing, Pigment, Coating, Copper, Zinc, Electrode, Solvent, Cathodic Protection, Pigmenting, Sodium Chloride, Exposure

TABLE OF CONTENTS

LIST OF FIGURES

LIST OF FIGURES (Continued)

LIST OF FIGURES (Continued)

LIST OF FIGURES (Continued)

LIST OF TABLES

1.0 INTRODUCTION

The objective of this research program has been to develop a methodology for predicting the lifetime of polymer coated metals exposed to aggressive environments. A major result of the work is the roadmap introduced in Fig.1 showing the steps involved in the degradation of the polymer/coating compound. Several relatively new concepts have been developed during the course of this study to evaluate the relative probability for a polymer coated metal to proceed to each of the steps in a global model for corrosive degradation. New experimental techniques such as electrochemical impedance spectroscopy have been developed for the study of polymer coated metals since it became obvious very early that traditional techniques such as measurements of the corrosion potential or the polarization resistance were not suitable to obtain the information which was thought to be necessary for the development and application of a lifetime prediction model. Previous work devoted to the determination of the corrosion mechanisms of polymer coated metals concentrated on the bulk transport of corrodents through the polymer coating. While the importance of the hydrophobic nature and the barrier properties of the polymer coating in providing protection of the metal substrate against corrosion should not be ignored, it must be recognized that the initiation and propagation of corrosion is related to coating defects. Furthermore, the mechanical strength and adhesive properties of the coating play perhaps a more important role in the overall integrity of the polymer/metal compound than the transport of corrodents through the bulk polymer. Based on the information generated during the course of this project it is concluded that a general model of the interaction of the substrate, the coating/metal interface, the coating and the environment as represented in Fig. 1 provides the most fruitful means for evaluating the relative lifetime of polymer coated metals.

2.0 DESCRIPTION OF THE LIFETIME MODEL

The schematic in Fig. 1 contains the elements of the lifetime model which is the result of the research performed during the duration of this project. The elements of the model fall into the category of system variables describing the surface of the substrate, the coating and the environment, or the category of processes which determine the degradation of the coating/metal compound. These processes include formation of defects in the coating and at the metal/coating interface, transport of corrodents to the metal, loss of adhesion, corrosion and failure. The lines joining the processes and variables in Fig. 1 indicate the causal relationships of the system variables and processes and their independence.

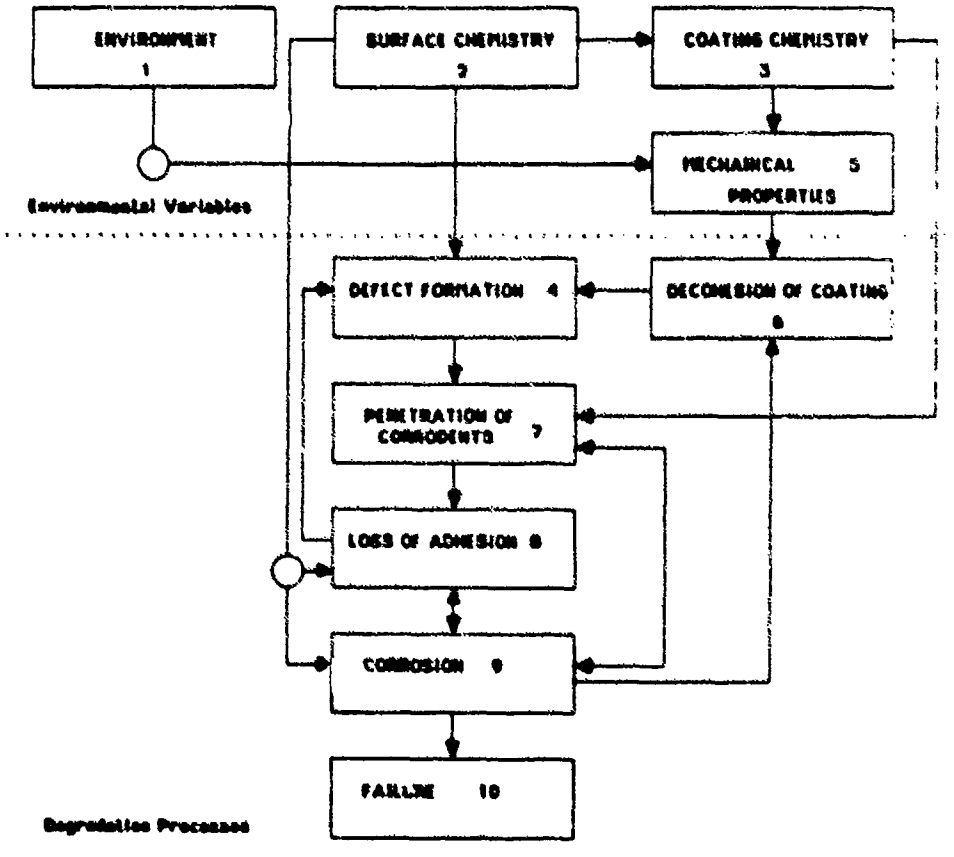

Fig. 1 Schematic of the lifetime prediction model.

2.1 System Variables

The environmental variables which may include UV and other radiation, pH, oxygen concentration, water activity, temperature, electrolytic conductivity, and the concentration of other corrosive species such as SO_2 or sulfide provide the driving force for the penetration of the corrodents (e.g., through the dependence of the diffusion rate on the activity gradient). The environmental variables may also have an effect on the mechanical properties of the coating (process 1-5 in Fig. 1). For example, water may swell the coating and UV radiation can have an embrittling effect on the coating which may lead to the formation of defects in the coating via decohesion of the film as shown by the lines 8-4 and 6-4 in Fig. 1.

The surface chemistry of the substrate is governed by the bulk chemistry of the metal and can be affected by the method of pretreatment. A "good" or "bad" surface resulting from a certain pretreatment process may lead directly to loss of adhesion (process 2-8 in Fig.1), corrosion (process 2-9) and defect formation in the coating as a result of poor wetting of the surface by the liquid coating (process 2-4).

Coating chemistry governs the mechanical properties of the coating[5] and the permeation rate of corrodents[7] such as oxygen, water and electrolyte. For example during the course of this research it has been found that a coating which is very hydrophobic, but also very brittle provides poor protection. Evidence exists to suggest[2,5-7] that corrosion itself contributes to the rupturing of the coating and hence the propagation of corrosion as indicated by the process 9-6 in Fig. 1.

2.2 Degradation Processes

The corrosion of polymer coated metals involves the processes of defect formation, penetration of corrodents, loss of adhesion and corrosion, which eventually lead to failure of the coated metal.[2] The defect formation accelerates the penetration of corrodents and provides initiation sites for the corrosion reaction. This can produce extensive corrosion leading to

failure provided a loss of adhesion takes place. Loss of adhesion is, in fact, promoted by corrosion itself through the formation of cathodic sites adjacent to the anodic defect. The reaction at the cathode in neutral NaCl:

$$1/2\ O_2 + H_2O \rightarrow 2OH^- - 2e^-, \qquad (1)$$

produces a local increase in the pH which has a detrimental effect on the adhesion of the polymer to the substrate. A number of mechanisms could account for this behavior including alkaline hydrolysis of the polymer, the oxide interphase or the metal oxide-polymer bond. Most likely a number of different effects contribute to this process.

The initial stages of the corrosion reaction at the metal/coating interface depend somewhat upon the surface preparation.[2-7] Certain surface preparations can remove metal sulfides from steel substrates which serve as initiation sites.[3] The presence of unremoved scale on the surface can cause formation of crevices and lead to poor adhesion or wetting which can provide sites of rapid initiation of corrosion.[8]

Inhibiting pigments placed in the coating slow down the corrosion rate of the metal and improve the lifetime of the coating/metal system. Experiments performed in this project have shown that chromates that are slightly soluble produce highly permeable and poorly adhering coatings on steel, but increase the lifetime of the coated metal if a sufficiently adhering layer exists next to the coating/metal interface.

The definition of ultimate failure of the coating/metal system depends somewhat on the use of the structure involved and the purpose for which the coating is applied. In many cases, all that is required of the coating is that the structural integrity of the system be preserved. In this case the appearance of small rust spots or filiform corrosion will not define failure. On the other hand, any corrosion in food containers will define failure

of the coating/metal system. In other cases any corrosion which provides a slight dimensional change defines failure. Coatings often protect against functional failure. Coated electrical components fail when the component does not operate properly despite the possible absence of any gross corrosion products.

The schematic shown in Fig.1 provides a roadmap to follow in specifying the rate determining step and the ultimate lifetime of polymer coated metals. For any given system a certain number of the paths shown in Fig.1 will be either active or inactive. The relative probability of a coating failure can in principle be determined by evaluating the probabilities for each of the processes leading to failure. Only a qualitative description of the mechanism of corrosion of polymer-coated metal can be made at present, although the relative rates for several of the processes described here have been evaluated for certain specific systems (polybutadiene or epoxy coatings on steel or Al) during the course of this project. The results of this work, however, suggest the validity of the overall mechanism outlined in Fig.1.

Any evaluation of the lifetime of coated metal should endeavor to find which of the pathways shown in Fig. 1 is followed and which process is rate determining in the failure sequence. The following section describes methods for evaluating the relative rates for each of the processes described in Fig. 1.

3.0 EVALUATION OF DEGRADATION PROCESSES

As shown in Fig.1 and discussed above, degradation of polymer coatings can occur in several steps which involve formation of defects, transport of corrodents, loss of adhesion and finally corrosion at the metal/coating interface. For the evaluation of these degradation processes a number a new techniques have been developed and applied mainly to coated steel during the course of this project.

3.1 Defect Formation

The formation of defects can occur during application of the coating, as a result of reaction of the coating with the corrosive environment and/or due to the build-up of stresses resulting from the formation of corrosion products at the coating/metal interface. Defect formation has been studied mainly with electrochemical impedance spectroscopy (EIS) during exposure to air-saturated NaCl solution. Some preliminary tests have been performed with the scanning impedance probe (SIPT). Use of these methods along with mechanical testing has demonstrated the importance of the mechanical properties of polymer coatings in determining the propagation of defects in polymer coated steel.

3.1.1. Electrochemical Impedance Spectroscopy (EIS)

EIS[4-12] provides an excellent tool for determining the presence and development of defects in polymer coatings on steels and aluminum. The frequency dependence of the electrochemical impedance distinguishes various properties of the polymer coating from the response of the polymer/metal interface.

For the evaluation of the impedance of a polymer coated metal, an equivalent circuit has been found to be most suitable which consists of the solution resistance R_Ω of the test electrolyte, the capacitance C_c of the nondefective portion of the coating layer, a resistance R_{po} that shorts the

coating dielectric, and a general impedance Z_I, which characterizes the reactions at the metal interface (Fig. 2a.). C_c depends on the dielectric constant and the thickness of the polymer:

$$C_c = \varepsilon \varepsilon_0 A/d, \tag{2}$$

where

ε = the dielectric constant of the coating
ε_0 = the dielectric constant of free space
A = the cross sectional area of the coated specimen
d = the coating thickness

Typical dielectric constants for polymer coatings range between 2-4.[13] Since the dielectric constant of water equals 80, absorption of even small quantities of water by a polymer film produces a significant increase. As a result C_c provides a sensitive measure of the penetration of the coating by water.[14]

R_{po} is referred to as a pore resistance because it results from the penetration of electrolyte into defects of the coating which causes a conductive path to the surface. These defects may be actual pores containing bulk electrolyte or they may be virtual pores of heightened ionic conductivity formed as a result of insufficient cross-linking.[13,16]

For the systems studied here, Z_I can be characterized by a polarization resistance R_p in parallel with a double layer capacitance, C_d (Model I in Fig. 2(a)) or by R_p in series with a Warburg or pseudo-Warburg impedance Z_σ (Model II in Fig. 2(a)).[4-8] Details of these interfacial models will be discussed in greater detail in Sec. 3.3 and 3.4, which deal with the interfacial phenomena of adhesion loss and corrosion, respectively.

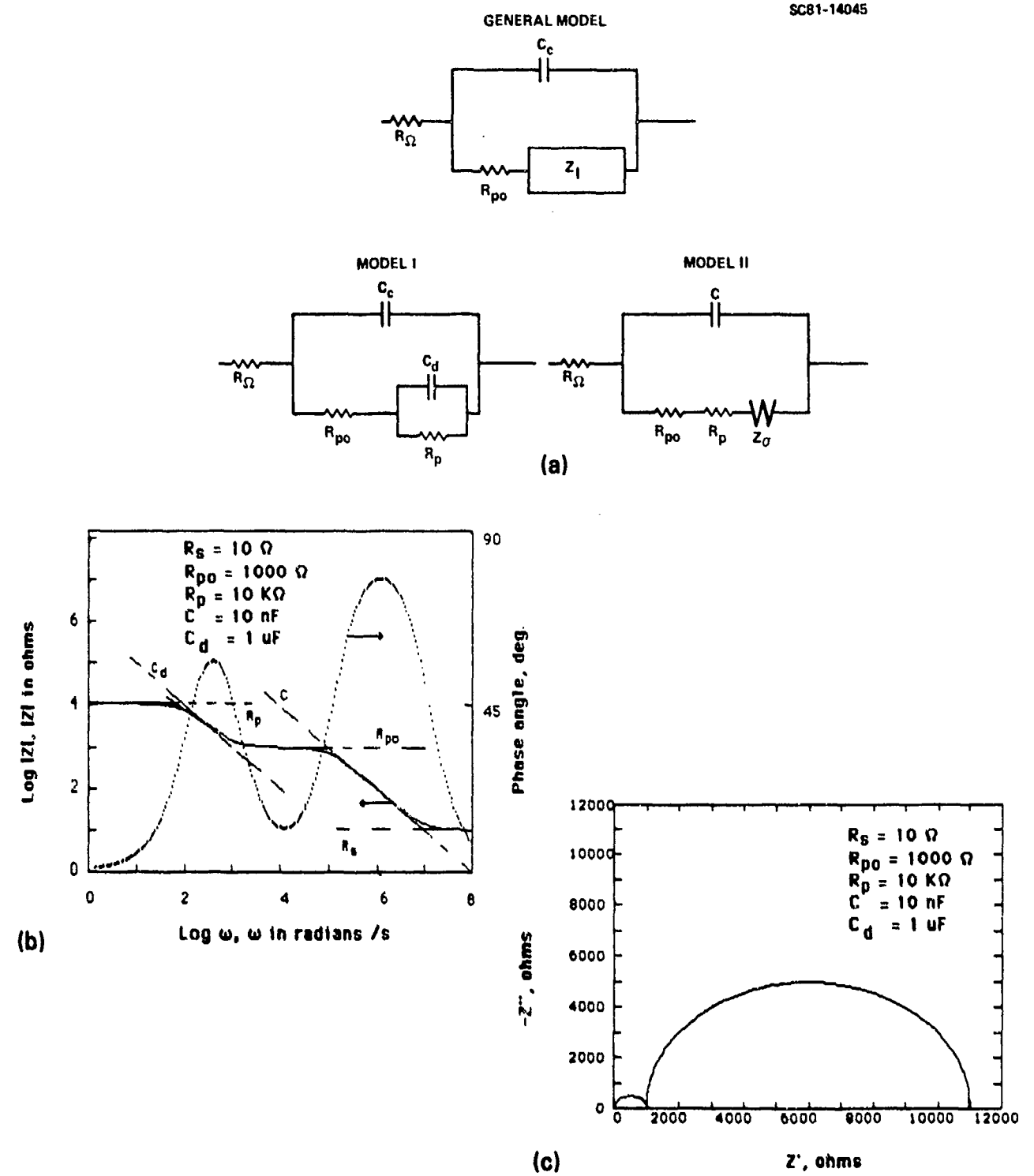

Fig. 2 Electrochemical impedance of polymer coated steel: (a) Circuit analogs, (b) Bode-plots for Model I with parameters in the inset, (c) Nyquist plot (-Z" vs Z')of spectrum in Fig. 2(b).

For simple cases, the frequency dependence of the impedance for a polymer-coated metal allows the different components to be evaluated. For example, Fig 2(b) shows a Bode-plot (log of the impedance modulus, log $|Z|$ ($|Z|$ in ohm), vs the log of the measurement frequency, log ω(ω in rad/s)) for a hypothetical case of Model I (Fig 2(a)). The dashed lines show the frequency characteristics for each of the elements of Model I. At high frequencies, $|Z|$ becomes independent of frequency and equal to R_Ω. At intermediate frequencies between $\omega \sim 10^3$ and 10^5 rad/s, a plateau in the log $|Z|$ vs log ω curve occurs as a result of the shorting of the coating capacitance by R_{po}. The impedance $|Z|$ for the plateau equals $R_{po} + R_\Omega$. Only at the lowest frequencies does the polarization of the interface become apparent as an increase of $|Z|$ with decreasing ω due to the ω^{-1} frequency response of the double layer capacitance C_d. For $\omega \to 0$, a limiting value for $|Z|$ is approached which is the dc limit $R_{dc} = R_\Omega + R_{po} + R_p$. In many situations $R_p >> R_\Omega + R_{po}$, for which case $R_{dc} \sim R_p$. The phase angle in Fig. 2(b) shows the presence of two time constants, which is typical for simple cases of filmed electrode surfaces.

Impedance spectra may also be presented as Nyquist plots (negative out-of-phase impedance (imaginary component), $-Z''$, vs in-phase impedance (real component), Z'). The Nyquist presentation of the example of Model I appears in Fig. 2(c), where two semicircles occur. The small, high frequency semicircle intersects the real axis at points equal to R_Ω and $R_\Omega + R_{po}$, respectively, and allows, therefore, an evaluation of R_{po}. Bode-plots are preferred for analysis of impedance spectra, since all frequencies are equally represented. The phase angle is very sensitive to the existence of additional time constants and/or deviations from a specific model used for analysis.

The measurement of the electrochemical impedance of polymer-coated steel has been described in detail in various papers resulting from this work.[4-12] A number of advances related to enhancing the speed and accuracy of the impedance measurement have been made.[17]

As a test of the validity of the model, Fig. 3 shows the impedance for a polymer-coated steel exposed to 0.5 M NaCl after a defect was placed in the polybutadiene coating with a pin. Very good agreement of the characteristic features with those of model I in Fig. 2(a) and the typical spectrum in Fig. 2(b) is observed. Two time constants occur as becomes obvious from the maxima of the phase angle at frequencies exceeding $2 \cdot 10^5$ Hz and at about 5 Hz. The capacitance C_c determined at the highest frequencies corresponds to that calculated from Eq. (2) for the exposed area A = 20 cm^2 and the coating thickness d = 8-10 μm. The pore resistance R_{po} has a value close to 500 Ω (10000 Ω • cm^2)and R_p is approaches $5 \cdot 10^4$ Ω. The analysis of this spectrum is facilitated by the wide separation of the two maxima of the phase angle.

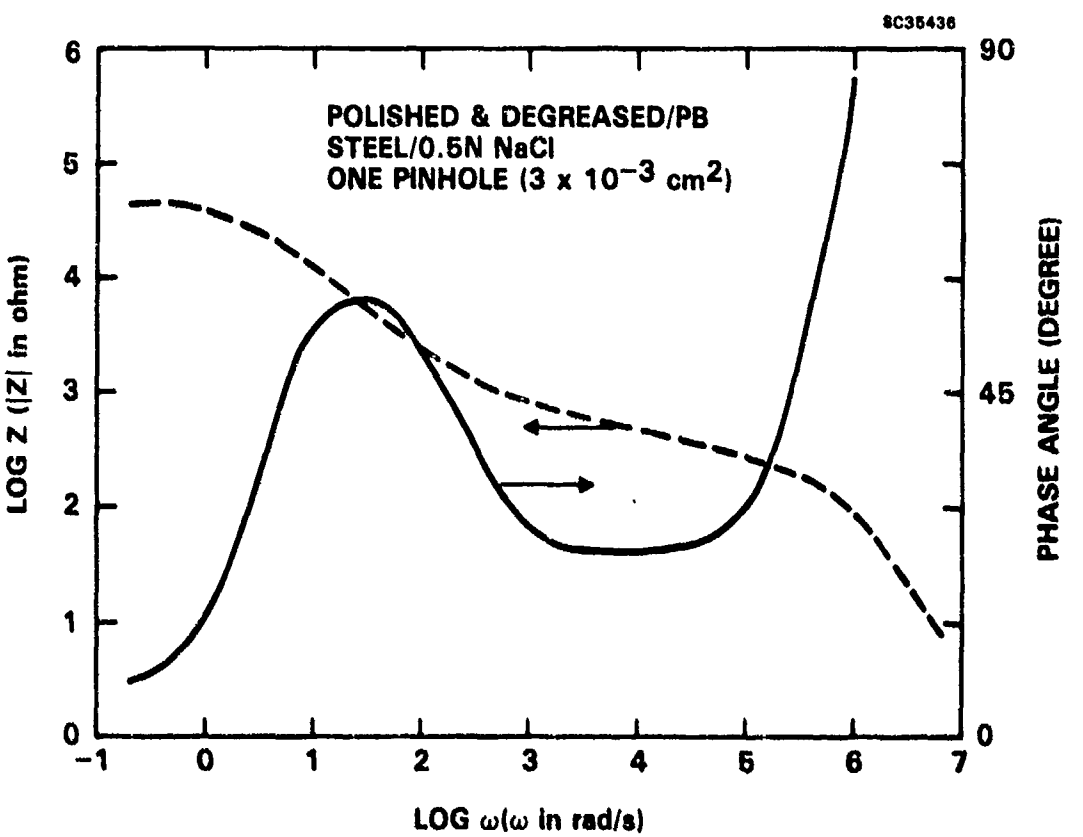

Fig. 3 Bode plot for a polymer coating after damaging with a pin.

EIS was applied to 8-10 μm polybutadiene coated specimens having the different pretreatments listed in Table 1. The pretreatments in Table 1 were used as discussed in Federal Specification TT-C-490B. Other pretreatment processes were selected in an attempt to produce a wide variety of initial surface structures.

Table 1

Surface Pretreatments

Treatment	Description
Degreased (D)	Trichloroethylene, 15 min TT-C-490 Method II
Polish (P)	Wet polish, 600 grit SiC
P + D	P followed by D
D + HA	Polished (P) followed by 5 min, 100°C hot alkaline treatment (TT-C-490)
D + AD	Degreased followed by alkaline derusting (AD) 10 min, 50°C, TT-C-490, method V, Type III
P +D +inh. HCL	Polished (P) and degreased (D) followed by treatment for 5 min in room temperature 42 v/o HCl + 5.8 g/l 2-butyne-1,4-diol
D + AE	Degreased (D) followed by an anodic etch for 2 min at 0.1 A/cm^2 in 30 v/o H_2SO_4
D + HNO_3	Degreased (D) followed by passivation for 30 min in concentrated HNO_3 at room temperature.

Examples for the changes of the impedance for coated steel during exposure to 0.5 M NaCl are given in Figs. 4-7. Figure 4 shows the Bode-plot for a surface which was degreased and then treated in the alkaline derusting procedure (Table 1). Deviation from capacitance behavior occurs only for frequencies below 1 Hz (Fig. 4). This deviation does not change very much with time. The coating capacitance stays constant at about 0.1 μF, indicating that the film thickness (about 6 μm) does not change during the short exposure time.

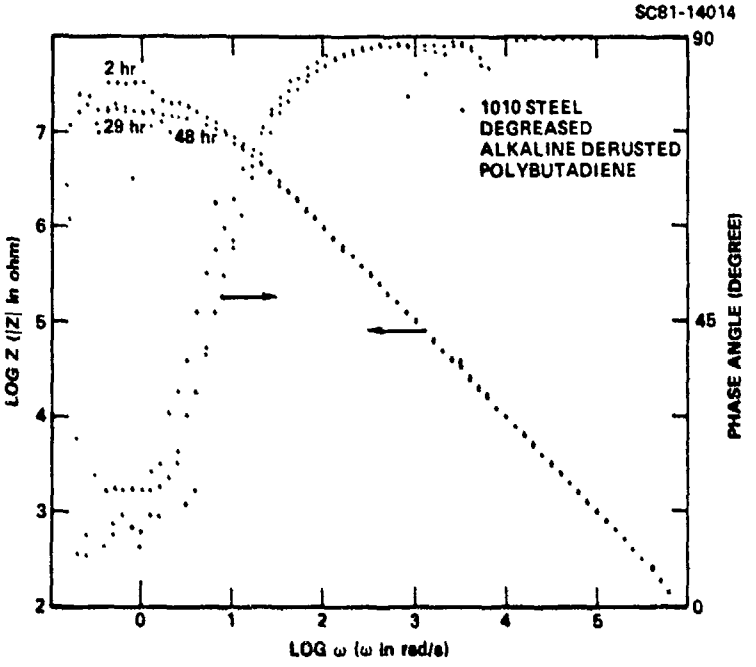

Fig. 4 Bode-plots for coated steel (D + AD).

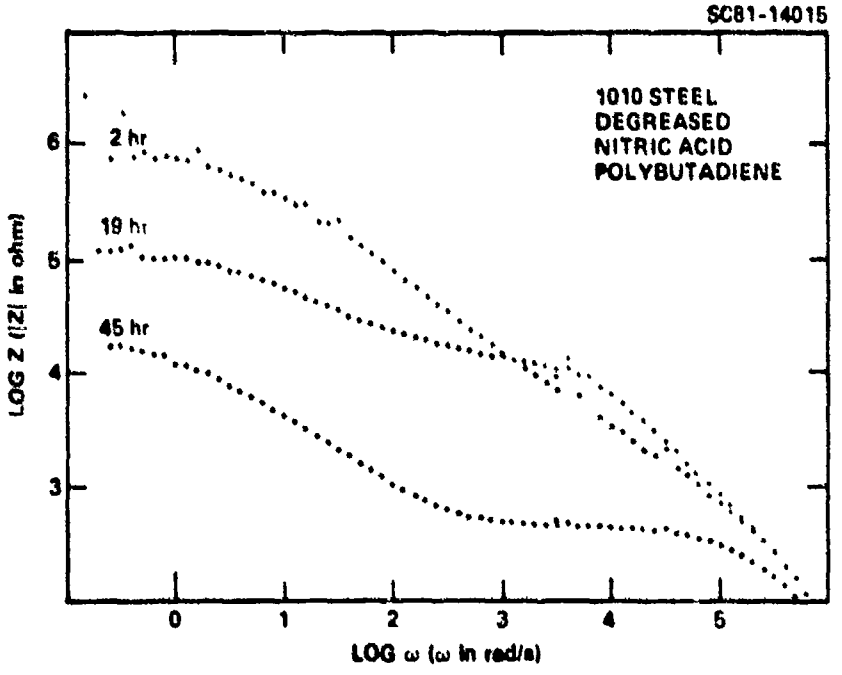

Fig. 5 Bode-plots for coated steel (D + HNO_3).

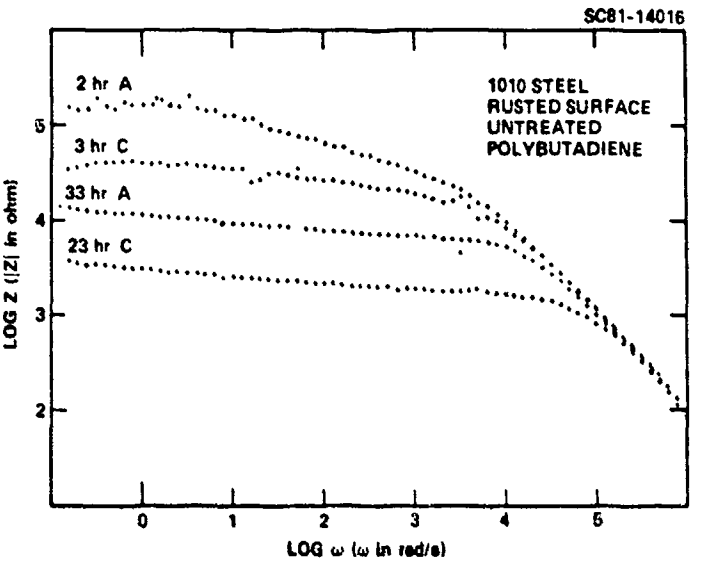

Fig. 6 Bode plots for coated steel (initial rust spots not removed).

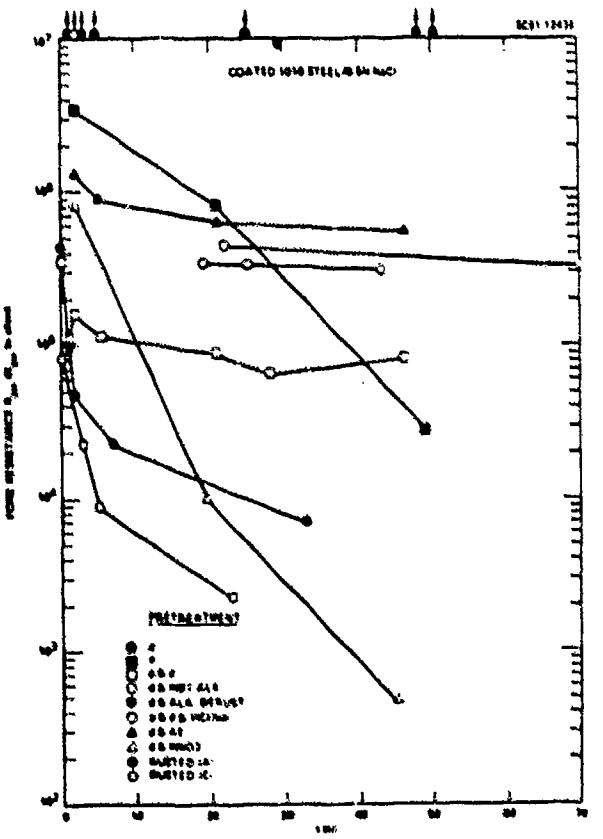

Fig. 7 Time dependence of pore resistance R_{po} for coated steel with different surface pretreatment procedures.

While the coating on the surface which was cleaned by alkaline derusting stayed very protective, relatively rapid deterioration of the protective properties of the coating occurred for the treatment of concentrated HNO_3 (Fig. 5). Already after 2 h exposure, pronounded changes from that of an intact coating can be observed. After 19 h and 45 h exposure, the impedance and the phase angle have changed drastically and two semicircles are observed in the complex impedance plot. Using a curve-fitting procedure for determination of semicircles in the complex impedance plot,[18] R_{po} and R_p were calculated as R_{po} = 12.8 kΩ and R_p = 122.2 kΩ for 19 h exposure and R_{po} = 395 kΩ, and R_p = 21.3 kΩ after 45 h. In both cases, the low frequency circle had its center below the real axis in a complex plane plot. After 45 h, the coating has become thinner or has an increased dielectric constant due to water uptake,[14] as indicated by the increase of the capacitance from 0.012 μF to 0.17 μF. A number of rust spots were observed after the 48 h test. This pretreatment gave by far the poorest results.

While for most surface pretreatment procedures (with the excpetion of HNO_3-passivation), very little degradation of the coating properties occurred as shown by the impedance measurements, relatively rapid changes were observed for surfaces from which rust particles were not removed before application of the coating. Figure 6 shows examples for surfaces with a small (A) and a large amount of rust particles (C). After 7 h exposure for the first case, R_{po} was about $2.3 \cdot 10^4$ Ω, while after 5 h, R_{po} was about $8.9 \cdot 10^3$ Ω for the second case. Complex impedance plots showed a semicircle at high frequencies corresponding to the time constant related to R_{po} and C_c. The lower frequency impedance behavior determined by $|Z|$ could not be accurately resolved into individual components. These results show that AC impedance measurements can detect in a very short time the harmful effects of surface contamination on the protective properties of an organic coating.

The impedance data for the coated steel seem to follow Model 1 shown in Fig. 2. Since in most cases very little corrosion occurred in the 48 h exposure period. R_p remained very high and could not be determined at the pres-

ent low-frequency limit of 20 MHz. The pore-resistance R_{po} has been determined from the experimental Bode-plots for the surface pretreatments in Table 1. Figure 7 shows the time dependence of R_{po} for exposure to 0.5 N NaCl. For the alkaline derusting treatment and the sample which was degreased only, the impedance at $\omega = 1$ rad/s (0.16 Hz) exceeded 10^7 Ω, at all times. The impedance for the sample with the hot alkaline treatment initially also exceeded 10^7 Ω, but then dropped to lower values with increasing exposure time and stayed below the values for the anodic etch and the acid pickling treatments. For polished surface and for passivation in concentrated HNO_3, R_{po} decreased faster than for the other surface treatments. For the surface from which rust was not removed before coating, the lowest initial and final (with the exception of the HNO_3 treatment) R_{po} values are observed.

The data in Fig. 7 can be used for a ranking of the effect of surface pretreatments on corrosion protection by the polybutadiene coating. This ranking in order of decreasing resistance to environmental effects based on the values of R_{po} at 48 h is the following: degreased ≈ alkaline derusting >> anodic etch ≈ HCl/Inh. ≈ hot alkaline > polished + degreased ≈ polished >> low rust ≈ high rust ≈ concentrated HNO_3.

This ranking results in four groups of different resistance to corrosion attack.

Figure 8 shows the variation of R_{po} with time in the first 7 days of exposure to 0.5 M naCl, for films formed on steel with different surface pretreatments, as compared to R_{po} for a free-film surface measured in the Hittorf cell. Since the exposed areas of the free film and the polymer-coated metal were different, the data for the free film have been normalized by multiplying the raw impedance data by the area ratio 5.1/19.7. The thickness of the free film was comparable to the thickness of the coating on steel, as determined from normalized capacitance data. The values of log R_{po} for the different surface pretreatments and the free film extrapolate back to nearly the same R_{po}^{o}, the value of R_{po} at zero time. However, R_{po} for the coatings on the metal substrate decreased in time, while R_{po} remains virtually unchanged for

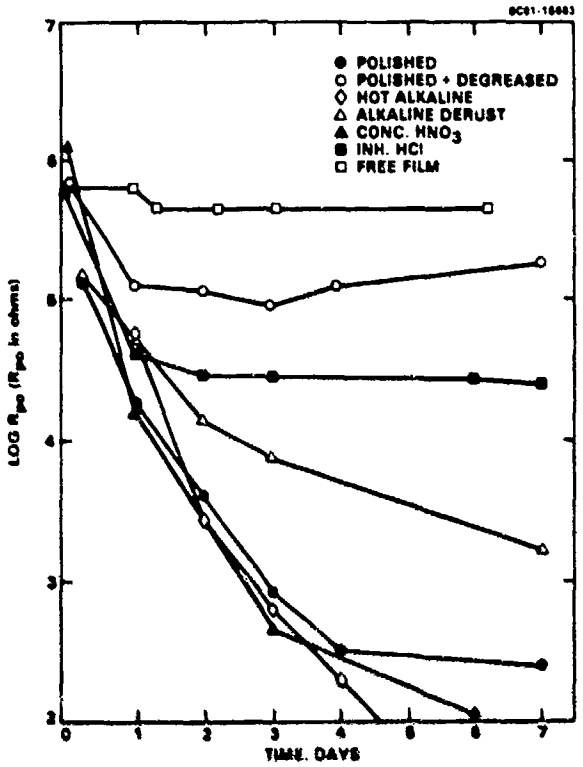

Fig. 8 Time dependence of the pore resistance R_{po} for a free film (polybutadiene) and for the same coating on steel with different pretreatments.

the free film. R_{po} for coatings on the metal substrates decrease by different amounts, depending on the surface pretreatment. The polished and degreased specimen showed only an order of magnitude decrease, but R_{po} for the samples which were polished or treated in concentrated HNO_3 or in the hot alkaline solution before coating decreased to a much greater extent upon prolong exposure. For the sample with the hot alkaline treatment (Table 1), R_{po} decreased by more than a factor of 10^4 after 7 days.

R_{po} would seem a priori to depend entirely on the nature of the polymer coating and would have no significant relationship to the surface preparation. In fact, at initial times before significant exposure to the electrolyte, R_{po} shows little variation with pretreatment (Fig. 8). However, as time progresses, the value for R_{po} of the coatings on differently prepared

substrates decreased at different rates. Significantly, R_{po} for the free film remains essentially constant. Clearly, the presence of the substrate enhances the short circuiting of the polymer film by the conducting electrolye. Although the chemical or electrochemical gradients across films formed on metals might provide the driving force which decreases R_{po} of coated substrates, it seems more likely that mechanical stresses produced by growing corrosion product films or H_2 evolution enlarge defects initially present in the polymer coating. Hence, for a given polymer coating, the coating/metal interface most susceptible to corrosion will induce the most rapid decrease in R_{po}.

These results emphasize the importance of the mechanical stresses provided by the generation of corrosion prducts at coating defects and lead to the model shown in Fig. 9 for the degradation of polymer coated steel. Corrosion initiates at critically present defects in the coating (pores or virtual pores of heightened ionic conductivity). As the corrosion reaction proceeds, oxide developes at the anodic site of the defect which drives the adjacent interface cathodic causing cathodic disbonding.[2] The stresses in the coating produced by the growing oxide rupture the coating, thereby propagating this process. Two mechanical processes, coating rupture and adhesive failure, are important to the propagation process and will be discussed in greater detail in Sects. 3.1.2 and 3.3.

3.1.2 The Role of Mechanical Stress

The evaluation of R_{po} for coatings as a function of coating extension demonstrates the role of stresses in propagating the development of coating defects. Figure 10 shows the dependence of R_{po} on strain for a PB-coated steel as compared to the stress vs strain behavior of the coated coupon. A significant decrease in R_{po} occurs between the elastic region of the metal and its yield point. R_{po} decreases further with additional strain. The decrease of R_{po} occurs within the elastic limit of the steel and indicates a brittle coating. A more ductile coating, however, will not show a significant decrease in R_{po} at such a small % strain, as is the case for the specimens

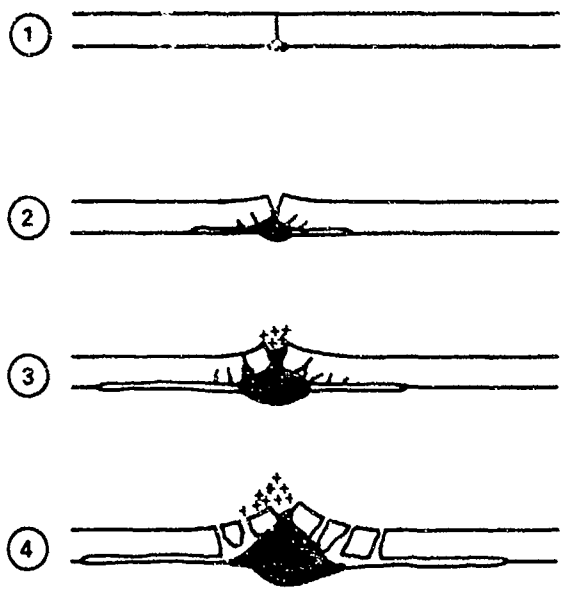

Fig. 9 Model for the coating degradation process due to build-up of corrosion products.

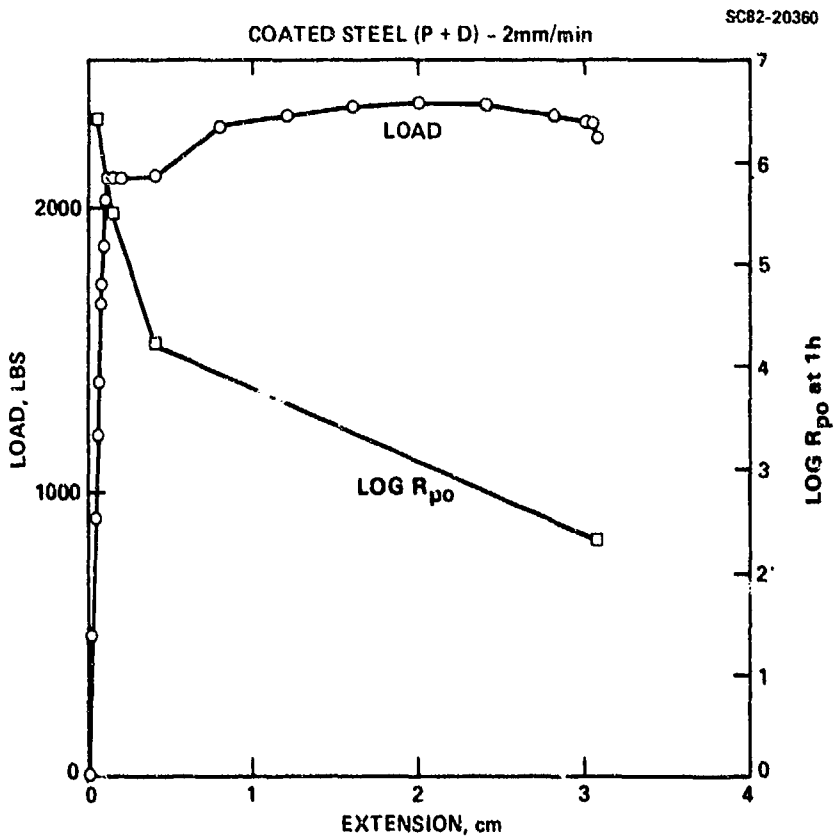

Fig. 10 Pore resistance R_{po} vs extension for coupons of polybutadiene-coated steel (P + D).

coated with epoxy (EPON 1001)/polyamide (Versamide 125), where the epoxy wt. fractions are 0.6 and 0.7, respectively (Fig. 11). The polyamide component of the epoxy, a condensation product of a polyamine with fatty acid, imparts ductility to the coating. Hence, the coatings having lower epoxy content (0.7 and 0.6 wt. fraction epoxy content) contain more polyamide than the 0.9 and 0.8 wt. fraction materials and are more ductile. Accordingly, they show no sharp drop in R_{po} upon going from an elastic strain (1.8% or 0.14 cm for the coupon) to plastic strain at 0.28 cm. Too much polyamide (0.6 wt. fraction epoxy), however, results in a coating which has an initial R_{po} that is toc low (ca. 10^4-10^5 Ω) for adequate protection. The more brittle 0.8 wt. fraction epoxy shows a high initial Rpo which drops rapidly with strain (Fig. 11). The most brittle material (0.9 wt. fraction epoxy) has a low initial R_{po} of 10^5 Ω which drops to a very low value of 100 Ω with only 5.2% strain (Fig. 11). The coating with 0.7 wt. fraction epoxy performs the best having a high initial R_{po} that changes little with up to 5.2% strain. These results demonstrate the need for a compromise between high initial R_{po} and polymer durability under strain. High polyamide fraction produces sufficient ductility, but lowers the initial R_{po}. Good corrosion protection requires high values of R_{po} (low number of defects or low ionic mobility within the coating), and no mechanism for R_{po} to decrease as a result of stress produced, for example, by growing corrosion products at the coating/metal interface.

3.1.3 Analysis with the Scanning Impedance Probe[19,20]

A potentially useful tool for detecting the presence of defects in coatings is the scanning impedance probe technique (SIPT), a schematic for which appears in Fig.12. This device evaluates the impedance between the tip of a porous fiber containing a neutral electrolyte and the substrate. The measurement is highly localized and the impedance measured at a constant frequency may be evaluated as a function of posititon of the probe tip on the specimen. For example, drops of concentrated NaOH were placed at one spot on a coated Al alloy. After a period of time, a point of low resistance appeared which could be mapped by the probe (Fig. 13). This technique has yet to be

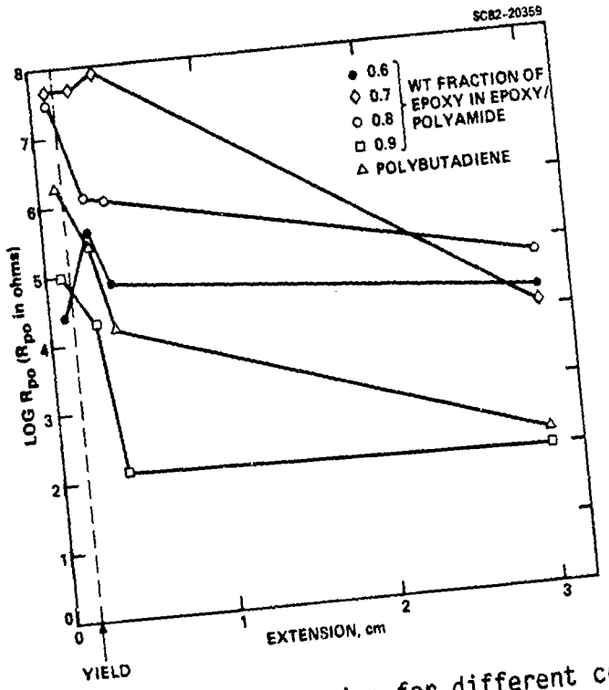

Fig. 11 Pore resistance R_{po} vs extension for different coupons coated with materials.

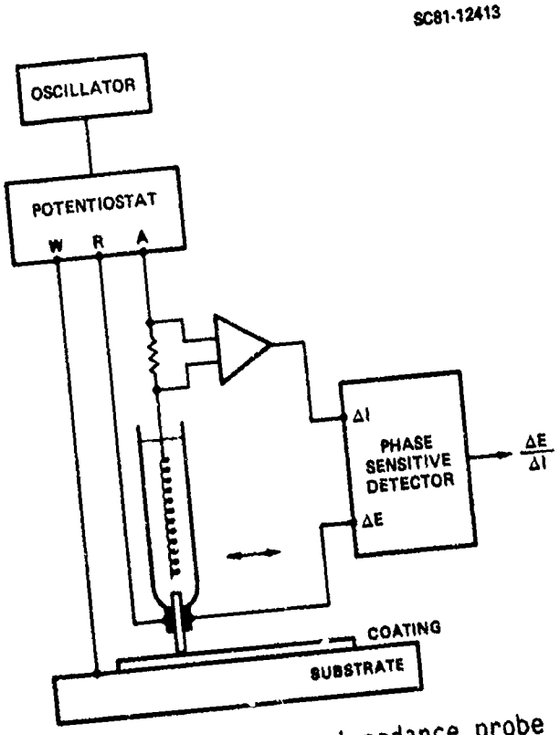

Fig. 12 Schematic for the scanning impedance probe technique (SIPT).

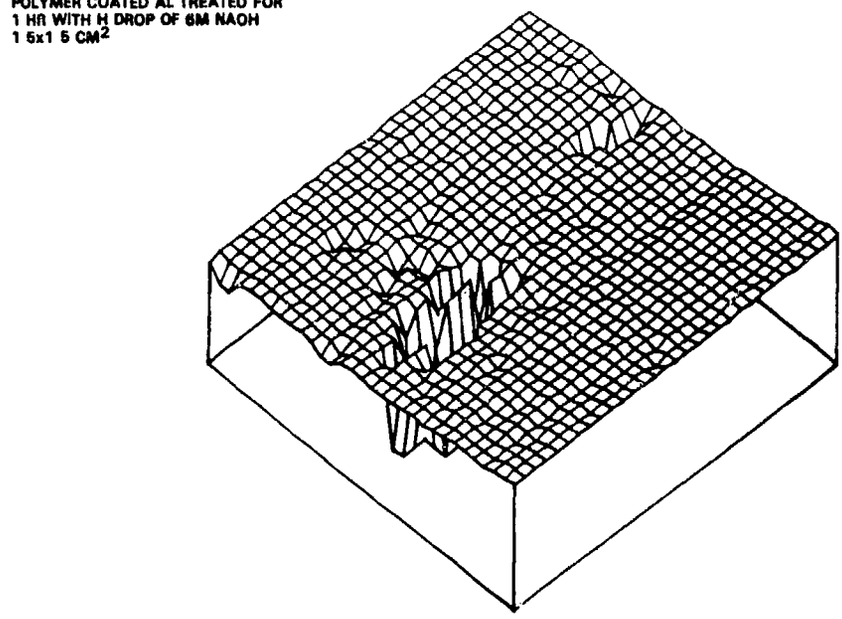

Fig. 13 SIPT map for polymer coated Al alloy subjected to localized degradation by 1.0 M NaOH.

exploited to its fullest. It will be most useful for evaluating the existence of defects which are initially present in polymer coatings on metals.

3.2 Transport of Corrodents

Permeation of organic coatings by various constituents of corrosive electrolyte has been studied extensively. The reader is referred to the literature covering this subject, in particular, the work by Ruggeri and Beck.[21]

Initially the coating itself represents the major barrier to the transport of corrodents to the interface. R_{po} as described in Sec. 3.1 is related to the transport of corrodents to the surface of the metallic substrate. The coating capacitance increases with water uptake. With time and after significant disbonding of the coating from the metallic substrate, significant transport occurs parallel to the coating/metal interface at the disbonded portion of the metal. Details of this process will be discussed in Sec. 3.4.

3.3 Loss of Adhesion

Once corrosive species have reached the metal/coating interface, corrosion and disbonding of the coating can occur. In some cases where the metal surface is quite corrosion resistant, loss of adhesion of the coating does not lead to corrosion damage. Disbonding of the coating has been studied in this project with the reflected pulse and the acoustic emission techniques. Some indirect evidence for the degree of disbonding has been obtained by recording impedance spectra between segmented electrodes under the coating as will be discussed in Sec. 3.4.2.

3.3.1 Cathodic Disbonding

As discussed above, the cathodic half of the corrosion reaction (Eq. (1)) is extremely detrimental to the adhesion of the polymer coating to the substrate. This fact may be demonstrated by a rather simple test. A scratch placed in a polymer-coated steel which was then exposed to 0.5 M NaCl and polarized to potentials more negative than the corrosion potential caused extensive disbonding of the polymer coating. On the other hand, when the same scratched surface was polarized to potentials positive to the corrosion potential, only highly localized anodic dissolution was observed with no significant disbonding at the perifery of the scratch.

This simple procedure forms the basis of a test similar to that of ASTM G8-79 for the relative susceptibility of a coating to undergo cathodic disbonding. Coated steel specimens were scribed using a silicon carbide chip to place two 2.5 cm marks bisecting at 90°. The specimens were polarized at -1050 mV vs SCE typically for 1 h. The time for the test may be modified for coating systems which have a high resistance to cathodic disbonding. The current and total charge passed during the test were recorded. Following the polarization, adhesive tape was immediately applied to the coated surface. A pull of the tape removed the portion of the coating delaminated by the cathodic disbonding. The area delaminated A_d was determined by integration from a photomicrograph.

During the polarization of the defect, most of the cathodic current eminates from the initial defect, and only a small amount of the current comes from the delaminated region. An estimate of the relative delamination rate may be made from the delamination efficiency ε_d:

$$\varepsilon_d = A_d/Q \tag{3}$$

where Q is the total cathodic charge that is passed.

Table 2

Cathodic Disbonding Results for Various Pretreatments

Treatment	Time of test (h)	A_d (cm^2)	Q (coul.)	ε_d (cm^2/coul.)
1. Polybutadiene				
HA	1	34	0.69	20.4
HNO_3	1	34	1.00	29.5
D	1	36	1.13	31.3
P + D	3	138	4.43	32.8
HA[1]	1	37	1.29	34.8
P	1	41	1.88	46.2
AD[2]	1	40	2.34	58.8
P + AE	3	140	8.45	60.4
inh.HCl	1	40	2.51	62.6
AD	1	40	1.7	67.9
2. EVA Laminate				
No adh. prom.	0.5	55	0.77	14.0
adh. prom.[3]	0.5	55	0	0.0

(1) No silicates
(2) Ending with cathodic cycle
(3) Formulated organosilane - Springborn A11861

Table 2 shows ε_d for specimens with the treatments described in Table 1. The samples with the hot alkaline treatment showed a significant resistance to cathodic delamination with ε_d = 20.4 cm^2/C as compared to the degreased, as received specimen (D) with ε_d = 31.3 cm^2/C. The HNO_3 treated and the polished and degreased surfaces (P + D) showed efficiencies similar to the blank (P + D) with efficiencies of 29.5 and 32.8 cm^2/C, respectively. The alkaline derusting and inh. HCl pretreatments apparently enhance the probability for cathodic disbonding to take place.

Delamination of an inflicted defect does not require mass transport through the coating. Thick (> 0.1 mm EVA) laminates also exhibited cathodic delamination from the steel in the absence of a suitable adhesion promoter (Table 2). The dimensions of these films preclude transport through the film during the short 0.5 h test. Consequently, the delamination results from lateral transport of the cathodically generated OH^- at the defect.

When the cathodic delamination results are comparted to surface properties obtained previously by Auger electron spectroscopy,[2,3] it is found that the cathodic delamination shows no preference for either substrates with thick oxide films (> 50Å) or thin films (< 50Å), nor for degree of hydroxylation of surface oxides as indicated by XPS analysis of surface OH^- concentration. Further analysis of these surfaces suggests that the presence of small quantities silicon-containing compounds on the surface improves the resistance of the coated surface to cathodic disbonding.

A number of methods for evaluating the loss of adhesion of a coating from the metallic substrate have been investigated. Disbonding about a cathodically polarized defect produced a dramatic change in the electrochemical impedance spectrum (Fig. 14), except for the ohmic resistance of the coating defect which remained constant at 11 Ω (Fig. 14a). After the polarization, an approximate 2.5 cm diameter region of delamination appeared around the defect and the corrosion resistance (approximately equal to the d.c. limit of the impedance spectrum) decreased from 583 Kohm to 4.6 Kohm. In addition, a large drop in the maximum of the phase angle and a decrease in the slope of the

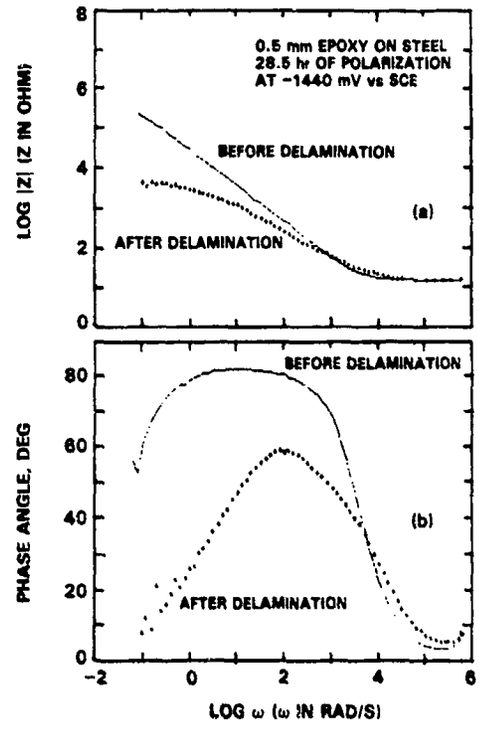

Fig. 14 Impedance spectra for a coating defect before and after cathodic disbonding around the defect.

log|Z| vs log ω curve in the 10-1000 rad/s region occured after delamination. This is consistent with the model for the delaminating defect shown in Fig. 15a which comprises a transmission line analog for the electrochemical impedance. A pore resistance, R_{pore}, and a shunt resistance, R_{sh}, define the initial defect, where the shunt resistance represents the polarization resistance at the initial defect. However as the disbonding takes place about the initial defect, parallel elements representing the corrosion resistance and double layer capacitances of the metal/coating interface (R_{pl} and C_{pl}) and a series resistance, R_{sl}, representing the series resistance of the crevice formed between the disbonded coating and the metal surface contribute to the impedance. The development of this transmission line type of impedance lowers the phase angle. This is illustrated in Figure 15b which shows the Bode plot for an interface with 10 elements representing the initiation of debonding and that for 1000 elements representing extensive disbonding. This qualitatively models the experimental results shown in Fig. 15a. The dc limit , i.e.,

corrosion resistance, is also lowered as more conducting elements R_{pi} short R_{sh} (Fig. 15b).

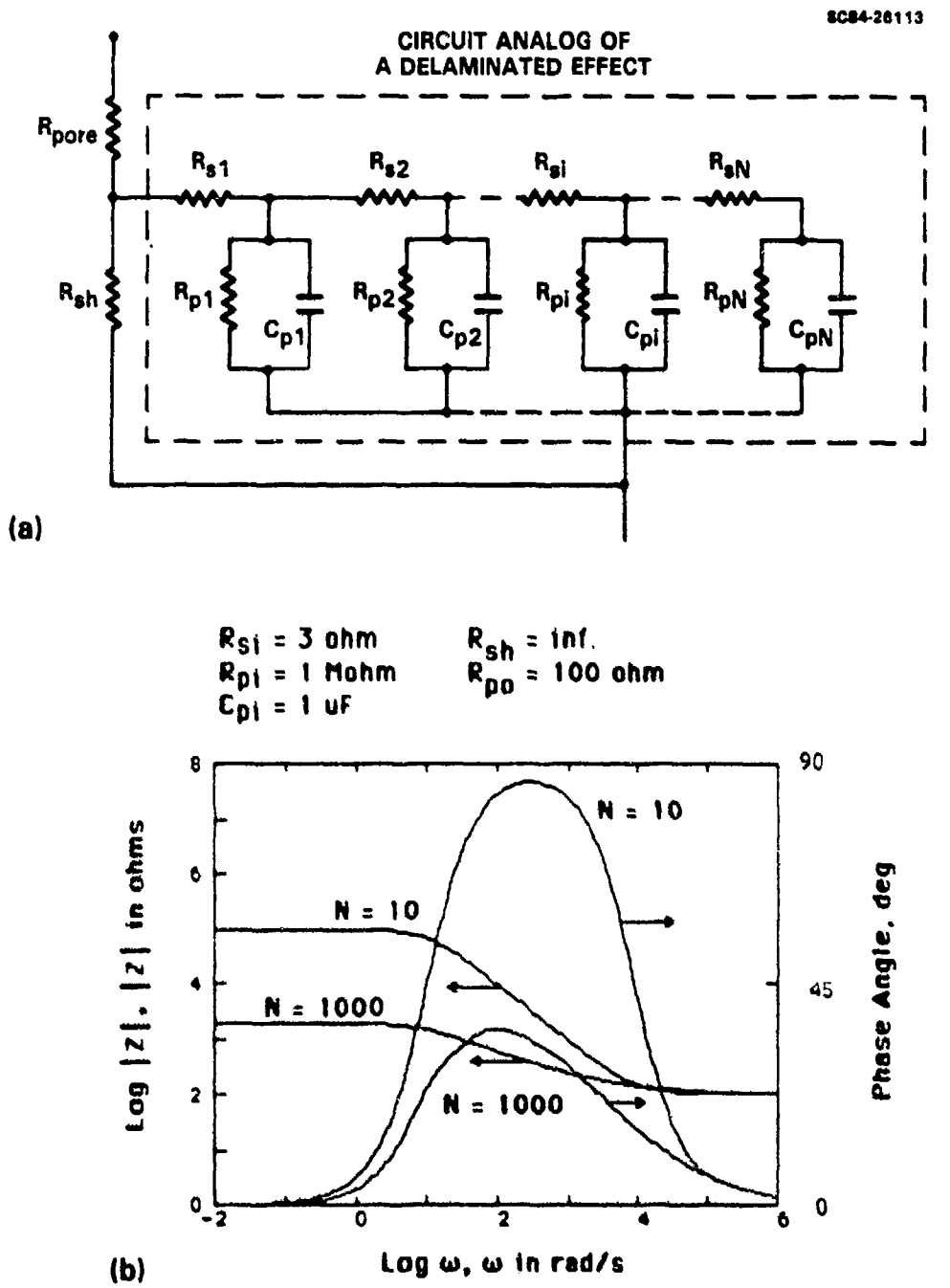

Fig. 15 Schematic for the electrochemical impedance for a cathodically disbonded region, (a) model and (b) Bode-plots.

3.3.2 Analysis with the Reflected Acoustic Pulse Technique

Reflected acoustic pulses provide a another nondestructive method for assessing the extent of disbonding or loss of adhesion at the coating/metal interface. Figure 16 a shows a schematic for the use of the reflected acoustic pulse technique for evaluating the integrity of the coating/metal interface. The time delay between the pulse reflected from the coating/metal interface (P_1) and that from the coating/couplant (water) interface (P_0) depends on the coating thickness and the velocity of sound in the coating (1.62 times that for water). A pulse P_2 also reflects from the back of the metal substrate, but this may be effectively eliminated by using a very thick substrate. Figure 16b shows a schematic for the apparatus which consists of a piezoelectric acoustic transducter mounted on a manipulator. The nominal center frequency for the pulse is 25 MHz. Signals may be stored on a digital oscilloscope for later transfer to a VAX 11/780 computer for analysis using the Interactive Signal Processing programs developed at the Rockwell International Science Center.

Figure 17 shows the reflected acoustic pulses for different thicknesses of epoxy (EPON 1001)/polyamide (Versamide 125) coatings containing 0.7 wt fraction of epoxy on a 0.5 cm thick carbon steel plate. The time difference between P_0 and P_1 for the pulses from the 25 μm-thick coating can just barely be resolved as the time between the two maxima, while a clear resolution of the time delay between P_0 and P_1 appears for coatings thicker than 100 μm. The time delay between P_0 and P_1 increases with the thickness of the coating as is to be expected. Figure 18 shows a linear dependence of the delay time on the coating thickness as measured by a micrometer. The slope of the thickness vs delay time curve (Fig. 18) equals $1.6 \cdot 10^5$ cm/s which is the velocity of sound at 25 MHz in the coating.

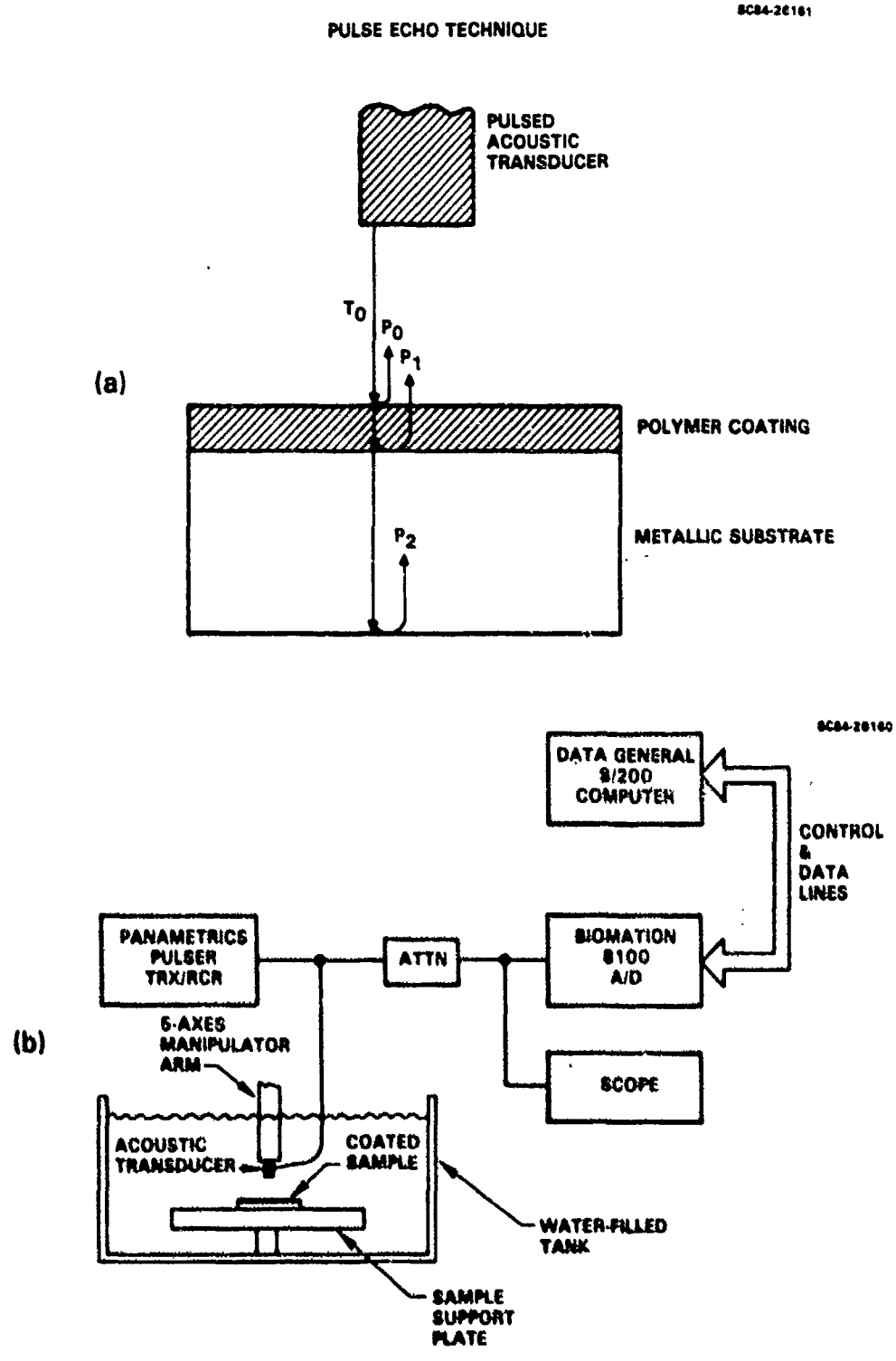

Fig. 16 Schematic of the reflected acousic pulse technique, (a) reflections and (b) apparatus.

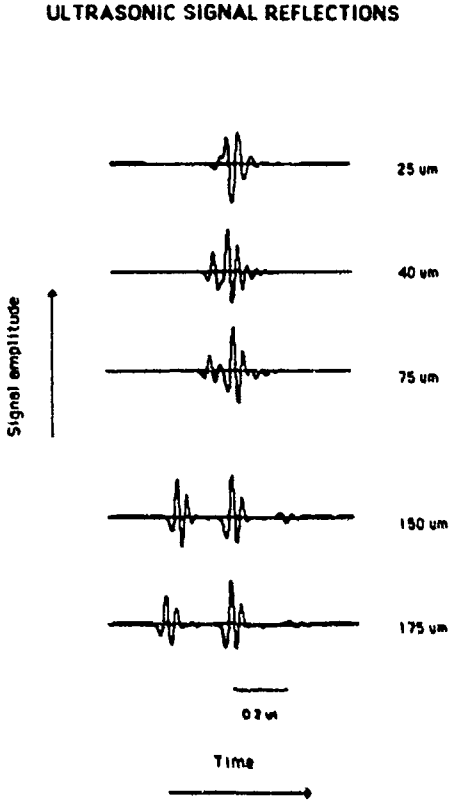

Fig. 17 Reflected 25 MHz acoustic pulses for coatings having different thicknesses.

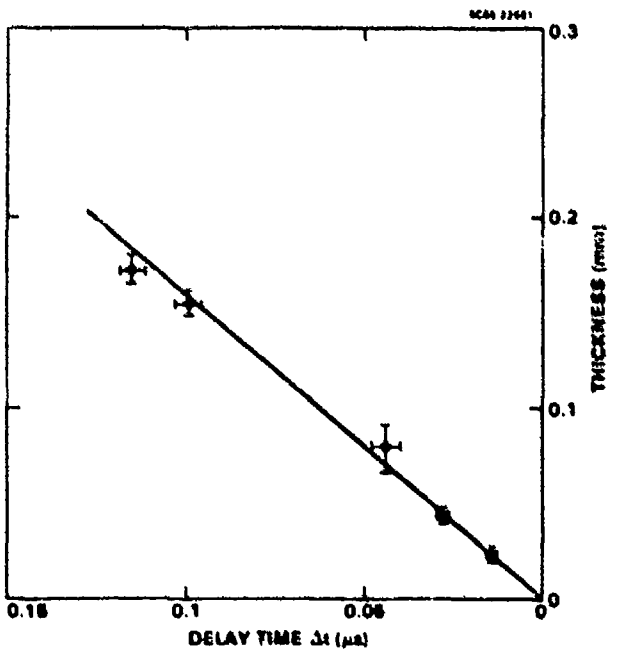

Fig. 18 Delay time Δt between P_0 and P_1 as a function of coating thickness.

The method can be used to observe gross disbonding of the coating from the substrate. Figure 19 shows a "waterfall" plot made by placing the transducer at different points near and over a defect (0.6 cm hole) in a coating which had been subjected to -1440 mV vs SCE for 30 h (-1.5 V vs $Cu/CuSO_4$ - see ASTM G8-79). The transducer was translated 1.25 mm before each waveform shown in Fig. 19 was collected. At the defect only one reflection due to the metal/water interface occurs, while both P_0 and P_1 appear when the transducer is over the coating. Where lift-off occurs, P_0 arrives earlier since the coating has been raised. The small signal between P_0 and P_1 in the lift-off region is a reflection from the polymer/water interface.

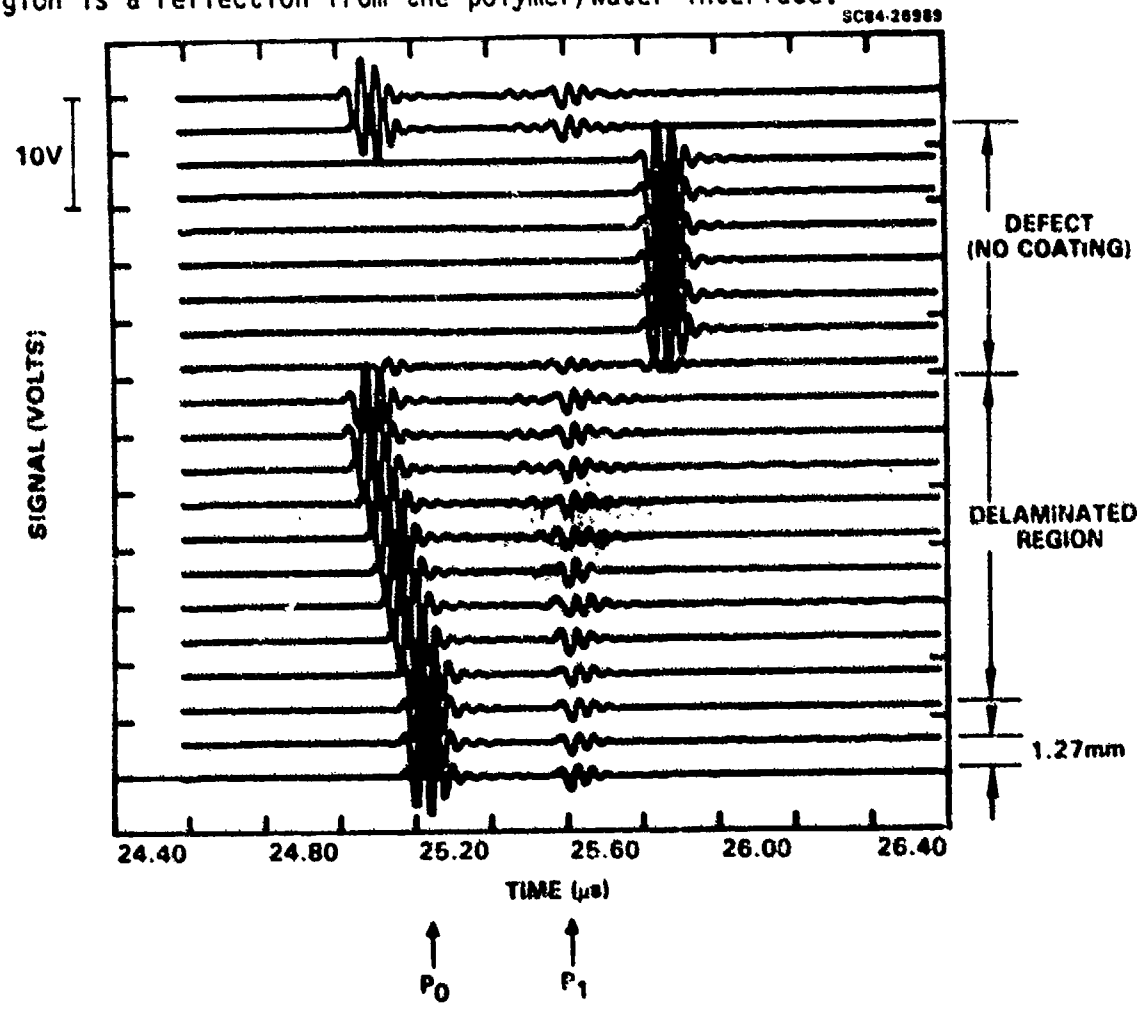

Fig. 19 Reflected 25 MHz acoustic pulse at a disbonded region next to a defect.

In addition to the time delay between P_0 and P_1, the frequency spectrum of P_1 has features which sense disbonding due to acoustical impedance differences at the interface when a disbond occurs as compared to when complete adhesion exists. The acoustic impedance of a material equals the density of the material times the velocity of sound in the material. When the acoustic impedance of the substrate exceeds that for the coating, as is the case for a well bonded coating/metal interface, then a positive spike in the phase angle spectrum of the frequency transform of the pulse appears as shown in Fig. 20b. On the other hand, when disbonding occurs a water layer which exists between the coating and the metal acts as the acoustic substrate. In this case the acoustic impedance of the substrate (i.e., the water layer) is less than that for the coating and thereby produces a negative phase shift as shown by the negative spike in the phase spectrum (Fig. 20a). This phase shift allows the signal from disbond initiation sites to be enhanced with the proper data transformation. The signal due to the phase shift can be enhanced by performing a transformation on the signal of the initial time domain signal, P_{old} into a new signal, P_{new}:

$$P_{new} = F^{-1}\{F(P_{old})/F(P_{ref})\} - P_0 \qquad (4)$$

where P_{new} = the transformed signal.
P_{ref} = a signal from a well-bonded region.
F and F^{-1} refer to the operations of fourier and inverse fourier transformation, respectively.

After placing a defect in a 350 μm coating on steel and exposing it to 0.5 M NaCl severe corrosion occured at the defect. In addition several small corrosion spots appeared at sites several centimeters removed from the defect. An attempt was made to detect the integrity of the coating at the smaller corrosion spots removed from the defect. Time domain acoustic pulse data gave some indication of the initiation of corrosion at these remote sites as shown for each 1.25 mm translation of the transducer position in Fig. 21.

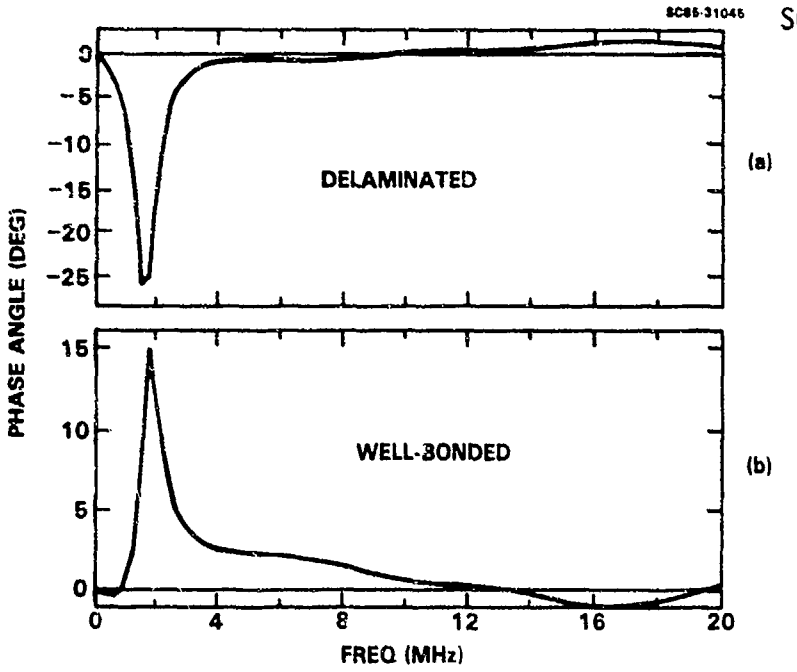

Fig. 20 Phase angle vs frequency for transformed pulse data from delaminated and well bonded regions.

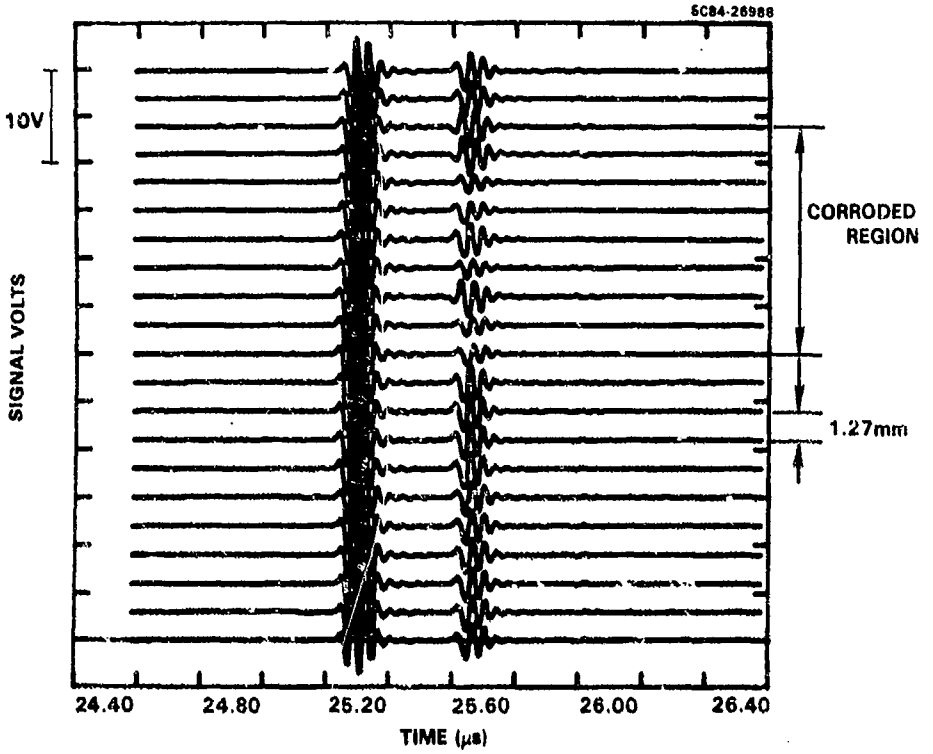

Fig. 21 Reflected 25 MHz acoustic pulse near a corrosion spot.

Very little differentiation appears for the time domain pulses shown in Fig. 21. However, upon transforming the data of Fig. 21 according to Eq. (4), the resulting signal pinpoints regions of disbonding as minima, shown in Fig. 22, due to the negative phase shift brought out by the transformation.

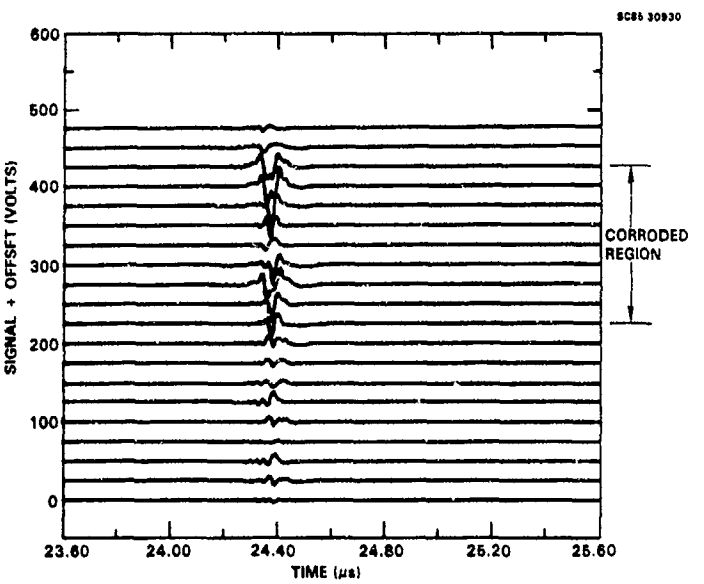

Fig. 22 Image enhancement of the data from Fig. 21.

The previously described tests were performed on relatively thick specimens that contained an artificially produced defect. In order to evaluate the ability of the method for detecting the earliest stages of corrosive degradation of the polymer/metal interface, a steel coupon coated with a 25 μm epoxy was exposed for over 600 h to 0.5 M NaCl and the electrochemical impedance spectra and reflected acoustic pulses taken from an approximate 6.5 cm^2 area were collected at different intervals of the exposure. The electrochemical impedance gave values for R_{po} which decreased rapidly in the first 200 h and then increased slightly after 300 h. Little change in the acoustic pulse spectra occur until after 672 h at which time a corrosion spot appeared under the coating which was detected by the reflected acoustic pulse. Figure 23a shows a plot of the transformed signals taken at initial time from the

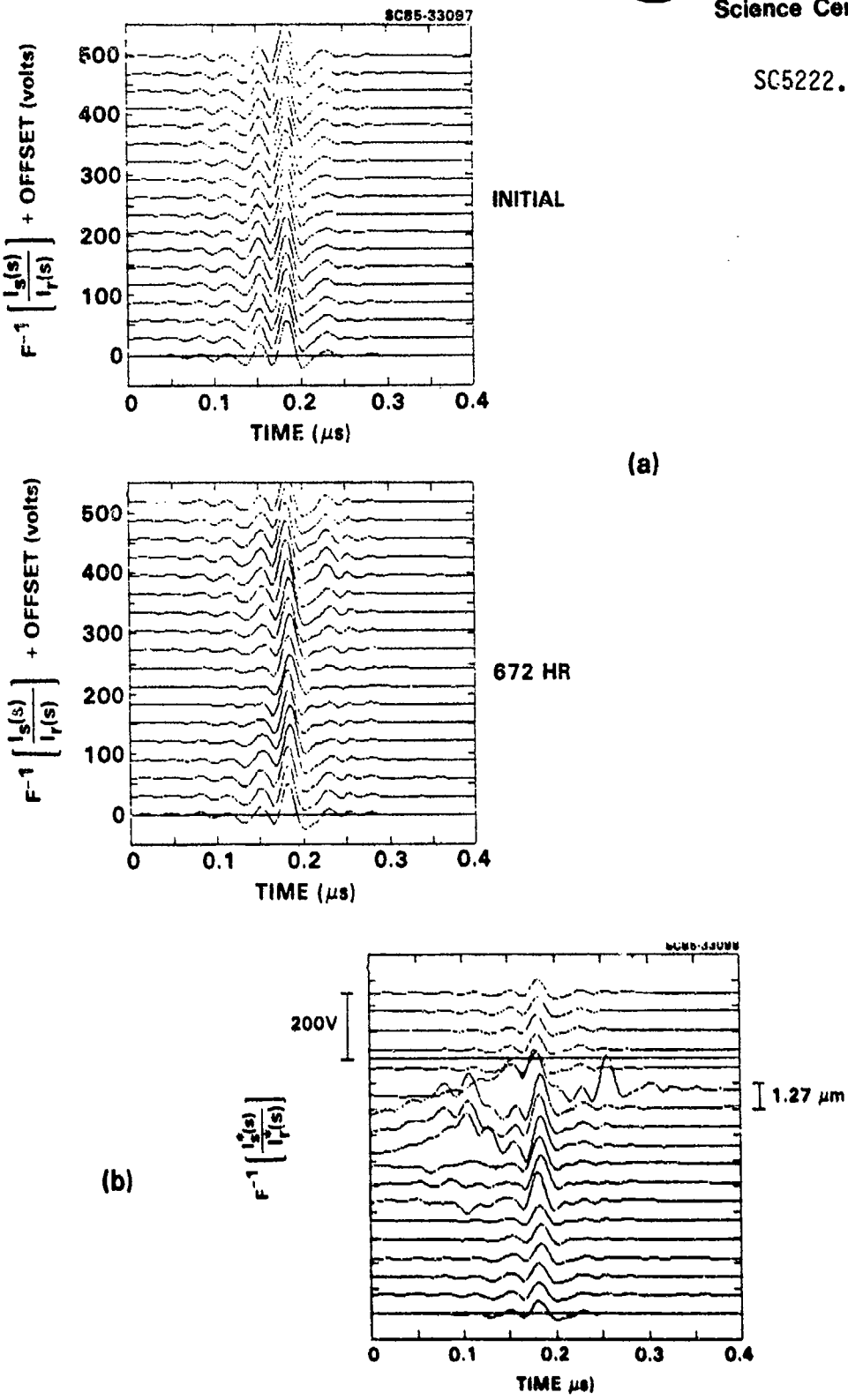

Fig. 23 (a) Reflected pulses from the same region of epoxy coated steel after 0 and 672 h exposure to 0.5 M NaCl. (b) Image enhanced reflected acoustic pulse of the 672 h data.

position where the corrosion spot eventually appeared, and after 672 h when the corrosion spot was initially detected. After enhancing the initial portion of the signal by a multiplication factor and performing the transformation, a clear indication of the position of corrosion spot appears in Fig. 23b.

With the application of signal processing techniques the reflected acoustic pulse method detects the loss of adhesion of polymer coatings from metallic substrates and the initial growth of corrosion products at the coating/metal interface. The technique can locate the initiation site(s) of corrosion at early times which is not possible with EIS. The impedance spectra suggest that defects in the coating have formed prior to the earliest detection of corrosion product by the acoustic pulse. The acoustic pulse method would be of use for evaluating nontransparent coatings and for assessing the earliest stages of adhesion loss.

3.3.3 Analysis with the Acoustic Emission Technique

A number of investigations have used acoustic emission (AE) emanating from polymer-coated steel pulled in tension to failure as a method for evaluating the environmental degradation of adhesion and microcracking of the protective coating.[22-21] A number of approaches have been used in this laboratory for separating the different types of acoustic events observed for coated steel with different pretreatments and exposure history.

Coupons (17.8 cm × 5.08 cm × 0.05 cm) of carbon steel were pretreated by 1) polishing (600 grit) and degreasing in hot xylene (P&D), 2) pickling in inhibited HCl (inh. HCl), 3) treating in hot NaOH (HA), or 4) passivating in HNO_3 ($HNO_{3)}$. 10 μm polubutadiene coatings were applied to the specimens and cured for 20 min at 100°C. From electrochemical impedance spectra R_{po} was determined as a function of time of exposure to 0.5 M NaCl at different intervals over a period of 70 h. After the 70 h, the specimens were pulled in tension at a rate of 2 mm/min in a 2000 lb Instron machine. Flat jaw grips were used to grip the specimen firmly. A gauge length of 7.6 cm was used.

The test set-up along with the AE monitoring system is shown in Fig. 24. The AE events were continuously monitored as the specimens were pulled to failure.

Figure 25a-d shows the event rate and the integrated event rate vs time for the coated steels of different pretreatments. For all of the specimens, counts occur when the metal yields; however, for the HA and inh HCl pretreatments which showed superior resistance to degradation, a smaller fraction of the total counts appeared at or near yield of the steel substrate as compared to the P&D and HNO_3 pretreated specimens which showed a substantial fraction of the counts in the first half of the total specimen elongation before rupture. At 50% elongation, the fraction of the total counts for the specimens with HA, inh. HCl, P&D and HNO_3 pretreatment were 0.13, 0.17,0.25 and 0.54, respectively (Figs. 25a-d). This order correlates inversely with the R_{po} results in Fig. 26. The sample with the greatest fraction of counts in the first half of the total elongation where yield occurs (HNO_3) shows the lowest R_{po} at 70 h exposure to the 0.5 M NaCl environment.

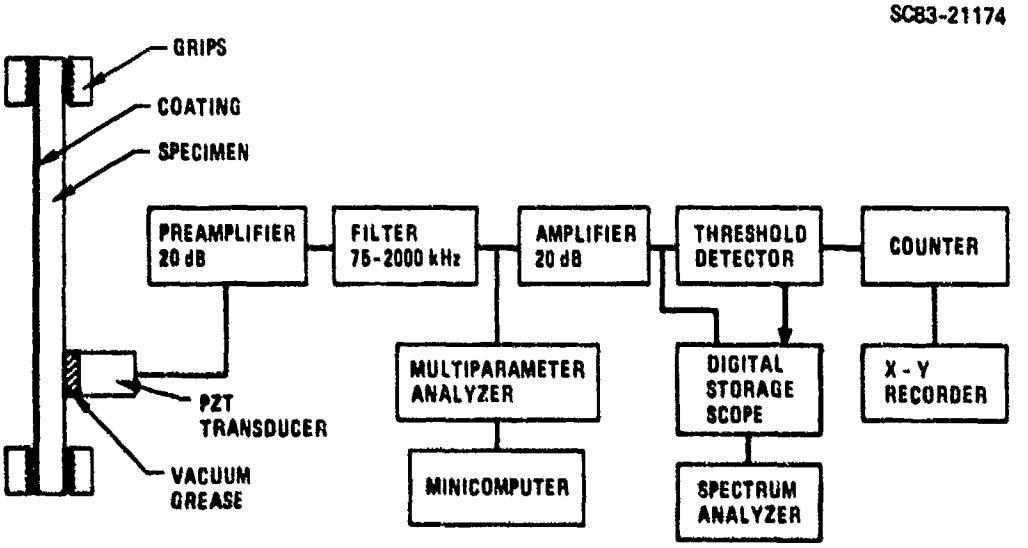

Fig. 24 Schematic of the acoustic emission apparatus.

SC5222.FR

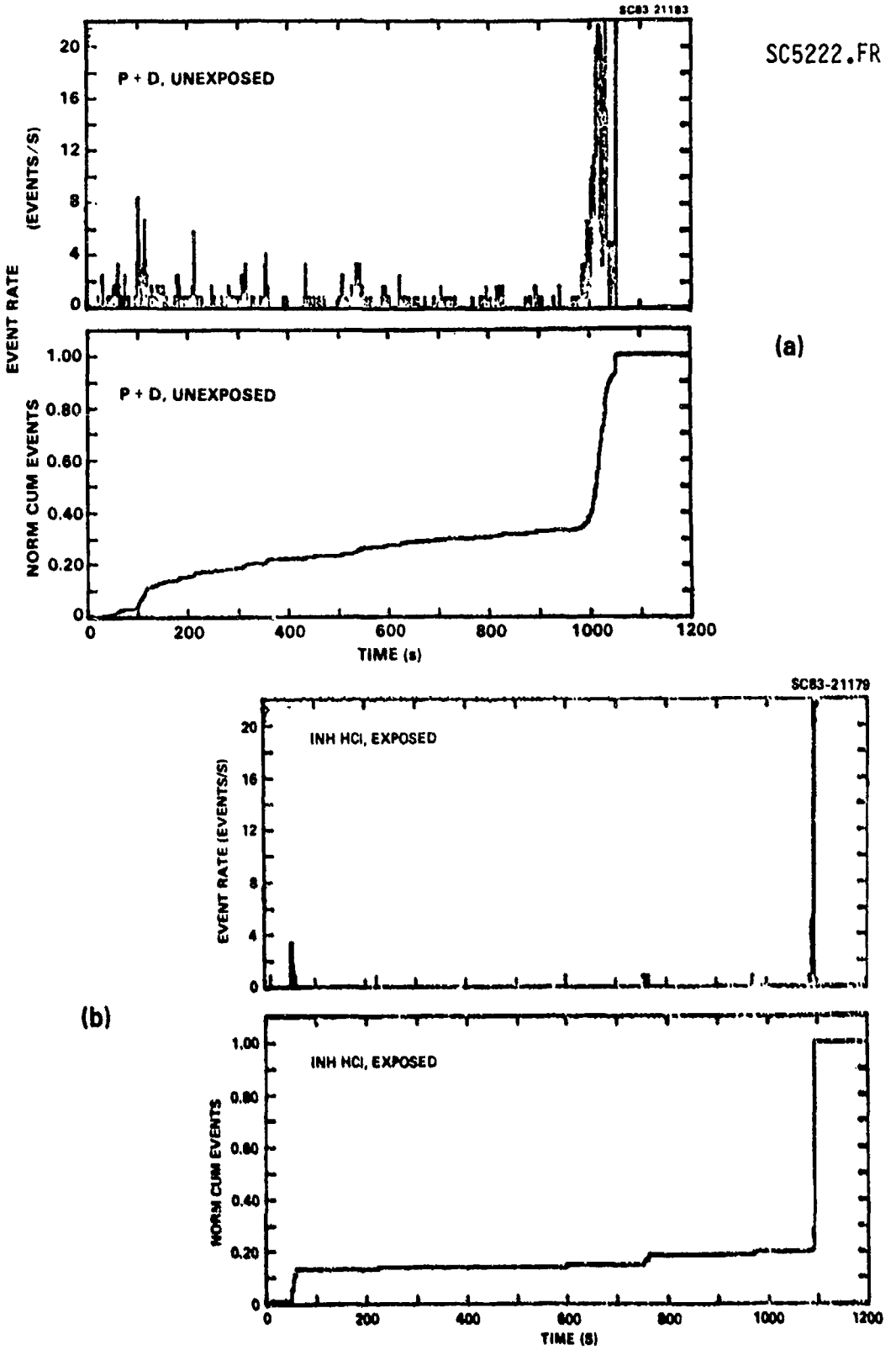

Fig. 25 AE event rate and cumulative events for polybutadiene-coated steel exposed for 70 h to 0.5 M NaCl, pretreatment: (a) P + D, (b) inh. HCl, (c) HA, and (d) HNO_3.

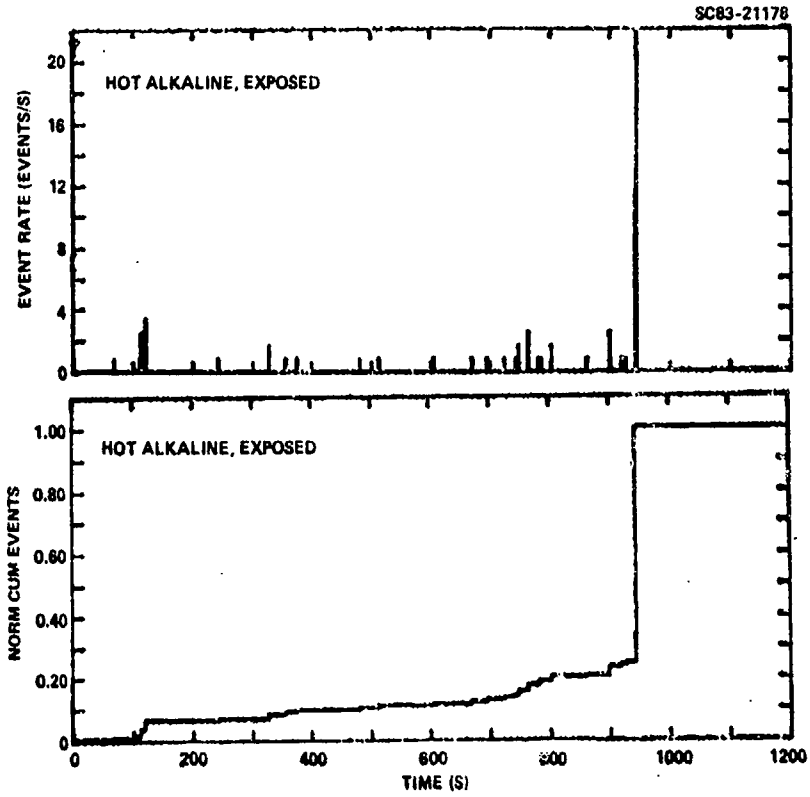

(c)

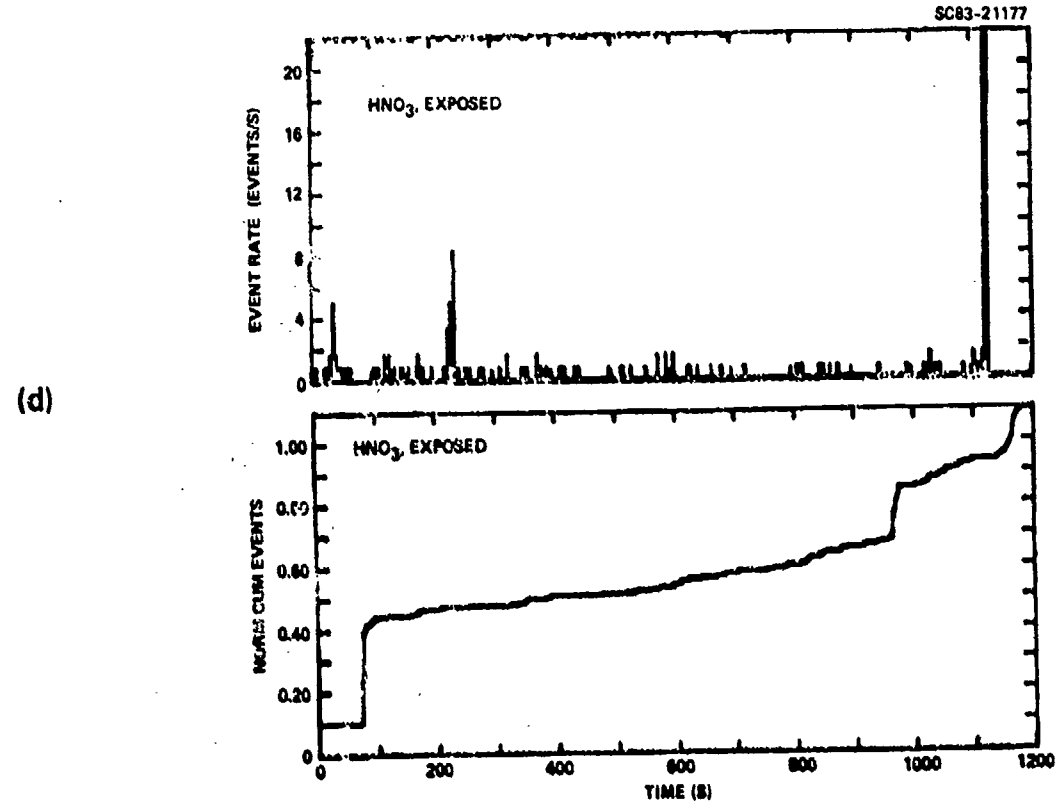

(d)

Fig. 25 (Continued).

The P&D (Fig. 25a) and the HNO_3 (Fig. 25d) treated specimens show the largest number of events before failure of the specimen. This correlates quite well with the Rpo data appearing in Fig. 26. The amplitude distribution for the AE of these specimens provides further information. The amplitudes for the coatings which are least degraded (HA and inh HCl) exhibit higher amplitude events (see Figs. 27b-c) than the P&D and HNO_3-treated sample (Figs. 27a and 27d). The two specimens exhibiting the greatest degradation have amplitude distributions characteristic of brittle failure of the coating.[1] This apparent embrittlement could result from the localized stress which occurs in corrosion products formed at the coating/metal interface for the coatings with more advanced degradation (see Fig. 9).

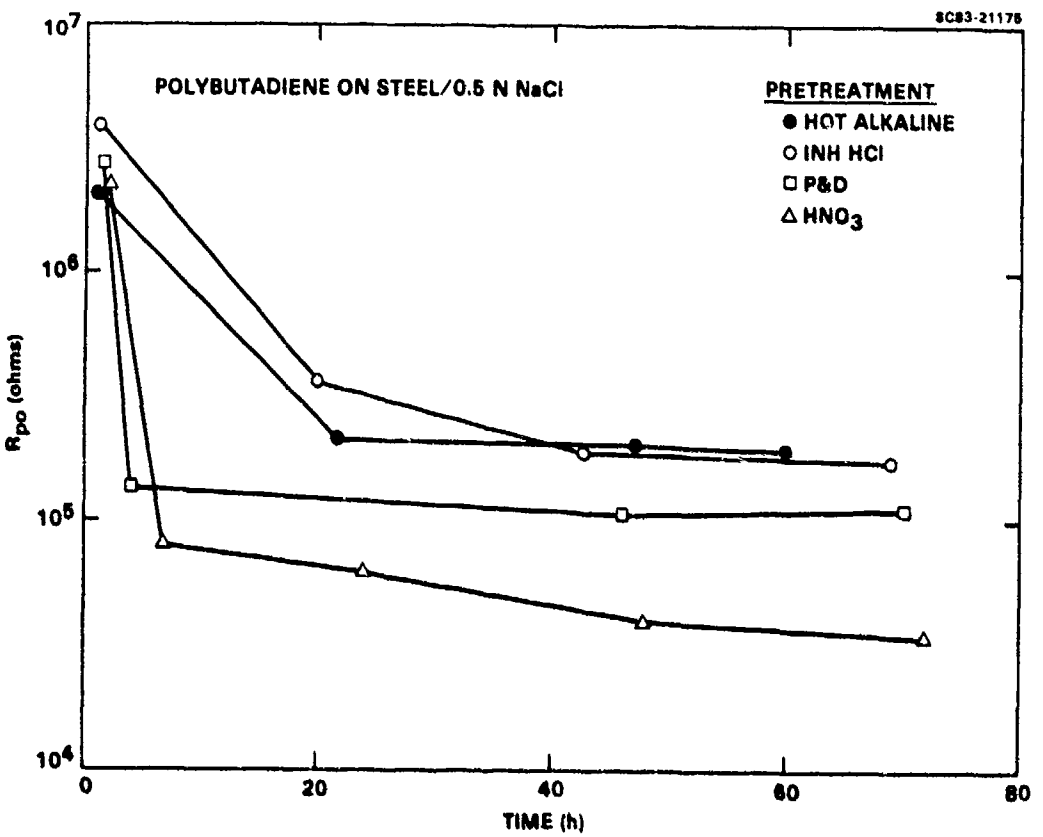

Fig. 26 Time dependence of R_{po} for PB-coated 1010 steel with different pretreatments.

SC5222.FR

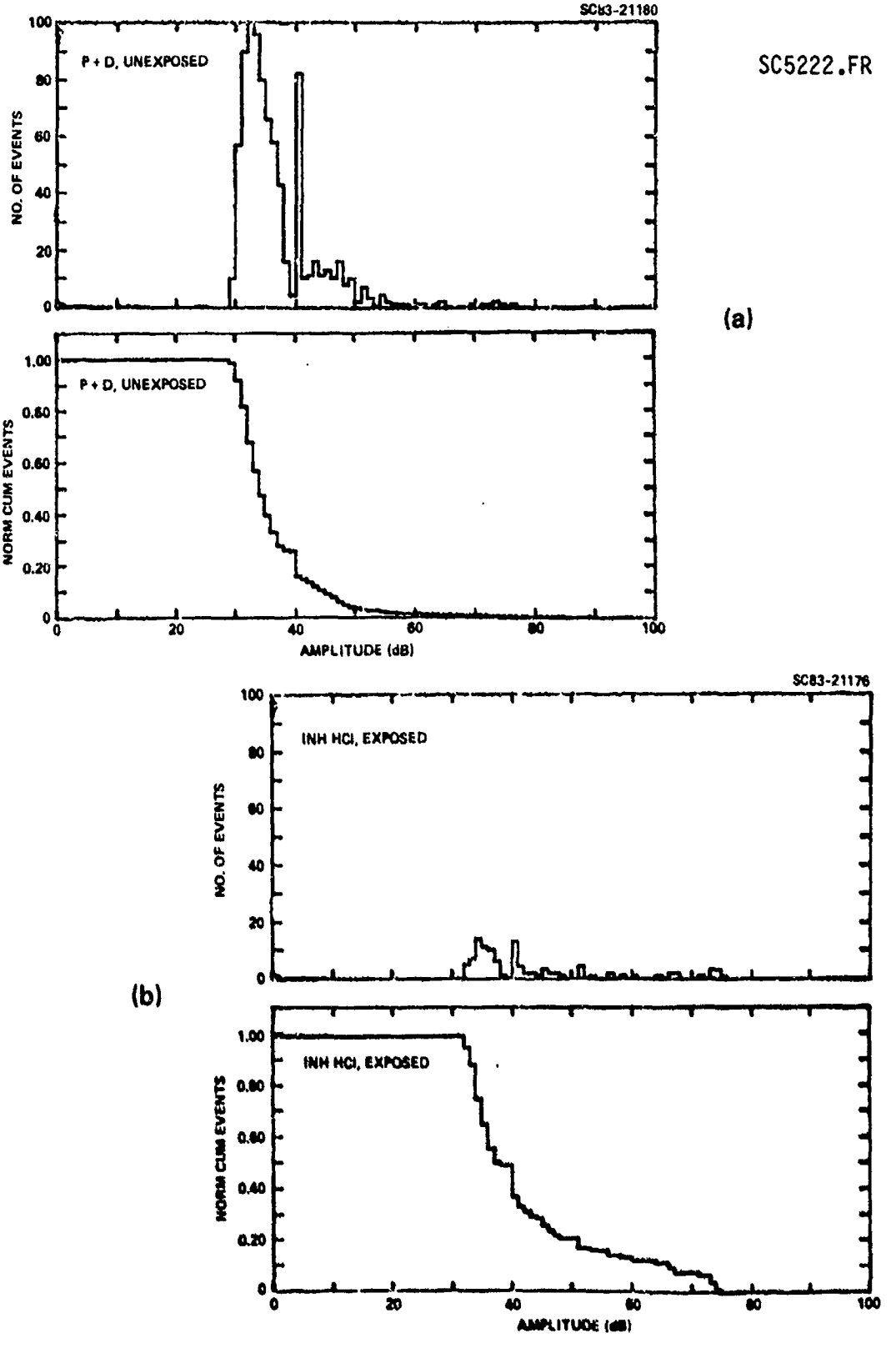

Fig. 27 Amplitude distribution for events observed for PB-coated 1010 steel with (a) P + D, (b) inh. HCl, (c) HA and HNO_3.

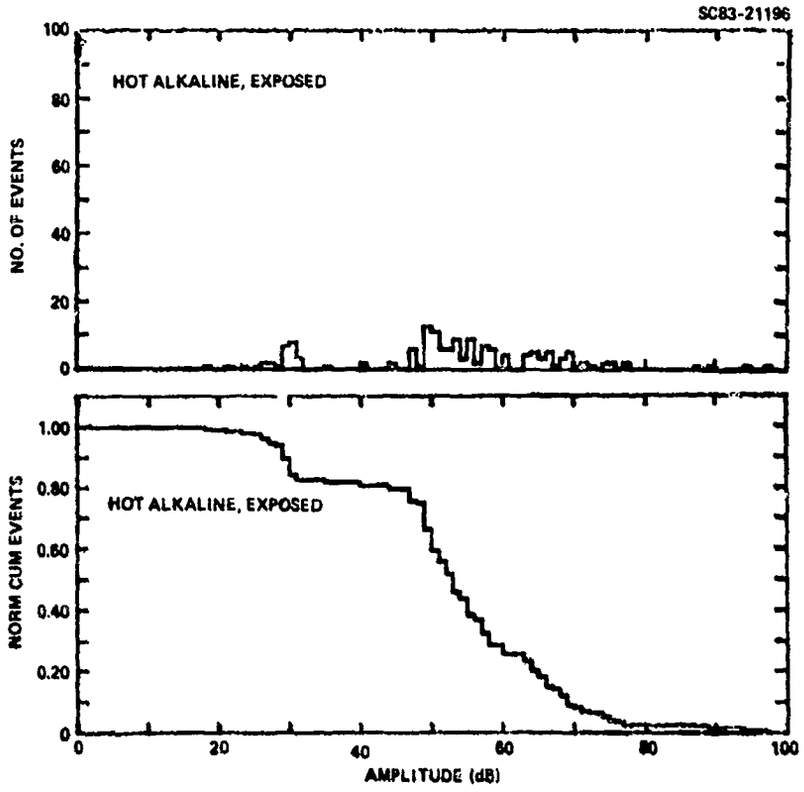

(c)

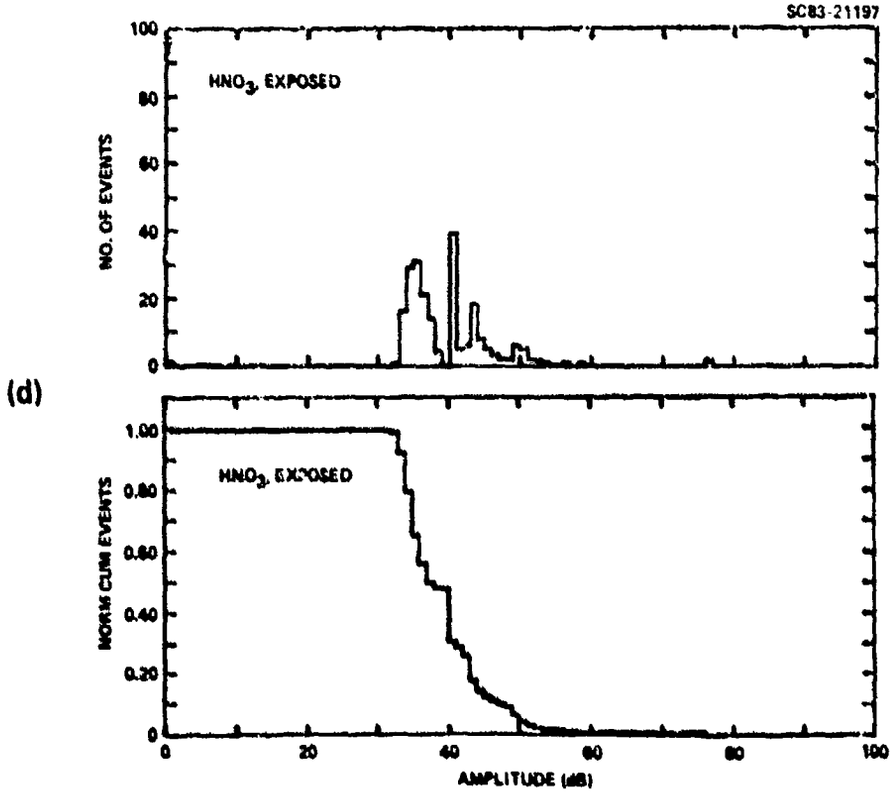

(d)

Fig. 27 (Continued)

The first events in the degradation of the coatings result from penetration of electrolyte and loss of adhesion. In the later stages of corrosion, corrosion products precipitate at local defects and locally produce high stress sites (see Fig. 9). In the early stages, then, AE will result from loss of adhesion producing the high amplitude, broadly distributed events (> 50 bB). For specimens in more advanced stages of degradation, more events will occur with amplitudes between the 40 and 50 dB level which are characteristic of the brittle behavior.

These results demonstrate the role of mechanical events in the degradation of polymer-coated steel. Adhesive failure of the coating interface during exposure to electrolyte leads to the growth of corrosion products that act as stress risers in the polymer film. This causes further degradation of the coating by enhancing the existing porosity and initiating new pores. Analysis of the amplitude distribution of AE from coated specimens loaded in tension to failure pinpoints events associated with brittle failure of the coating and adhesive failure at the interface. Most importantly, the number of acoustic events which occur near the yield point correlates with the extent of degradation of the coated coupons as determined from impedance analysis.

3.4 Corrosion

The combined effects of defect formation, transport of corrosive species to the metal surface and loss of adhesion can lead to corrosion of the surface. As discussed above, corrosion products and reaction products of the electrochemical reactions such as OH^- (Eq. (1)) can lead to further destruction of the coating. For the study of corrosion reactions at the metal surface, which in many cases might be covered by a (hydrated) oxide, impedance techniques provide again the most promising approach. The use of segmented electrodes allows to measure the impedance of the surface under the coating and compare the results with those for measurements across the coating. Corrosion inhibition by primers in the coating and by surface modification through phosphating of steel and anodizing or conversion coating of Al has also been evaluated using EIS.

3.4.1 Determination of the Corrosion Rate of the Substrate

As discussed in Sec. 3.1, the electrical analog of the polymer-coated steel interface contains the polarization resistance, R_p, which is inversely proportional to the corrosion rate. In principle, the actual corrosion resistance and its changes can, therefore, be evaluated from impedance spectra. While EIS has provided useful new information concerning reactions in the coating, as expressed by C_c and R_{po} (Fig. 2a), it has been difficult to determine values of the polarization resistance R_p and double layer capacitance C_d for the corroding surface as a function of exposure time. This is due to the fact that R_p and C_d are accessible only at very low frequencies for corrosion resistant polymer-coated metals. If R_p is less than R_{po}, then its accurate determination becomes difficult, if not impossible.

The changes of the capacitance with increasing porosity and corrosion rate can be used to determine the area fraction θ at which active corrosion occurs.[10] For an experimentally determined value of the capacitance C and the known values of $C_c = 6.2\ 10^{-9}$ F (Eq. (2)) and $C_d = 4\ 10^{-4}$ F, one can calculate θ from Eq. (5):

$$C = (1 - \theta)\, C_c + C_d \qquad (5)$$

The corroding area fraction θ and the pore resistance R_{po} are two parameters which can be used to characterize the deterioration of the coated metal.

3.4.2 Investigations of the Metal/Coating Interface

The study of the reactions occurring at the metal/coating interface, such as corrosion and loss of adhesion, is very important from both fundamental and practical standpoints. An attempt to evaluate such reactions has been made using a variation of the experimental technique for obtaining EIS data in coated metals. Impedance measurements are carried out under the coating and are compared with those for the more traditional approach of measuring impedance data across the coating.[12] These data have been obtained with an

electrode system which is used in the atmospheric corrosion monitor (ACM). It consists of a number of parallel steel plates which are isolated from each other.[12] A steel/steel ACM, which consisted of 20 steel plates 1 mm wide and 6.5 cm long, was used as the substrate. The steel (A366) plates were separated by a 50 μm thick mylar foil. Alternate steel plates were connected to establish a two-electrode system. The epoxy coating was 20 μm thick and consisted of 0.7 weight fraction epoxy and 0.3 weight fraction polyamide. After curing of the coating, an electrochemical cell, which contained the SCE reference electrode and a large Pt counter electrode, was attached to the active part of the ACM. The test electrolyte was aerated 0.5 N NaCl. The counter and reference electrodes were used for measurement across the coating; the measurement was carried out at the open circuit potential of the coated steel. The measurement under the coating was carried out at 0 mV applied potential. The ac signal was applied between alternate plates. EIS data have been obtained as a function of exposure time (t_{corr}) to aerated 0.5 N NaCl for clean steel surfaces and for surfaces which were exposed to diluted NaCl before coating.

Figure 28 gives a typical result for the changes of the electrode impedance $|Z|$ as a function of t_{corr} for measurements across the coating and under the coating, respectively. In the former case, the capacitive behavior observed at frequencies $f = \omega/2\pi$ exceeding 10 Hz corresponds to that of a 20 μm epoxy film (C_c in Fig. 24). At lower frequencies, the pore resistance R_{po} becomes apparent. It slowly decreases with t_{corr} up to 14 days, but remains at the high values observed earlier for 20 μm coatings.

For measurements under the coating, a much lower impedance, which changes significantly with t_{corr}, is observed. The initial capacitance at high frequencies corresponds to that of the bare steel/mylar/steel system. After longer exposure times, a -0.5 frequency dependence of the impedance is observed at intermediate frequencies which points to transmission line effects.

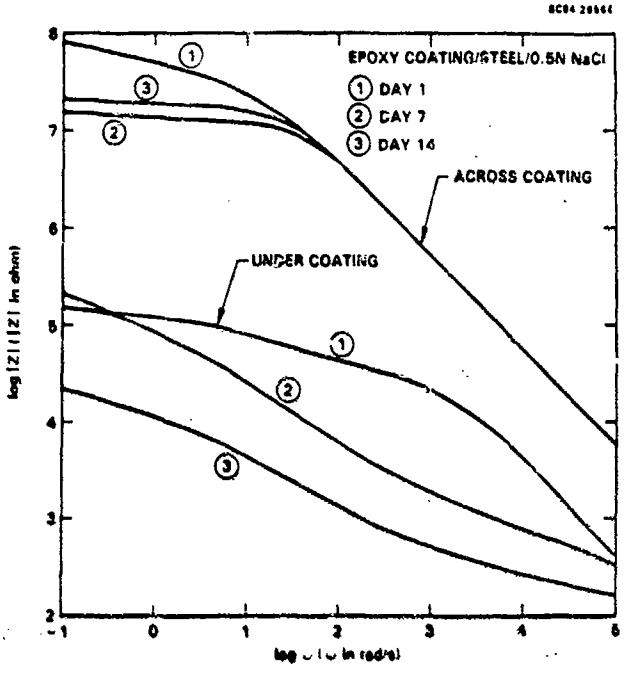

Fig. 28 Bode-plots for coated steel/steel, spectra measured across coating and between plates.

As observed earlier with EIS and well-known in practice, contamination of the steel surface before coating can lead to rapid corrosion and loss of adhesion of the coating. This effect was simulated by covering the ACM surface with a solution of 1 mM NaCl containing some ethanol which was allowed to dry. The epoxy coating was applied to the resulting surface. As Fig. 29 shows, much more rapid changes of the impedance occur in this case for both types of measurements. After t_{corr} = 1 day, R_{po} is already lower than the value for t_{corr} = 7 days for an uncontaminated ACM surface. For measurements under the coating, rapid changes occur even after R_{po} has become constant. The slope of -0.5 is found at intermediate frequencies. Figure 29 also shows an impedance spectrum for the bare surface which is dominated by the capacitance of the mylar spacers.

The impedance spectra in Figs. 28 and 29 have been analyzed using the model in Fig. 30 with the goal of obtaining an estimate of the corrosion rate at the metal surface and the degree of delamination. A transmission line model[16,12] has been used to fit the data to

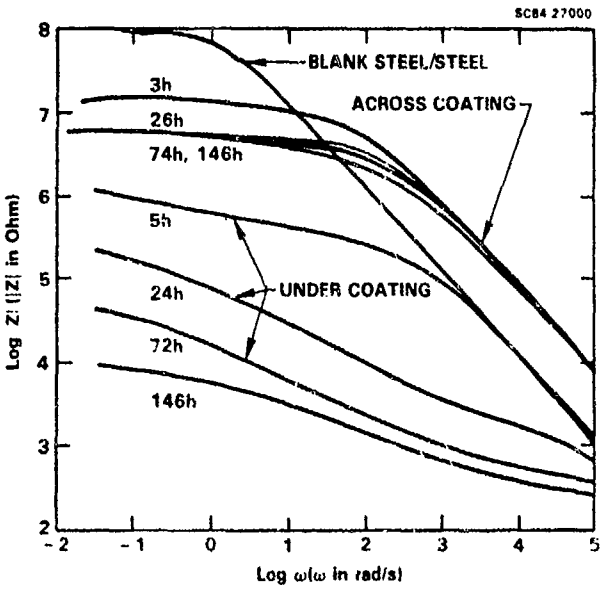

Fig. 29 As Fig. 28, but with NaCl pretreatment of the steel surface.

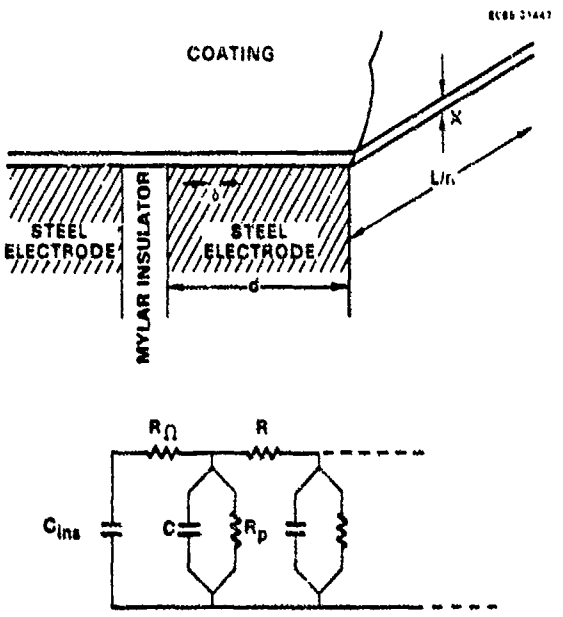

Fig. 30 Model for impedance at the coating/metal interface.

$$|Z| = R_\Omega + \frac{R}{2} + \sqrt{\frac{R^2}{4} + \frac{RR_p}{1 + j\omega R_p C}} \quad . \tag{6}$$

The polarization resistance R_p^o of the delaminated area is given by

$$R_p^o = \frac{R_p C}{C_d^o} \quad , \tag{7}$$

and the effective volume of delamination V_{eff} by

$$V_{eff} = \frac{C\rho d}{RC_d^o L} = x\, f^2\, dL \quad , \tag{8}$$

where C_d^o is the specific capacitance (F/cm^2) for the interface. Equation (8) defines R which is essentially a resistance related to the ionic resistance within the disbonded region. For the calculation of R_p^o and V_{eff}, the assumption is made that ρ equals the bulk resistance of the electrolyte (20 Ω•cm) and C_d^o = 30 $\mu F/cm^2$. In Eq. (8), x is the thickness of the delaminated area, and f is the fraction of the steel plate of length L = 20•6.5 cm which is delaminated. The values of R_p^o and V_{eff} in Table 3 are strongly affected by the surface pretreatment, with a lower R_p^o and a higher V_{eff} for the surface which had been exposed to NaCl before coating. The R_p^o values are much higher than those determined for corrosion of steel in bulk electrolytes ($< 10^3$ Ω•cm^2). This suggests that the corrosivity of the electrolyte at the coating/metal interface is lower. The effective delaminated volume V_{eff} is very small perhaps because in these experiments much of the corrosion activity was located along the steel plates, but did not overlap two adjacent plates and contribute to the measured impedance. Figure 31 shows the appearance of the coated steel ACM after t_{corr} = 14 d for the untreated surface and for t_{corr} = 7 d for NaCl pretreatment. For the former case, only a few areas exist where the corrosion spots cover adjacent plates. In the latter case, many more such areas have developed despite the shorter t_{corr}. The explanation may be that the assumed values for C_d^o and ρ might not be entirely correct and might contribute to some error in the calculated values of R_p^o and V_{eff}.

Table 3

Corrosion Resistance R_p^o and Effective Delaminated Volume V_{eff} for Coated Steel ACMs Exposed to 0.5 N NaCl

Time (h)	R_p^o ($\Omega \cdot cm^2$)	V_{eff} (cm^3)
	I, Clean Surface	
24	2.7×10^5	9.0×10^{-9}
168	6.9×10^5	9.3×10^{-8}
336	1.1×10^5	3.1×10^{-6}
	II, NaCl Treated Surface	
5	1.4×10^5	4.2×10^{-9}
24	1.7×10^5	6.9×10^{-9}
72	1.4×10^5	1.5×10^{-6}
146	1.5×10^4	3.8×10^{-6}

Investigations of the reactions at the metal/coating interface have also been carried out with epoxy coated segmented Cu/steel and Zn/steel electrodes in order to obtain information concerning the role of electrode polarization on corrosion and delamination. In addition to the impedance, the galvanic current flowing between the plates has been measured continuously as an additional qualitative indication of the developing corrosion activity. For Cu/steel corrosion and delamination occurred fairly soon as shown in Figs. 32 and 33. Initially the impedance measured between the Cu/steel plates is strictly capacitive, but already after two days deviations occur (Fig. 32b). From measurements across the coating, Fig. 32a, the deterioration of the coating becomes apparent after about one week and the impedance spectrum does not follow any more the simple model in Fig. 2. After two weeks the frequency dependency for measurements under the coating has changed to a -0.5 dependence as also observed for the steel/steel electrode (Figs. 28 and 29). The impedance measured across the coating degraded further and showed a similar

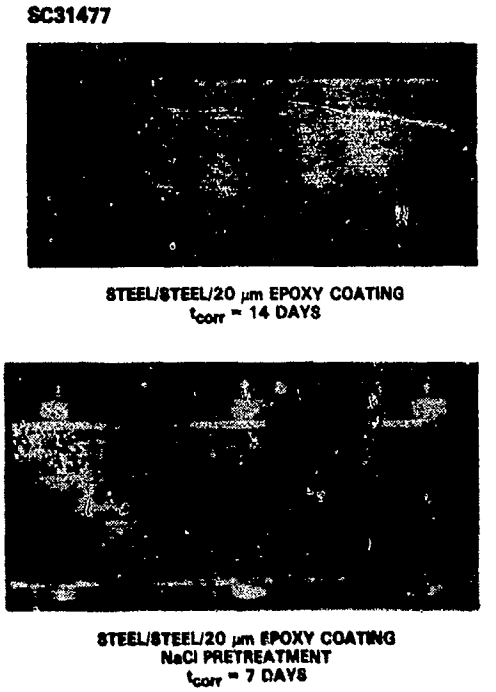

Fig. 31 Photograph of coated steel/steel surface after (a) t_{corr} = 14 days for clean surface and (b) t_{corr} = 7 days for NaCl pretreatment.

frequency dependance at the lowest frequencies as observed for measurements between the plates (Fig. 33a). Figure 34 gives a summary for the measurements with coated Cu/steel electrodes. As the pore resistance R_{po} decreases by a factor of 100 in an exposure period of two weeks, the effective delaminated volume V_{eff} increases by a factor of 1000 and the galvanic current I_g by about the same amount. V_{eff} and I_g show, in fact, a very similar time dependence. The corrosion potential E_{corr} rises initially to values close to that of Cu, but then drops sharply to values characteristic of corroding iron. The corrosion resistance R_p^o first decreases and then increases again.

For Zn/steel the time at which corrosion of the metal was first detected was much longer. Figures 35-37 show selected examples of the impedance spectra measured across the coating and between the plates. While the impedance spectrum determined across the coating changes fairly rapidly to a

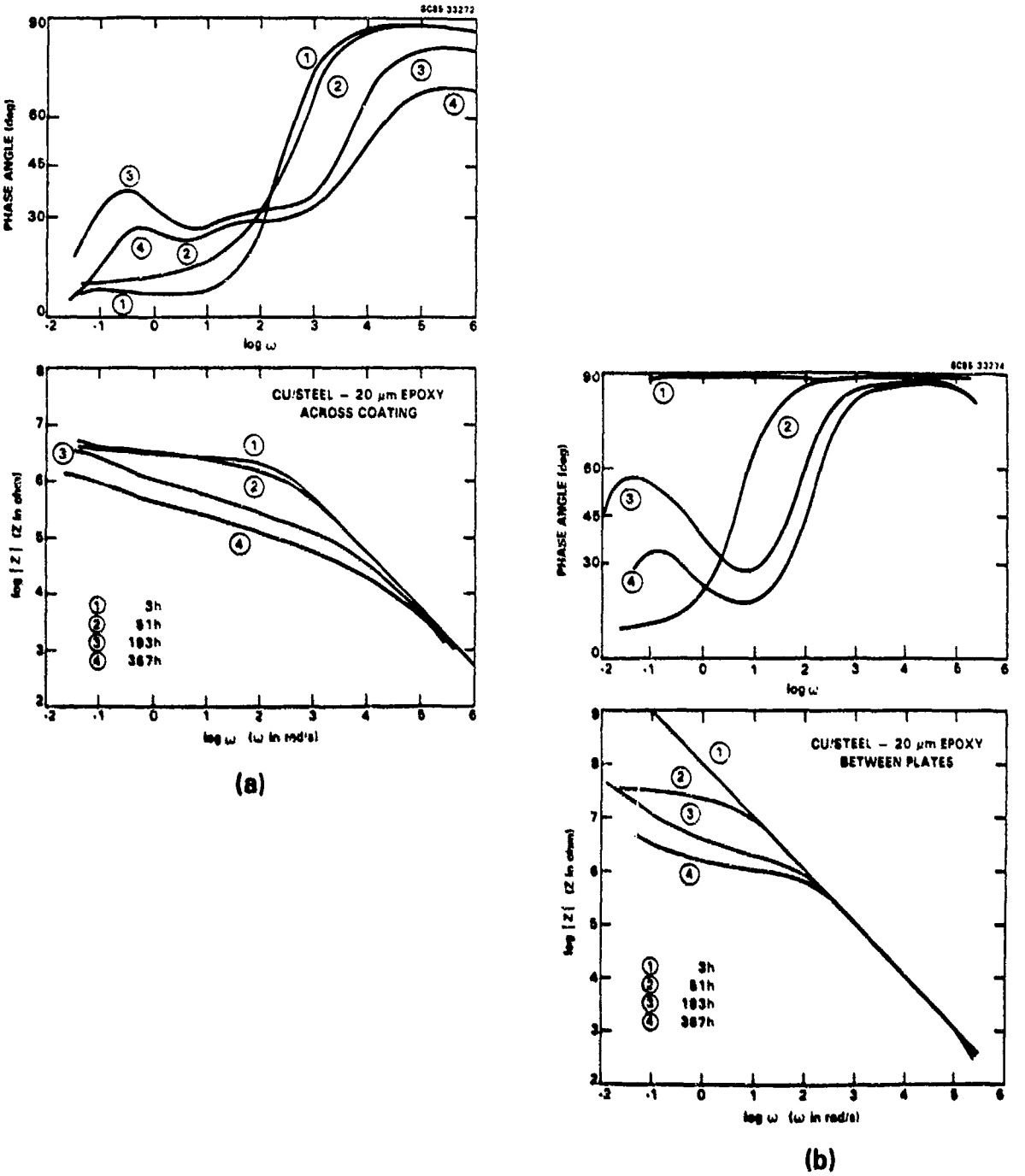

Fig. 32 Bode-plots for coated Cu/steel, spectra measured across coating (Fig. 32(a)) and between plates (Fig. 32(b)).

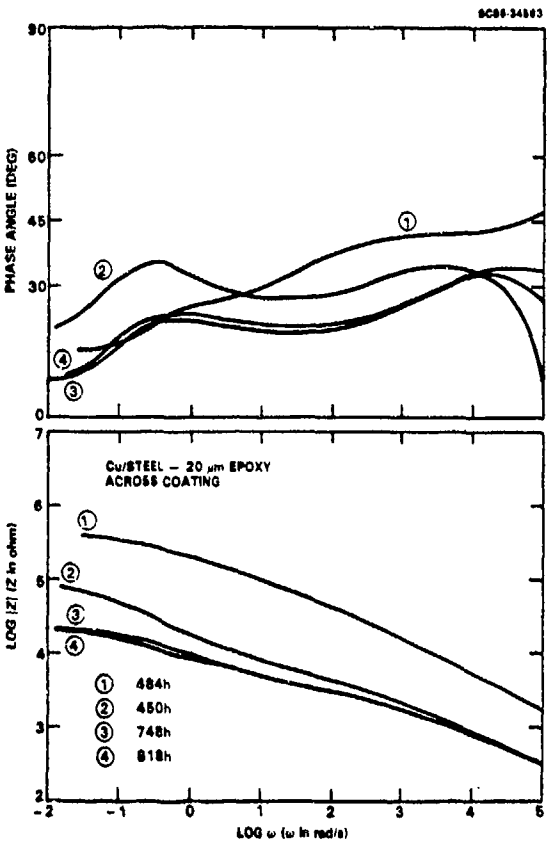

(a)

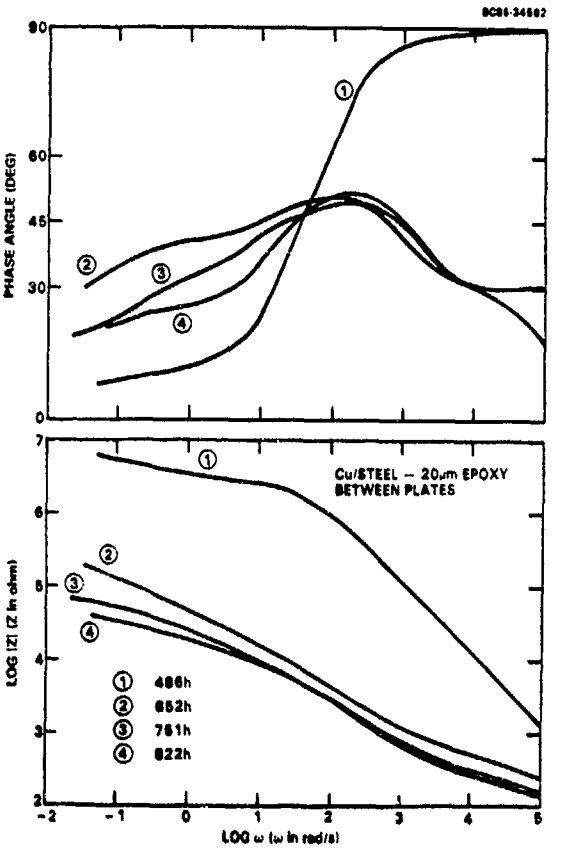

(b)

Fig. 33 As for Fig. 32, but for longer exposure times.

SC86-34581

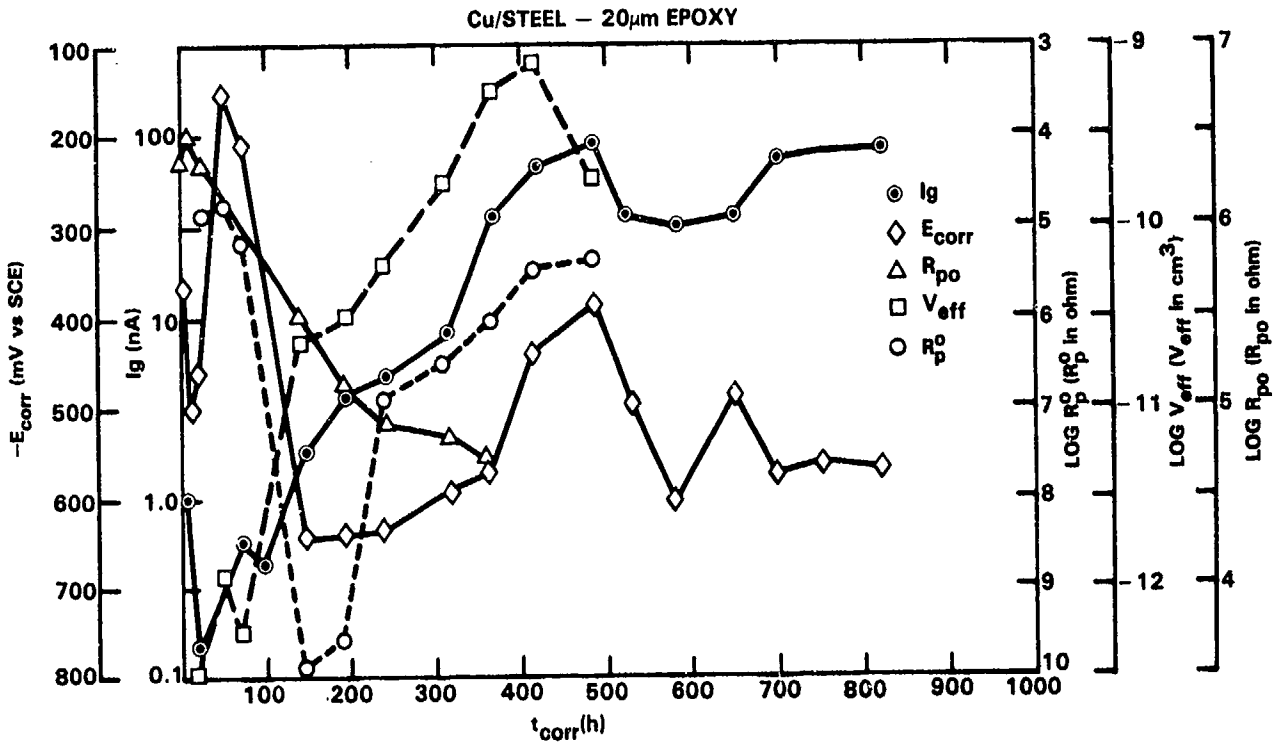

Fig. 34 Time dependence of pore resistance R_{po}, polarization resistance R_p^o, delaminated volume V_{eff}, corrosion potential E_{corr} and galvanic current I_g.

more or less constant value of $2 \cdot 10^5$ Ω at frequencies below 100 Hz, a deviation from strictly capacitive behavior occurs only after about 554 h. This indicates that after this time some delamination has occurred although it is not possible yet to calculate the value of V_{eff}. As can be seen in Fig. 38, V_{eff} and R_p^o could be calculate only for times exceeding 900 h despite the fact that fairly significant changes occurred in the spectra measured between the plates (Fig. 37(b)). After about six weeks two time constant dominate these spectra. The spectra recorded across the coating for steel/Zn are very similar to those obtained in other investigations for coated galvanized steel. E_{corr} dropped to the value measured for zinc after about 100 h.

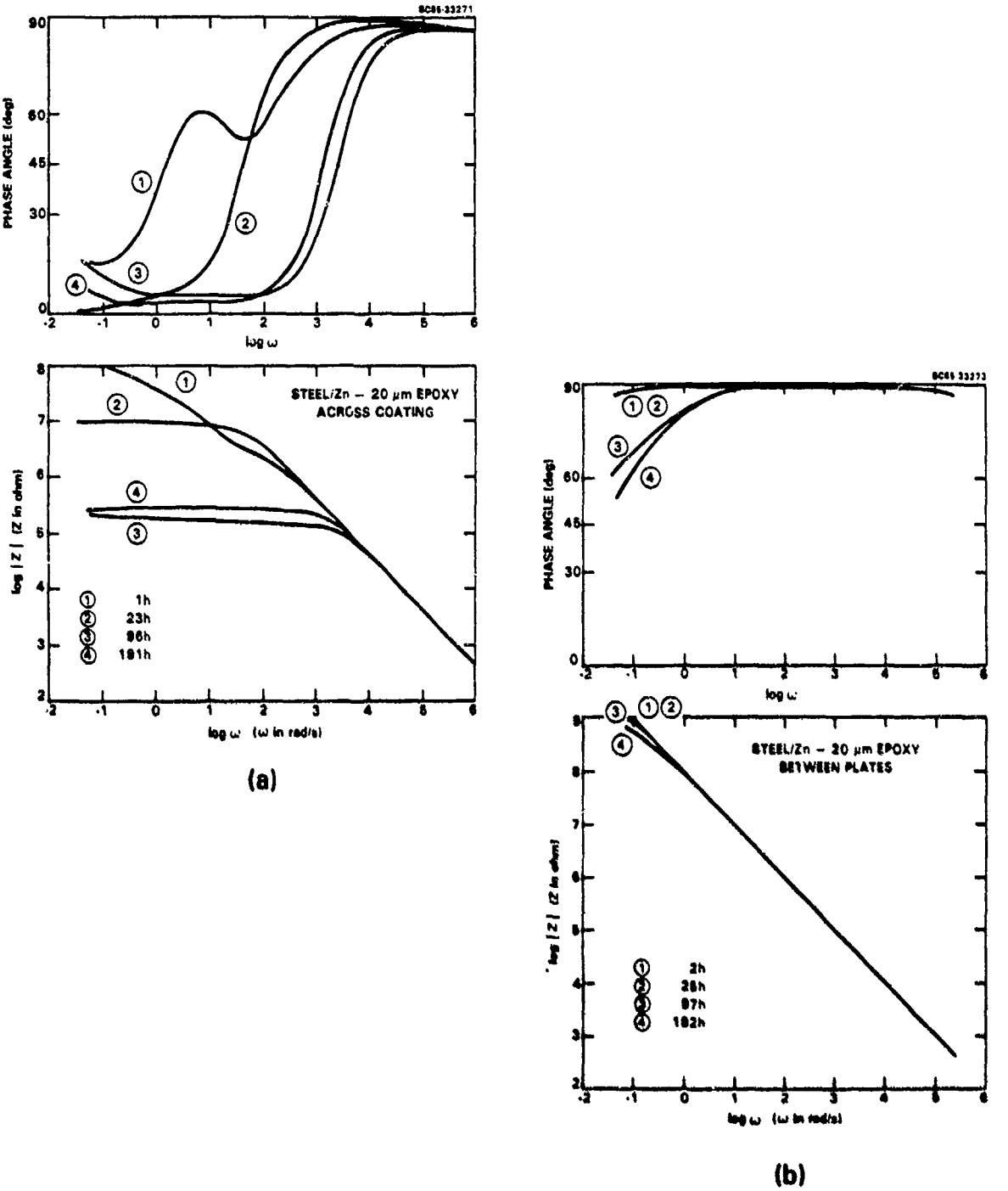

Fig. 35 Bode-plots for coated Zn/steel, spectra measured across coating (Fig. 35(a)) and between plates (Fig. 35(b)).

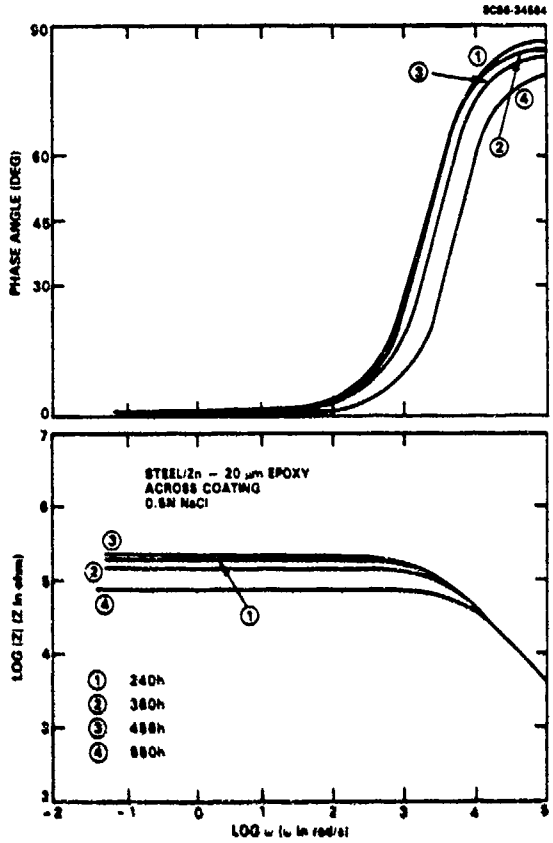

(a)

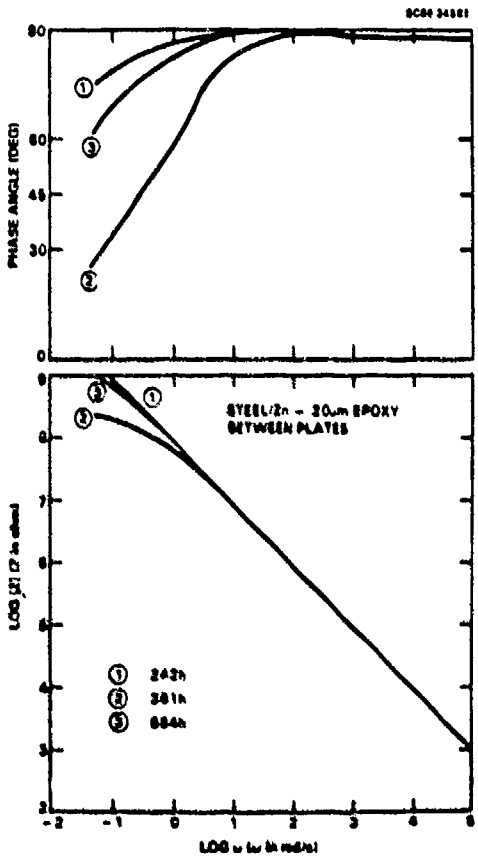

(b)

Fig. 36 As for Fig. 35, but for longer exposure times.

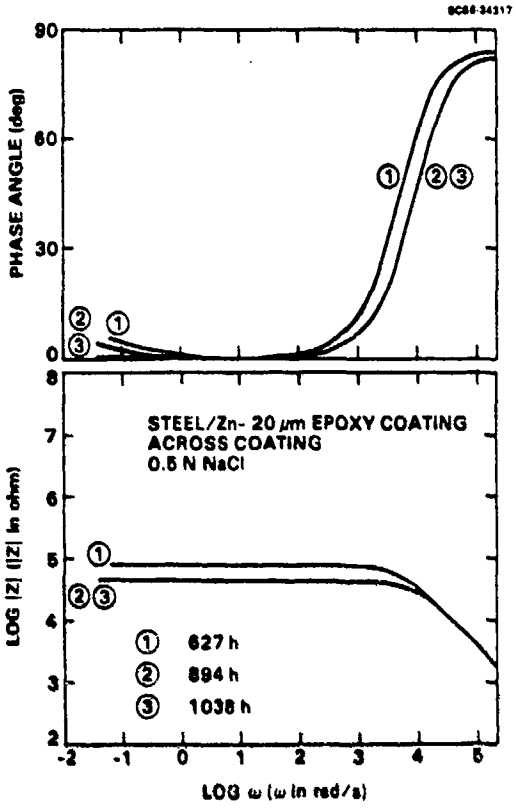

(a)

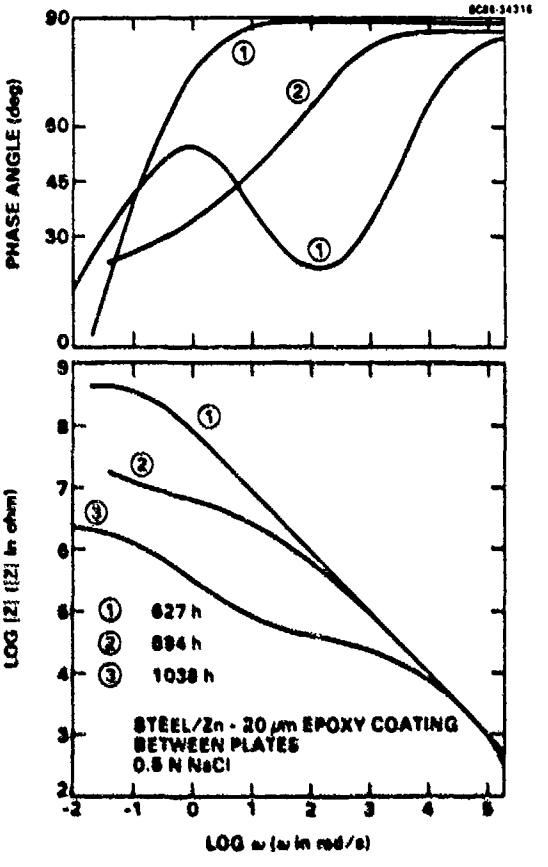

(b)

Fig. 37 As for Fig. 36, but for longer exposure times.

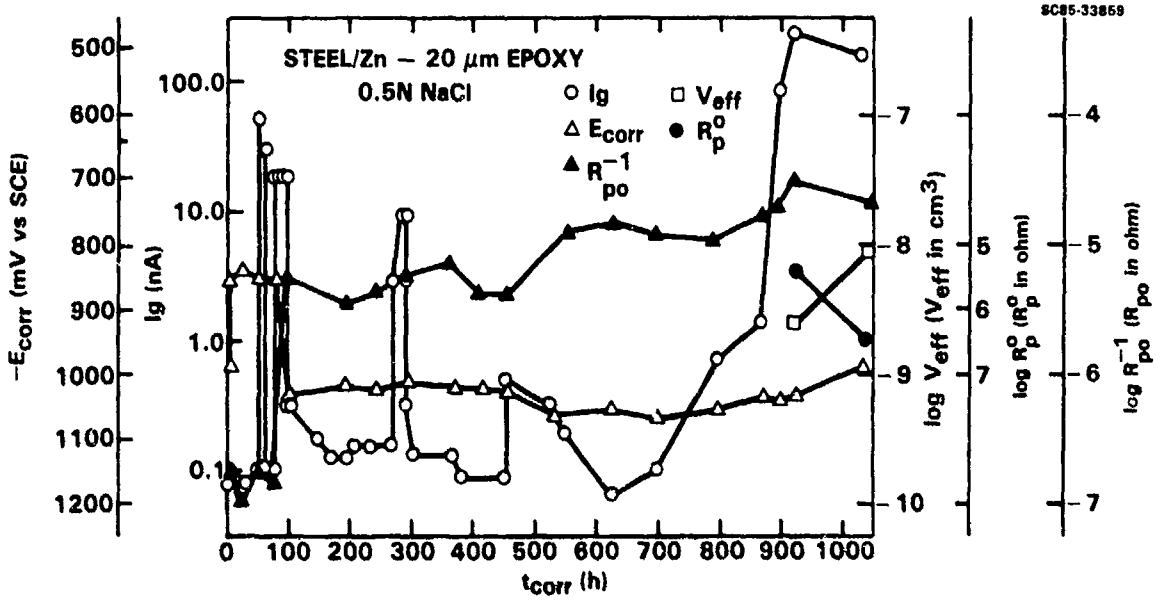

Fig. 38 Time dependence of coating porosity R_{po}^{-1}, polarization resistance R_p^o, delaminated volume V_{eff}, corrosion potential E_{corr} and galvanic current I_g.

Visual observation of the Cu/steel surface throught the clear coating showed rusting along part of the length of three of the steel plates, while the Cu plates remained bright and shiny. The rest of the steel plates also remained unattacked. Apparently the adhesion of the coating stayed good enough in these areas and on the Cu plates to prevent corrosion. For the Zn/steel assembly all steel plates were as bright and shiny at the end of the test as after polishing. Two Zn plates had developed a corrosion layer which covered one half of one plate, but did not spread to the neigbouring steel plates. This suggests that delamination had not occurred to a significant extent. On the other Zn plate corrosion was more localized over a short length of the plate.

Important information can be obtained from the measurement of the galvanic current I_g. After 3 or 4 days sharp spikes of I_g occurred accompanied by a drop of E_{corr} to values characterisitic of Zn. I_g then stayed more or less constant at very low values except for another series of spikes close to

300 h which are probably related to delamination and corrosion occurring for some time. I_g finally increases drastically in the last 300 h of exposure by a factor of 1000. Again this increase of Ig parallels the drastic changes of the impedance during this time period (Fig. 37b). While the coating delaminates and corrosion occurs, more current can flow between the plates.

A comparison of the results for Cu/steel (Fig. 34) and Zn/steel (Fig. 38) shows that the presence of the Zn plates provides cathodic protection. The level of I_g = 100 nA is reached after about 500h for Cu/steel, but only after 900 h for Zn/steel.

3.4.3 Effects of Surface Modification

The corrosion resistance of coated metals can be increased by surface modification. For steel, phospating improves the adhesion of the polymer coating. The phosphated surface itself is not more corrosion resistant than the bare surface as was shown by a few simple immersion tests. For Al alloys surface modification by anodizing or by conversion coating, which also improve the corrosion resistance of the uncoated surface, increases the corrosion resistance of the metal/coating compound.

3.4.3.1 Phosphating of Steel

Zinc phosphate coatings were applied on 1010 steel surfaces which had been cleaned according to the procedures in Table 1. A characteristic difference of the impedance spectra for phosphated and coated steel with different surface pretreatments can be seen at longer exposure times when a Warburg-type impedance occurs with either a slope of -1/2 or -1/4 in the Bode-plot and corresponding maximum of the phase angle of 45° or 22.5°. The former case is illustrated in Fig. 39 for the alkaline derusting treatment, and the latter case, which could correspond to semi-infinite diffusion in pores, can be seen in Fig. 40 for the surface which was degreased only before phosphating. A slope of -1/4 was observed only for this sample and the polished sample. For these two different types of impedance spectra, observation by SEM showed pronounced differences in the crystal size of the phosphate.[3,10]

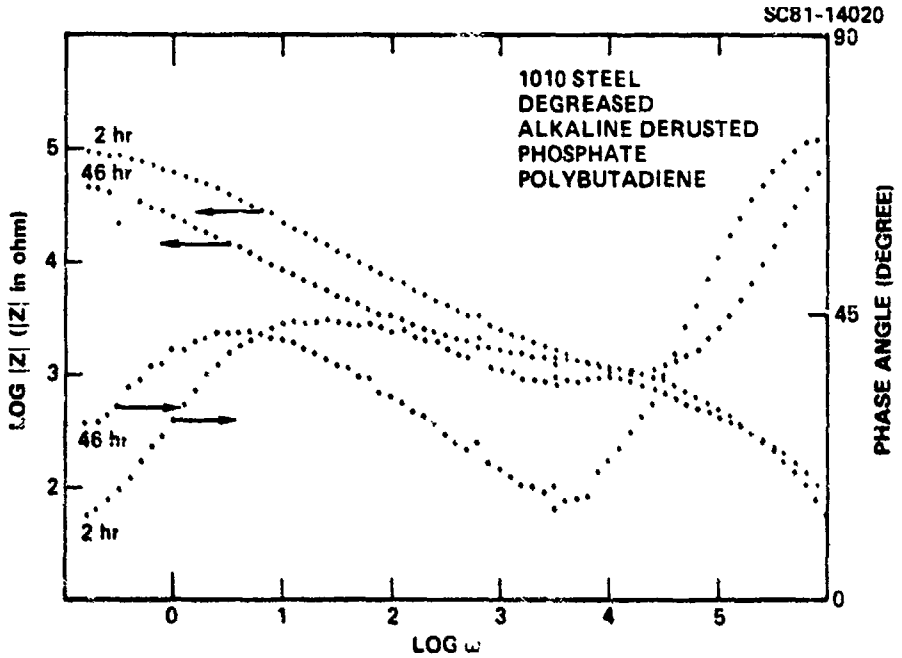

Fig. 39 Bode-plots for phosphated and coated steel (D +AD).

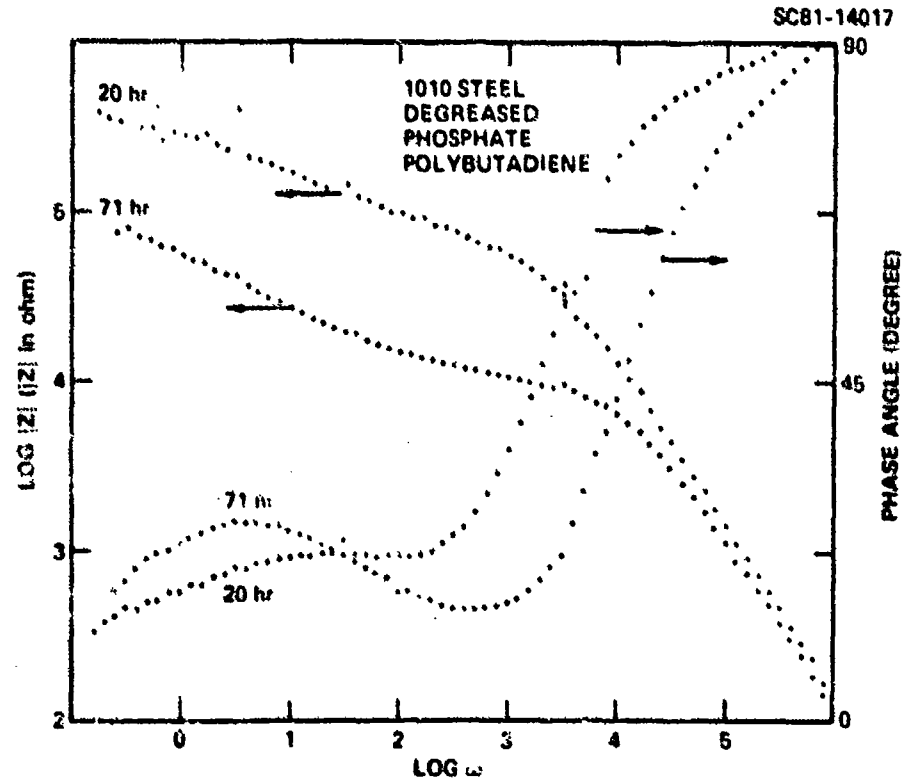

Fig. 40 Bode-plots for phosphated and coated steel (D).

As discussed elsewhere,[5] the results for the phosphated and coated steel can be explained by a generalized Warburg impedance in Model II (Fig. 2) in the form $W = k(j\omega)^{\alpha}$. When W behaves as a true diffusion impedance, $\alpha = 0.5$, and $k = \sigma\sqrt{2}$, where σ is the Warburg coefficient. The general case for $-1 < \alpha < 0$ can result from tangential penetration of electrolyte at the coating/metal interface or from heterogeneous penetration which gives rise to a distribution of time constants. This argument is supported by the observation that a different frequency dependence was found for two different crystal structures as discussed above.

3.4.3.2 Anodizing and Conversion Coating of Aluminum

The importance of a proper surface pretreatment can be illustrated by the case where Al 2024 was pretreated either with a conversion coating (Alodine 1200) or anodized (sulfuric acid with dichromate seal) before application of a 55 μm polyurethane coating which is used in airplane fuel tanks. The impedance spectra obtained during exposure to aerated 0.5 N NaCl for the pretreated and coated Al samples appear in Figs. 41 and 42. The panel with a conversion coating pretreatment develops a considerable amount of porosity of the coating after one week of exposure, resulting in the development of two time constants as can be seen from the appearance of two maxima in the phase angle vs frequency curves of Fig. 41. The pore resistance R_{po} for the H_2SO_4 anodized and coated panel, however, does not become sufficiently low for the observation of the second time constant (Fig. 42). Figures 43 and 44 show the changes of the pore resistance R_{po}, the capacitance C_c and the corrosion potential E_{corr} as a function of exposure time to 0.5 N NaCl. The much faster decay of R_{po} for the conversion-coated sample and the larger increase of C_c for the conversion-coated sample are readily apparent. The corrosion potential is increased markedly by the anodization treatment.

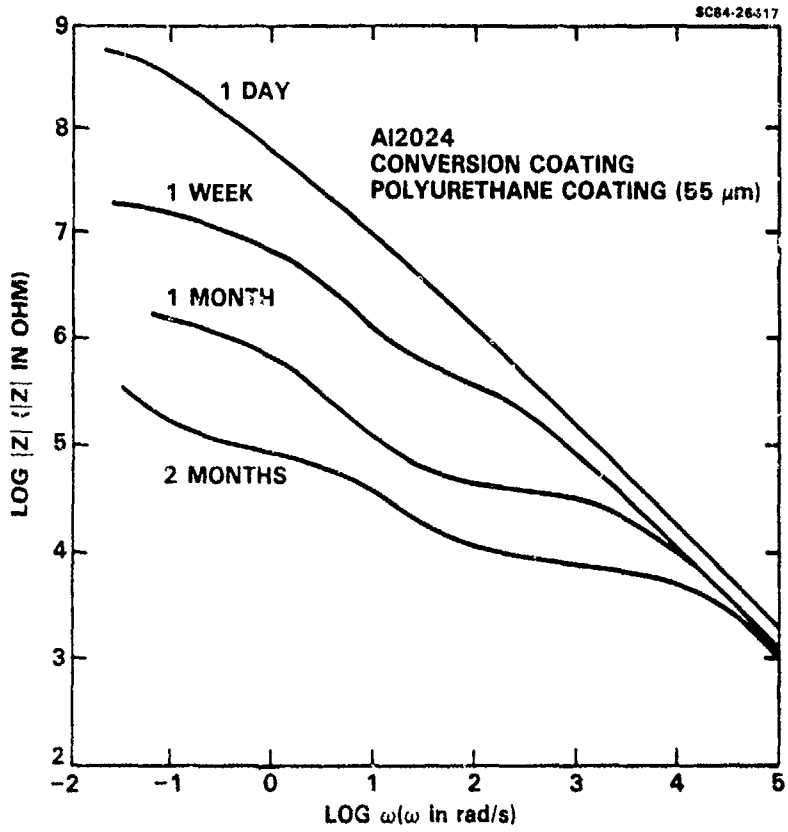

(a)

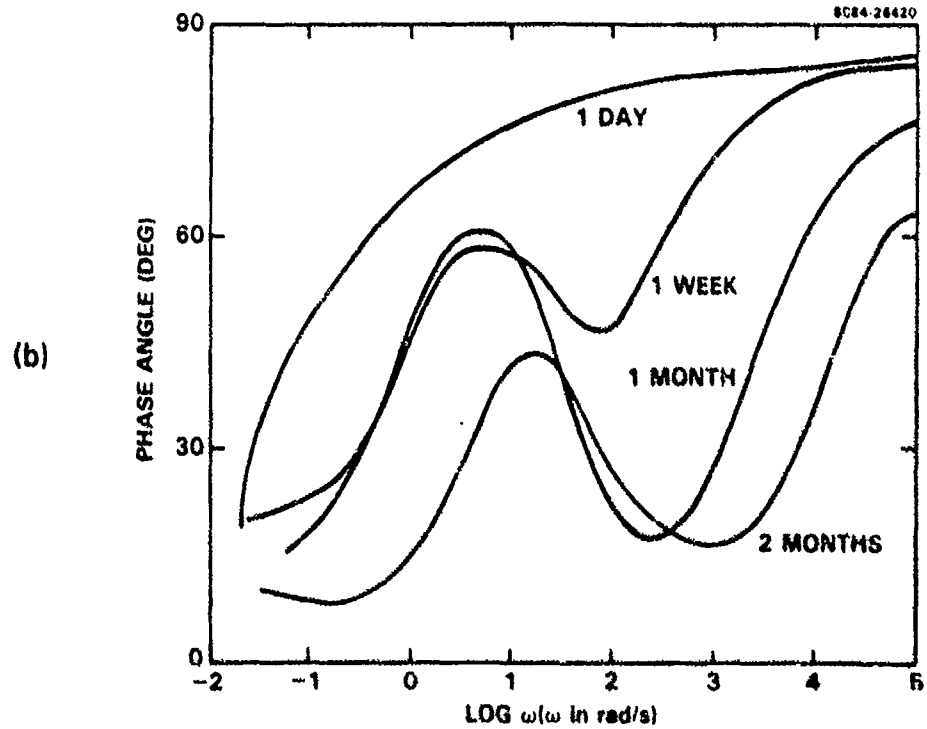

(b)

Fig. 41 Bode plots for Al 2024, conversion coating with polyurethane coating.

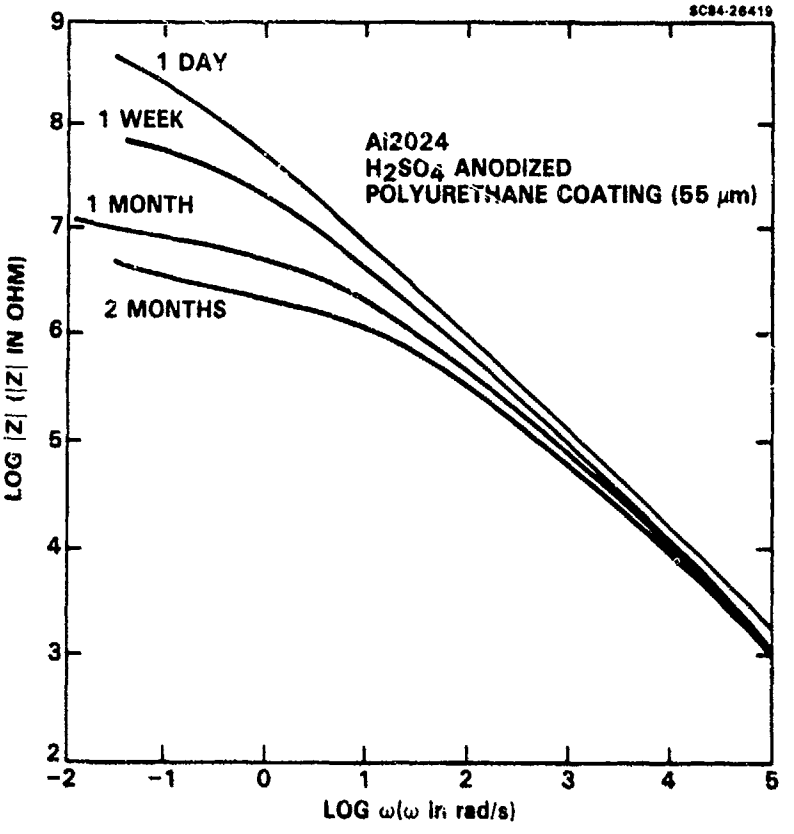

(a)

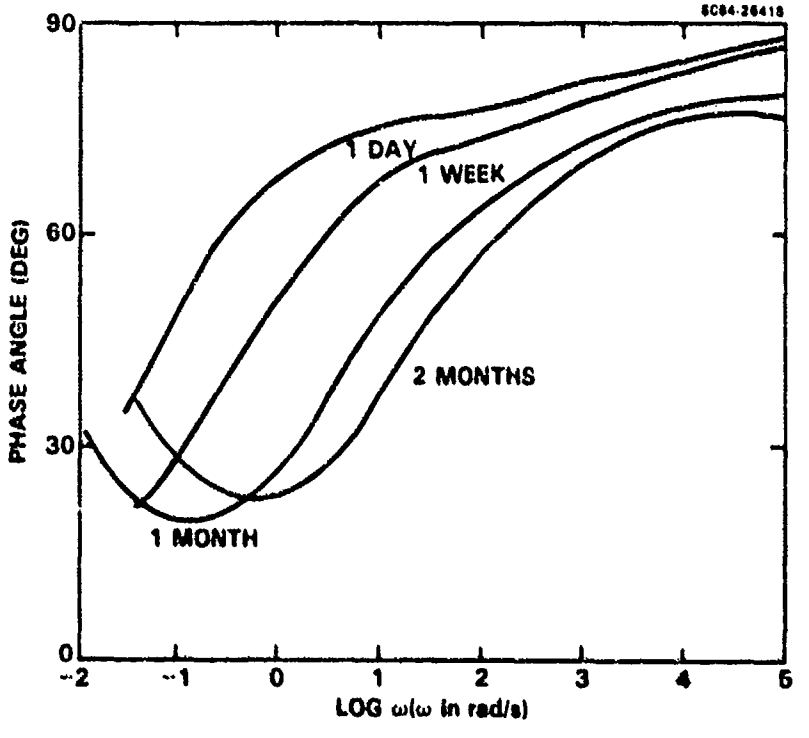

(b)

Fig. 42 Bode-plots for Al 2024, suluric acid anodized with polyurethane coating.

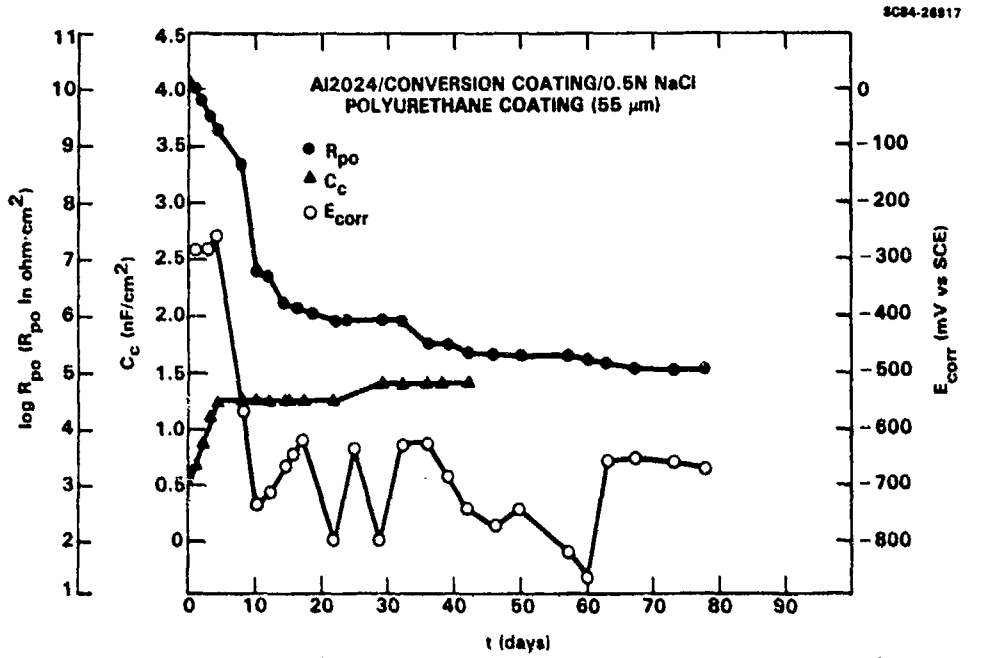

Fig. 43 Time dependence of pore resistance R_{po}, coating capacitance C_c and corrosion potential E_{corr} for coated Al 204 (conversion coating).

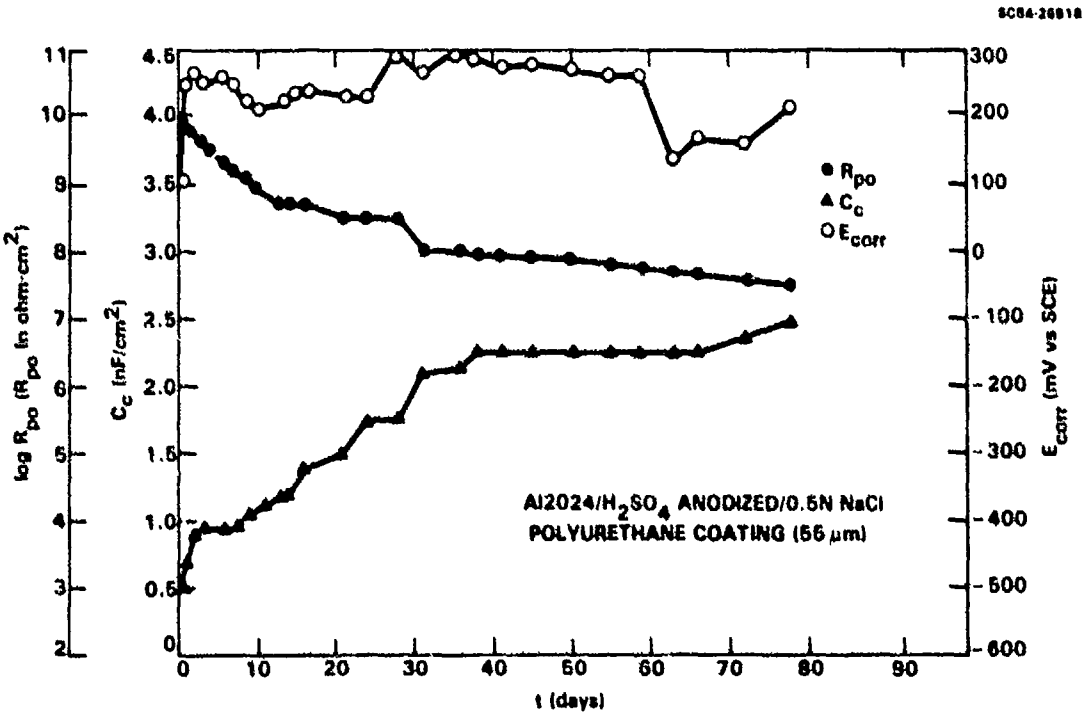

Fig. 44 Time dependence R_{po}, C_c and E_{corr} for coated Al 2024 (sulfuric acid anodized).

Table 4 shows that after exposure for one day, R_{po} is nearly equal for both pretreatments, exceeding 10^{10} $\Omega \cdot cm^2$. These high, nearly identical values for R_{po} indicate that no differences exist between the specimens with regard to the presence of initial defects. The specimen pretreated by conversion coating clearly shows the greatest rate of degradation, as evidenced by the greater drop in R_{po} and R_p throughout the two-month test (Table 4). After two months of exposure, the porosity of the conversion coated specimen, as measured by $1/R_{po}$, is nearly 500 times greater than that for the H_2SO_4 anodized specimen, and the corrosion rate for the conversion coated Al 2024, as estimated from $1/R_p$ is more than 35 times that for the anodized Al 2024.

Table 4

Pore Resistance and Polarization Resistance (in $\Omega \cdot cm^2$) for Polyurethane-Coated Al 2024 with Conversion Coating or Sulfuric Acid Anodizing Pretreatment

	Pore Resistance R_{po}		Polarization Resistance R_p	
Time	Conversion Coated	H_2SO_4 Anodized	Conversion Coated	H_2SO_4 Anodized
1 Day	1.4×10^{10}	1.2×10^{10}	$> 10^{11}$	$> 10^{11}$
1 Week	1.2×10^{7}	2.2×10^{9}	3.0×10^{8}	$> 10^{10}$
1 Month	8.4×10^{5}	1.9×10^{8}	3.2×10^{7}	$> 10^{9}$
1 Month	1.2×10^{5}	5.2×10^{7}	1.6×10^{7}	$> 6 \times 10^{7}$

Additional information can be obtained since C_c is proportional to the dielectric constant, ε, of the coating (Eq. (1)). The capacitance used in Eq. (1) must be that of the polymer dielectric and must not include faradaic or double layer components. This may be assured by using sufficiently thick coatings or by evaluating C_c only from the region in the impedance spectrum where $Z \propto \omega^{-1}$. Since ε is very sensitive to the uptake of water, a number of studies have used capacitance measurements to estimate the water uptake by polymer coatings. Using the equation of Brasher and Kingsbury[14]

$$C_p(t)/C_p(0) = 80^x \qquad (6)$$

where x = volume fraction of water, Leidheiser and Kendig[13] showed that for sufficiently thick coatings, such that the measured capacitance at 1000 Hz could be assured as being that of the coating dielectric, the calculated water content compared well with that observed from gravimetric data. By measuring the impedance for a coated metal over a sufficiently wide range, the ω^{-1}-region, where the impedance is strictly capacitive, can be determined, and therefore the polymer capacitance can be extracted with great confidence. Sufficiently well resolved ω^{-1}-regions for the spectra in Figs. 41 and 42 appear above 10^4 rad/s (1.6 kHz). C_c was readily evaluated using a least squares fit of the spectra from which the effective dielectric constants were obtained (d = 55 μm, Area = 20 cm^2). The volume fractions of water taken up by the coatings between one day and one week are shown in Table 5 as calculated from Eq. (6). Equation (6) assumes a uniform distribution of water and is valid only for low volume fractions. Nevertheless, clearly the polymer film over the conversion coated surface shows a greater water uptake after one week despite its initially lower capacitance.

Table 5

Effective Dielectric Constant and Water Uptake of the Coating

Pretreatment	Dielectric Constant 1 Day	1 Week	v/o Water Increase in 1 Week
Conversion Coating	8.7	19.3	18
Anodized H_2SO_4	10.3	16.5	11

3.4.4 The Role of Pigments

Polymer coatings often contain corrosion inhibiting pigments for lowering the corrosion rate of the substrate. Pigments used for this purpose can inhibit corrosion by a variety of mechanisms. Phosphates act as buffering

agents to limit the localized build-up of hydrogen ions formed by the localized concentration and hydrolysis of anodic corrosion products. Chromates are presumed to inhibit through the formation of a passive film on the surface of the substrate where local defects in the coating occur. Zn dust may act by galvanic protection or by enhancing the barrier properties of the coating due to the growth of a voluminous ZnO which seals defects in the film. The necessity of transporting the corrosion inhibiting pigment to the interface has been discussed frequently.

In order to evaluate the role of different types of corrosion inhibiting pigments and their transport to the metal surface, experiments using the two types of specimens shown in Fig. 45 were performed. For the specimen in Fig 45a, two ~ 13 μm layers of epoxy coating containing 50 v/o of pigment are spin coated onto a polished and degreased steel substrate and cured. For the specimen schematically shown in Fig. 45b, a 13 μm layer of epoxy is first deposited and partially cured followed by a 13 μm layer of pigment containing coating. For each pigment in Table 6 one of each of the specimens in Fig. 45 were formed and then exposed to air saturated 0.5 M NaCl. At intervals during the exposure the electrochemical impedance spectrum of the exposed surface was collected. An evaluation of the extent of corrosion and delamination was also made following the criteria of ASTM D610. The rating is based on a 10 point scale from 1 (50% coverage by corrosion or delamination) to 10 (no corrosion or delamination).

Table 4 and Figs. 46a-i summarize the results for these experiments. The duplex, unpigmented, 22 μm thick epoxy coating (EX/EX) (Fig. 46a) shows good protective properties and the corrosion rating, corr, does not drop below a value of 4 (10% coverage by corrosion product) before 2000 h. The generalized pore resistance, R_{po} ,that describes paths of low resistance that short the coating reaches a steady-state plateau value, R_{pt}, which is slightly below 1 megohm ($2 \cdot 10^7$ $\Omega\,cm^2$) (Fig. 46a and Table 7).

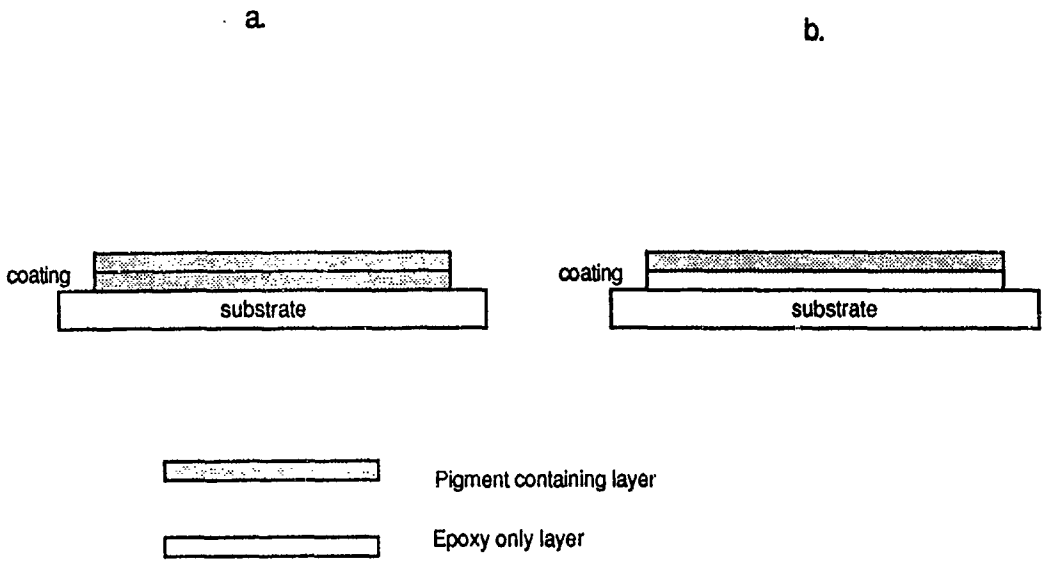

Fig. 45 Schematic for the two types of pigment-containing coated specimens: (a) two layers of pigment containing polymer (duplex coating), (b) two-layer coating with the layer nearest to the substrate not containing pigment.

Table 6

Pigment Data

Material	Density gm/cm^3	Specific Resistance Ω/cm	Dispersion Hegman	Dispersion Microns	Source
Sr Chromate (SrChro)	3.8	750-1000	5-6	38-25	Davis
Zn Phosphate (ZnPhos)	3.2	25000	7-8	6	Davis
Zn Ba Phosphate (ZnBaP)	3.6	N/A	7-8	6-8	Davis
Zn Dust	7.0	0.0000059	7-8	5	St. Joe

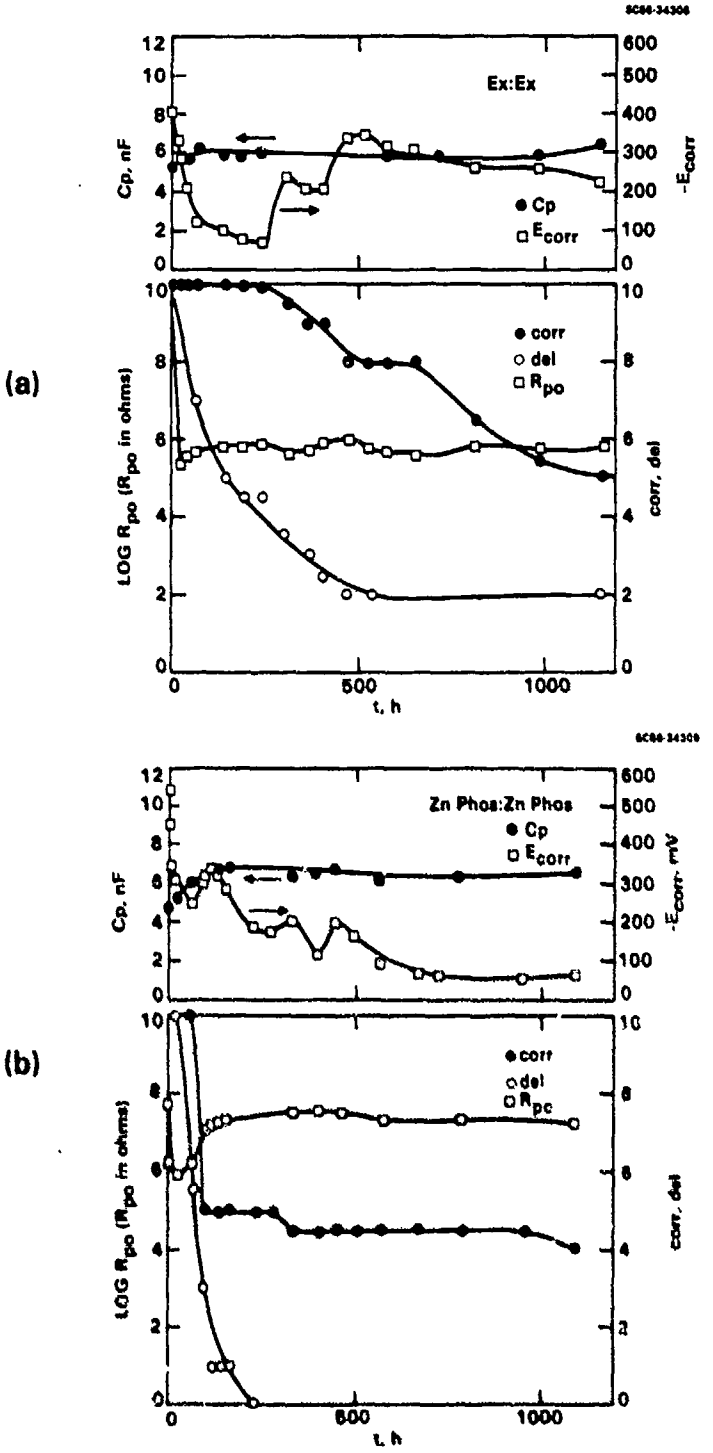

Fig. 46 R_{po}, C, corr, del and E_{corr} for steel with epoxy coatings containing: (a) layer 1-epoxy only (EX); layer 2-epoxy only (EX); (b) ZnPhos/ZnPhos; (c) EX/ZnPhos; (d) ZnBaP/ZnBaP; (e) EX/ZnBaP; (f) SrChro/SrChro; (g) EX/SrChro; (h) EX/Zn and (i) ZnZn.

(c)

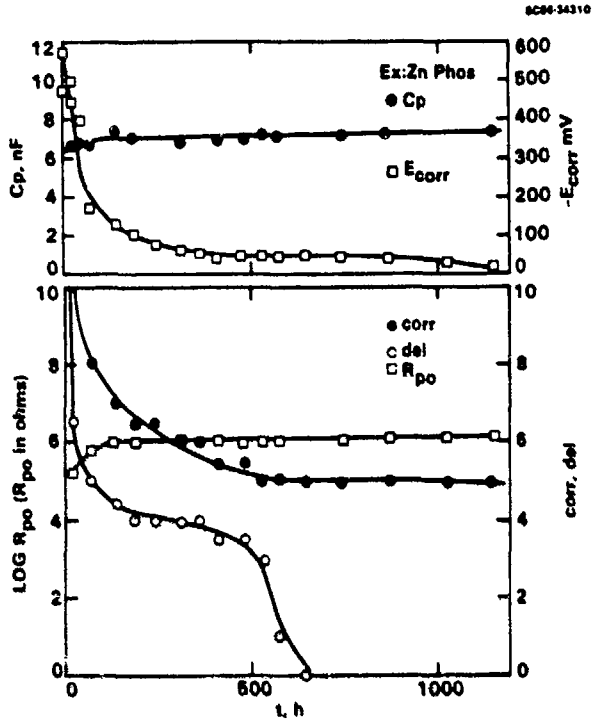

(d)

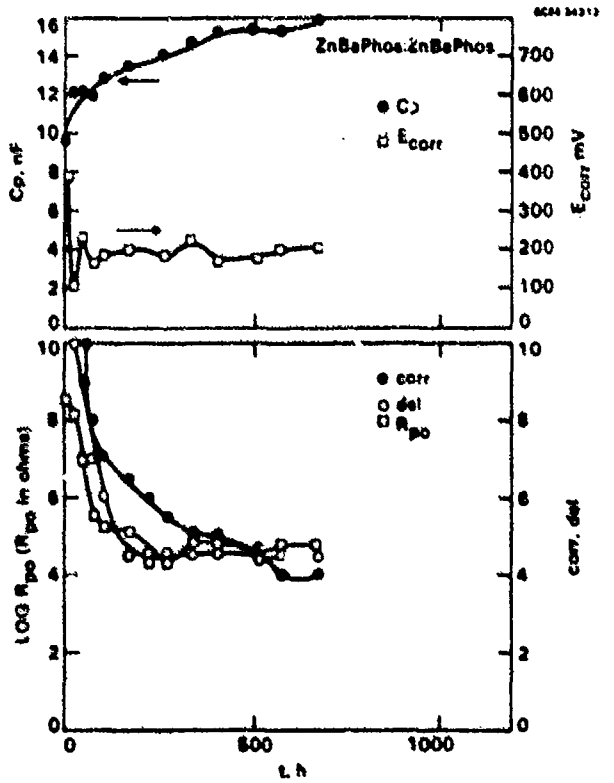

Fig. 46 (continued)

(e)

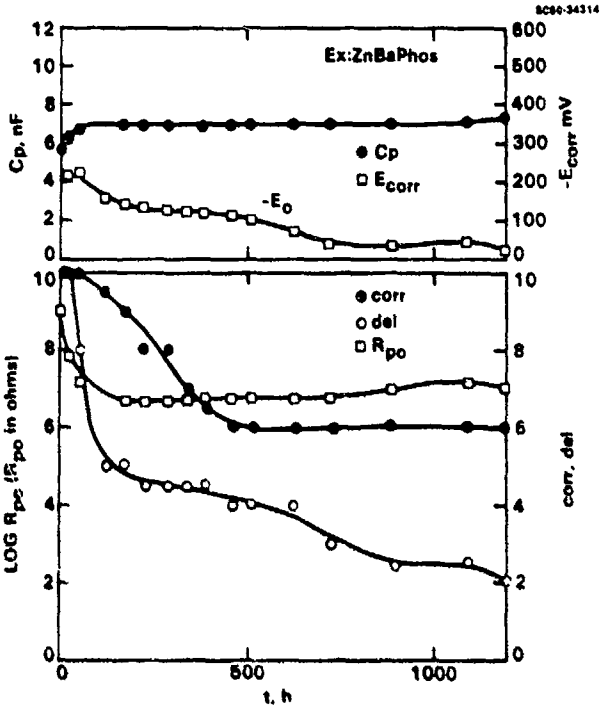

(f)

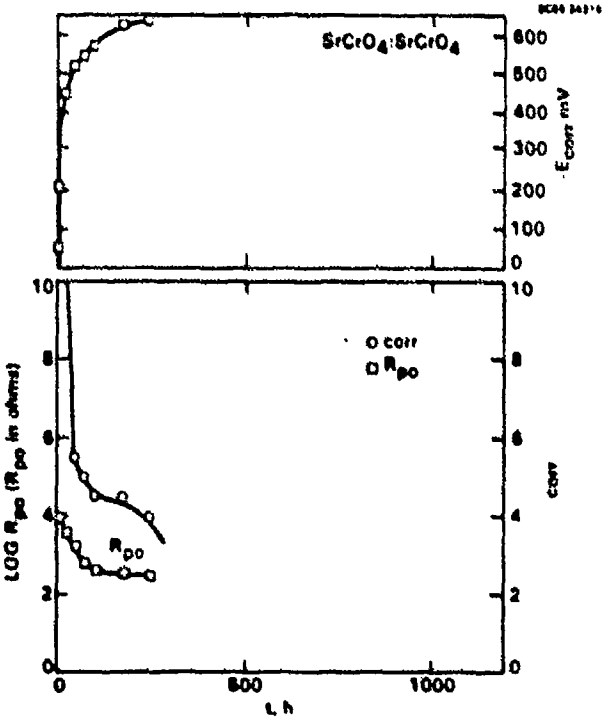

Fig. 46 (continued)

(g)

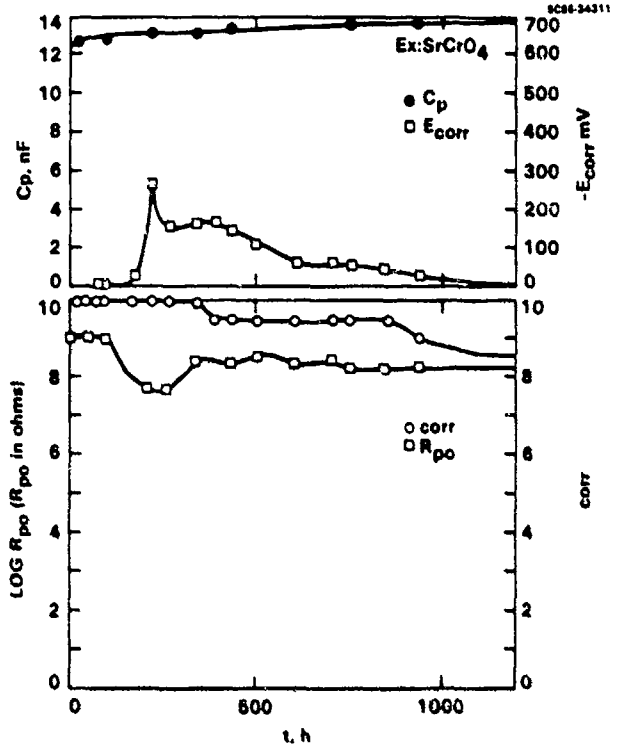

(h)

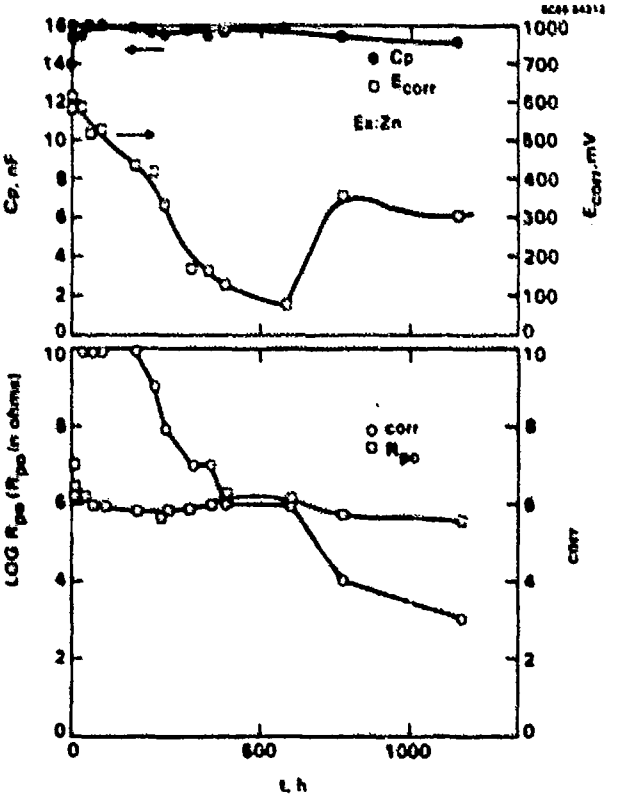

Fig. 46 (continued)

(i)

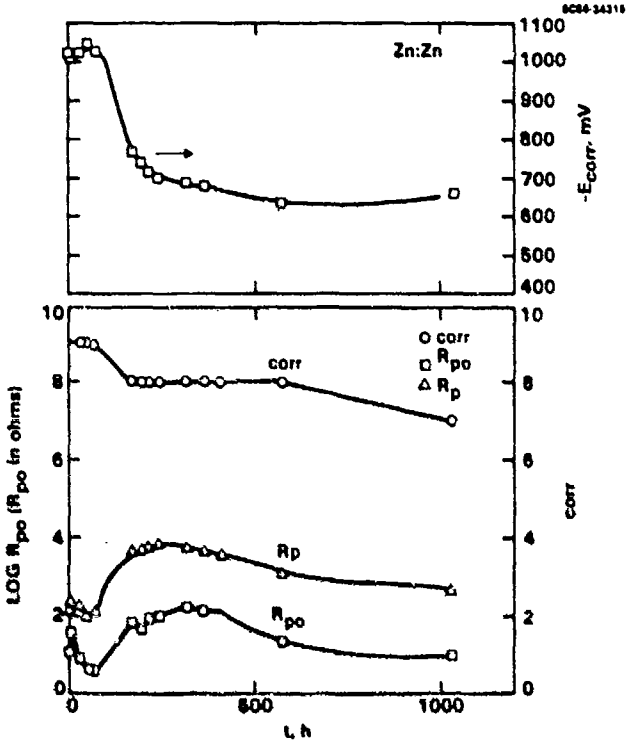

Fig. 46 (continued).

Table 7

Summary of Pigment Data - Coating Properties, Corrosion Behavior and Pore Resistance

Coat 1	Coat 2	d (μm)	pH	Log R_{pt}	E_{corr} trend	E_k (mV vs SCE)	τ^{corr} (h)	τ^{del} (h)	$Corr_k$	C_s/C_o
EX	EX	22	n.	5.8	v.	-260	>2000	250	5.5	1.17
EX	ZnPhos	30	4	6.1	i.	-35	1500	300	5.0	1.14
ZnPhos	ZnPhos	33	4	7.4	i.	-50	1100	80	4.4	1.33
EX	ZnBaP	27	4	6.8	i.	-40	>2000	550	6.0	1.17
ZnBaP	ZnBaP	20	4	4.7	c.	-200	570	>580	<4.0	1.55
EX	SrChro	24	7	8.2	v./i.	-25	>1370	n.d	8.9	1.10
SrChro	SrChro	27	7	2.5	d.	n.	240	n.d.	<4.0	n.d.
EX	Zn	30		6.0	i./v.	-300	720	n.d.	3.2	1.14
Zn	Zn	30		1.0	i.	-650	>1400	n.d.	7.0	n.d.

d: coating thickness
i.: generally increasing
c.: constant
v.: varies
n.d.: not determined or not applicable
Zn: Zn dust
EX: epoxy
ZnPhos: Zn Phosphate
ZnBaP: Zn Barium phosphate
SrChro: Strontium Chromate
R_{pt}: plateau value of the pore resistance (in Ω for A = 20 cm^2)

E_k: E_{corr} at 1000 h
τ^{corr}: time to corr = 4 (10%)
τ^{del}: time to del = 4
$Corr_k$: corr value at 1000 h
E_{corr}: corrosion potential

For the case of the duplex Zn phosphate containing coating (ZnPhos/ZnPhos), the pigment causes poor adhesion when in contact with the surface as can be seen by the rapid drop in the delamination rating, del, (Fig 46b), but interacts with corrosion products to form a good barrier film as shown by the relatively high values of R_{pt}. Better adhesion is produced when an epoxy

layer (EX/ZnPhos) separates the pigment portion from the interface as can be seen by a slower drop in del (Fig. 46(c)). Both ZnPhos/Zn/Phos and the EX/ZnPhos coating show relatively high values of R_{pt} due to the barrier enhancement produced by the ZnPhos (see Table 7 and Figs. 46(b-c)).

A duplex zinc barium phosphate coating (ZnBaP/ZnBaP) shows poor adhesion and poor corrosion resistance as can be seen by the rapid decrease in corr, del and R_{po} (Fig. 46d). However, the EX/ZnBaP system provides good protection as a result of the combined good adhesion afforded by the epoxy and good barrier property afforded by the pigment. In fact, the pore resistance of the EX/ZnBaP increases with time probably due to interaction with corrosion products (Fig. 46e).

The slightly soluble SrChro pigment produces a very poor coating when dispersed throughout the two layers. R_{po} drops below 1000 Ω and corr decreases to values below 4 in less than 300 h of exposure (Fig. 46f). When the soluble chromate is dispersed throughout the coating, the resulting poor barrier properties due to pigment solubility and poor adhesion allow a corrosion rate which is too large to be countered by the slightly soluble chromate. As a result the chromate accelerates corrosion. When a good barrier and adhesion layer is provided by a first layer of pigment-free epoxy followed by a second layer containing the inhibiting chromate pigment, the most corrosion resistant system of this series results (Fig. 46g). The pore resistance for this coating (EX/SrChro) remains above 10^8 Ω for more than 1000 h of exposure to 0.5 M NaCl (Fig.46g). This system combines the good adherence afforded by the epoxy and sufficient chromate activity to entirely eliminate corrosion at any initially present defects.

The results for the Zn pigmented coatings demonstrate the necessity for the Zn to form continuous paths to the substrate. For the EX/Zn system where no initial contact of the Zn with the substrate is made, the pore resistance, R_{po}, remains near 1 Mohm throughout the 1000 h test and the corrosion potential rises to values as high as -100 mV (Fig. 46h). However, when the Zn contacts the substrate as in the case of the Zn/Zn specimen

(Fig 46i), the effective "pore" resistance remains below 100 Ω throughout the test. For this case (Fig. 46i), R_{po} is most likely due to the electronic conductivity of the coating provided by the metallic Zn rather than due to the presence of ionically conducting pores. Further evidence of the steel/Zn contact in the case of the Zn/Zn coating appears in the corrosion potential which remains below -600 mV. The conductivity of the Zn particulates expressed as $1/R_{po}$ correlates inversely with the polarization resistance of the particulates (see Fig. 46i). As observed by Szauer and Brandt,[22] the increase in R_{po} after 100 h coincides with an increase in E_{corr}.

Additional evaluation of the role of Zn concentration was made by forming epoxy coatings containing Zn dust at concentration levels of 10, 20, 30, and 50 wt. % in addition to the 90 wt. %. These specimens were evaluated using electrochemical impedance spectroscopy after 1, 4 and 24 h exposure to 0.5 M NaCl. Figure 47 shows a Bode plot for 24 h exposure. The 10, 20 and 30 wt. % specimens appear as dielectric coatings with a pore resistances greater than 10^5 ohm, while the 90 wt. % containing coating has an entirely different spectrum. The high frequency resistance for the 90 wt. % specimen of nearly 10 Ω represents the resistance of the coating and the low frequency limit relates to the corrosion of the Zn particulates coupled to the steel. The 50 wt. % material represents a transition between these extremes. A plot of log R_{po} vs time after 1, 4 and 24 h of exposure appears in Fig. 48, where a dramatic decrease in R_{po} occurs for concentrations of Zn above 30 wt. %. This is also reflected in the mode of protection of the steel substrate by the Zn as shown in Fig. 49 by the dependence of E_{corr} on the wt. % of Zn. Above 30 wt. % Zn galvanic protection by Zn occurs with a significant lowering of the potential to that of metallic Zn. However, below 50 wt. % Zn, E_{corr} tends toward more positive values which are typical for the other epoxy coatings discussed above.

SC5222.FR

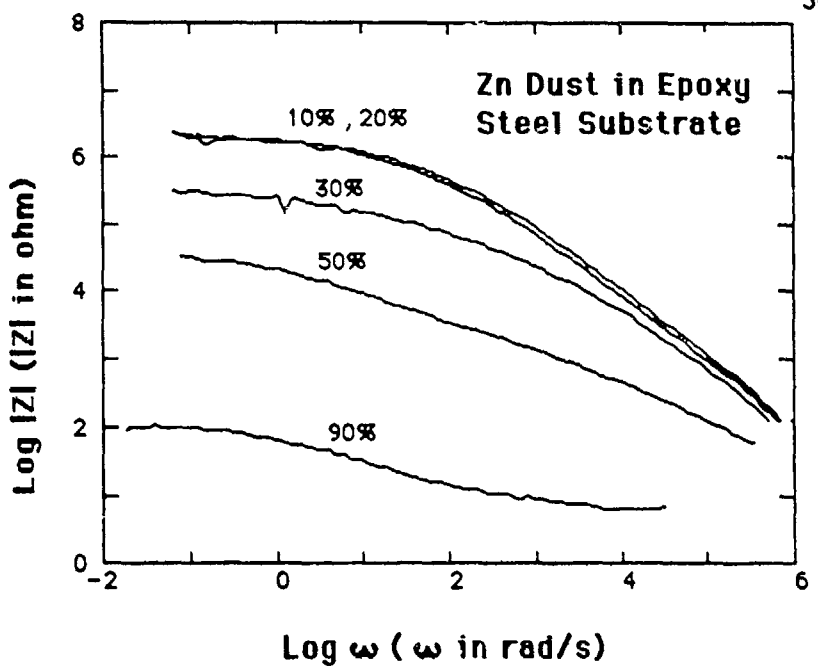

Fig. 47 Bode-plots for epoxy coatings with varous wt. % of Zn dust on P + D treated steel.

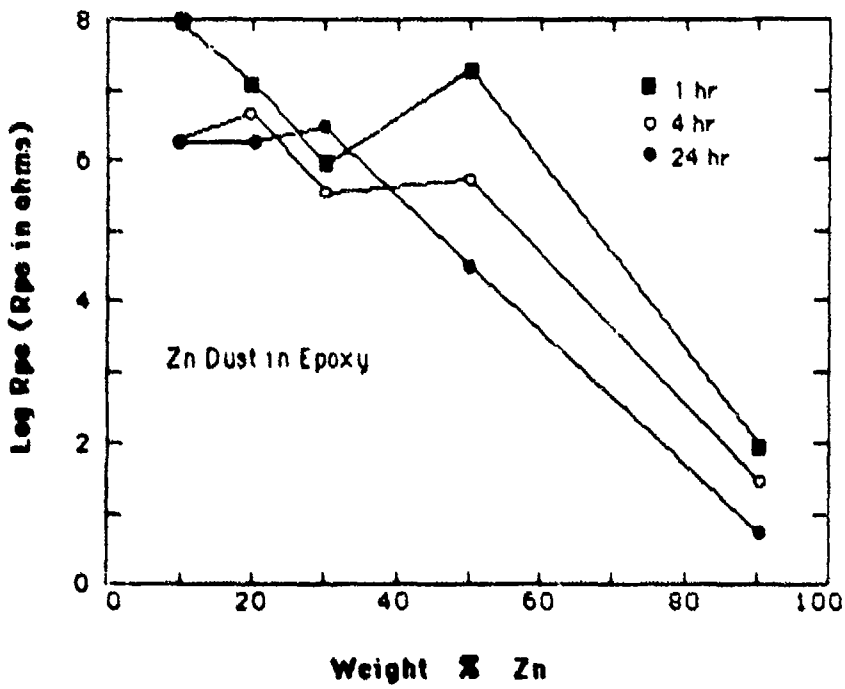

Fig. 48 Dependence of R_{po} on wt. % of Zn in duplex epoxy coatings for steel samples (P + D) after 1, 4 and 24 h exposure to 0.5 M NaCl.

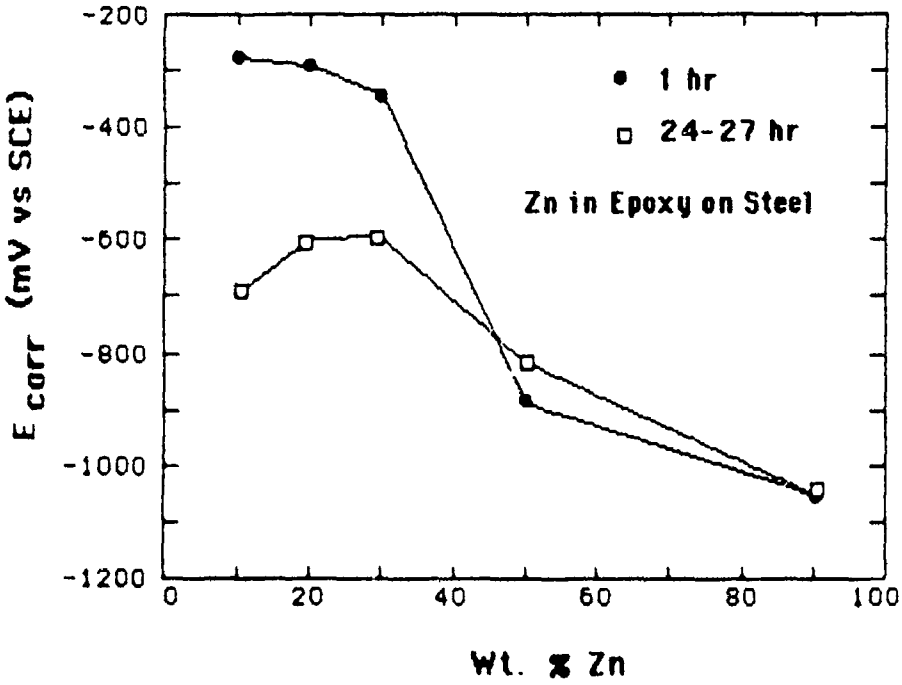

Fig. 49 Dependence of E_{corr} on wt fraction of Zn in the epoxy coating on steel (P + D) after 1 and 24 h exposure to 0.5 M NaCl.

The capacitance for all specimens typically increases rapidly to a plateau value within the first several days (Fig. 46a-i) which suggests that the water uptake of the coating is very rapid and reaches a steady-state value at early times relative to the degradation of the coating. The ratio of the steady-state capacitance, C_s, to the initial capacitance, C_o, provides a measure of the water uptake (Table 7). It is to be noted that the duplex ZnPhos and ZnBaP pigmented coatings show the greatest water uptake as evidenced by the largest values of C_s/C_o. The EX/Zn coating shows a very rapid rise in capacitance. However, for longer times its capacitance steadily decreases (Fig. 46i).

These results demonstrate that pigments may act by different means (passivation of small defects in the case of the soluble chromates, enhanced barrier behavior imparted to the film by the ZnBaP), but will only provide protection as long as a good interfacial bond exists. The Zn containing coatings behave in a special way. The impedance shows that the ohmic resistance between the Zn and the substrate increases with exposure to a corrosive

medium and correlates with galvanic protection as determined from E_{corr} measurements. The results of this work also show that Zn concentration must exceed 50 wt. % for galvanic protection to occur at initial times, but requires a larger concentration of Zn for longer term galvanic protection.

4.0 SUMMARY AND CONCLUSIONS

This work shows that the lifetime of polymer coated steel depends on a number of complex interrelated processes. The relationships between surface preparation, physical and chemical properties of the coating, adhesion and corrosion have been established and are summarized in Fig. 1. Several important conclusions can be drawn from this work.

It has been shown that penetration of the coating by the environment by itself will not cause failure of the coated metal. However, loss of adhesion between the coating and the surface and cohesive failure of the coating brought about by the corrosion reaction provide the major driving forces for the propagation of failure. Clearly, efforts to design coating systems which only minimize the transmission of corrosive electrolyte without attention to the adhesive or cohesive properties will bring no significant benefits with respect to corrosion protection. Surface preparation for optimum adhesion and polymer strength provide perhaps more important factors for the longevity of polymer coated metals exposed to adverse environments. Proper pretreatments for steels as well as aluminum have been shown to have a significant influence on the long term stability of polymer coatings.

The importance of adhesion in determining the corrosion rate has been demonstrated most dramatically by the simultaneous observation of the measured electrochemical impedance under the film and across the film. For coated steel for which corrosion has initiated, ionic and mass transport underneath the film represent the primary path for the charge transfer reaction to occur as shown by the fact that the under-film impedance for this corroding surface is several orders of magnitude less than the across-film impedance. The impedance across the coating reflects the extent of the damage to the coating caused by corrosion, but it does not characterize the ongoing corrosion reaction once corrosion has initiated.

Two nondestructive methods have been shown to be useful for the evaluation and prediction of the corrosion behavior of polymer coated metals.

These methods include the use of a reflected acoustic pulse to detect the early stages of adhesion loss, and the application of electrochemical impedance spectroscopy for the evaluation of the degradation of the polymer coating. While the electrochemical impedance method has great sensitivity for the earliest stages of degradation of the coating by the corrosion process, the reflected acoustic pulse has the ability to locate the regions of disbonding of the polymer from the metallic surface and provides a useful nondestructive tool for evaluating the kinetics of corrosion induced adhesive failure.

5.0 RECOMMENDATIONS FOR FUTURE RESEARCH

1. Additional EIS-data should be collected for coated segmented electrodes to obtain information concerning the reactions at the metal/coating interface combined with measurements across the coating which reveal the changes in the coating during the exposure to corrosive environments. This novel approach to the evaluation of the corrosive degradation of coated metals allows a complete analysis of the changes of the metal/coating compound. In this program, only epoxy coatings have been evaluated during continuous exposure to aqueous NaCl. Other types of coatings containing some of the pigments for which increased corrosion protection has been observed need to be studied. Other types of environments should be used in the study of corrosive degradation such as humid air containing various pollutants such as SO_2, NO_x and/or O_3. This should be followed by exposure at environmental test sites where the environmental parameters are monitored. As corrosion sensors the new atmospheric corrosion rate monitors (ACRM) and the data loggers for exposure studies (ACRMDL) should be employed. Such an integrated approach for the evaluation of coated metals under "real life" conditions is needed to provide additional inputs to the lifetime prediction model developed in the present project in laboratory conditions.

2. Stresses produced by growing corrosion products under the coating have been shown to play a significant role in the degradation of adhesion and cohesion of polymer coated steel. It is recommended that the mechanism by which corrosion induced stresses are relieved by cohesive or adhesive failure be investigated using acoustic emission. Acoustic events from coated steel coupons exposed to NaCl solution and pulled to failure have been explained by cohesive and adhesive failure. Events produced in the absence of tensile extension from corroding or cathodically polarized coated steel should

occur if reaction products induce cohesive or adhesive failure. Accordingly, acoustic emission from polymer coated steel exposed to various environmental conditions should be collected and analyzed as a function of time of exposure, coating chemistry, and surface preparation.

3. Adhesion appears to function as a major component in the mechanism of protection of metals by polymer coatings. It is recommended that the molecular steps involved in adhesion and corrosion induced adhesion loss should be investigated. It should be possible to form a monolayer of an epoxy coating on a steel surface by starting with available volatile epoxide and polyamide oligomers in an ultra high vacuum apparatus equipped with Auger and X-ray photoelectron spectroscopic capability, in addition to an attached electrochemical cell. Spectroscopic evaluation of a "monolayer" or thin layer of a model polymer interphase as a function of exposure to water, water vapor, or cathodic and anodic electrochemical polarization, and surfac pretreatment will give information on the type of adhesive bonding and the mode of their attack by the corrosion processes. Previous spectroscopic evaluation of the cathodic disbonding process has been carried out by examining samples after various treatments in the laboratory.[29,30] Questions concerning the existence of chemical changes occurring after the treatment at the disbonded interface have been raised.[31] Experiments performed in a chamber[32] that allows easy transfer from the electrochemical cell to the spectrometer vacuum chamber will provide direct evaluation of the chemical changes of the polymer/metal interface or interphase associated with the cathodic disbonding process.

Recognizing that adhesion in the presence of water and dissolved ions is critical to the stability of polymer coatings, the wetting forces at a model three-phase metal/organic/water interface can be directly

measured as a function of applied potential and electrolyte chemistry using the Wilhelmy plate method.[33,34] It is recommended that these experiments be performed using compounds in the organic phase having various organic functionality found in polymer coatings. Results from these tests could aid in the design of adhesion promoters, coatings or surface preparation techniques that resist corrosion enhanced adhesion loss.

4. Quantitative in-situ, nondestructive evaluation of the rate of cathodic disbonding about a defect should be performed as a function of environment, potential, surface preparation or modification, and polymer chemistry. Previously, cathodic disbonding has been studied only by destructive analysis or qualitatively by visual inspection. A need for a nondestructive in-situ method for detecting the disbond front exists.[35] The development of signal-enhancements for the ultrasonic reflected pulse techniques in this laboratory now allows in-situ nondestructive detection of the disbond front. This method can therefore be used to quantitively and nondestructively follow the disbonding as a function of time.

ACKNOWLEDGEMENT

The principal investigators gratefully acknowledge the help of their colleagues in the various tasks. Mrs. Sue Tsai, Sam Jeanjaquet and Art Allen prepared the coatings and performed most of the electrochemical tests. Arvin Arora collected and analyzed the acoustic emission data, Lloyd Ahlberg the acoustic pulse data. A number of summer students, among them Sheryl Jeanjaquet, Dan Cher and Daric Wong, provided support during the course of the project. A successful conclusion of this program would not have been possible without the enthusiastic support and helpful suggestions of the Project Officer, Dr. Phillip Clarkin.

6.0 REFERENCES

1. M. Kendig, F. Mansfeld and A. Arora, "Evaluation of Protective Coatings with Acoustic Emission and Impedance Measurements," 9th Int. Congr. on Metallic Corrosion, Toronto, Canada (1984),Vol. 4-73

2. M. Kendig, S. Tsai and F. Mansfeld, "Influence of Surface Preparation of Steel on Coating Performance and Cathodic Delamination," Materials Performance 23, 37 (1984).

3. F. Mansfeld, J.B. Lumsden, S.L. Jeanjaquet and S. Tsai, "Evaluation of Surface Pretreatment Methods for Application of Organic Coatings," Corrosion Control by Organic Coatings, H. Leidheiser, ed., NACE (1980), p. 355.

4. F. Mansfeld, M. Kendig and S. Tsai, "Evaluation of Organic Coating/Metal Systems by AC Impedance Techniques," Proc. 8th Int. Congress on Metallic Corrosion, Mainz, West Germany (1981), p. 1014.

5. M. Kendig, F. Mansfeld and S. Tsai, "Determination of the Long-Term Behavior of Coated Steel with AC Impedance Measurements," Corr. Sci. 23, 317 (1983)

6. F. Mansfeld and M. Kendig, "Electrochemical Impedance Tests for Protective Coatings," ASTM STP 866, p. 122 (1985).

7. M.W. Kendig , A.T. Allen, S.L. Jeanjaquet and F. Mansfeld, "The Application of Impedance Spectroscopy to the Evaluation of Corrosion Protection by Inhibitors and Polymer Coatings," Paper No. 74 , NACE, Corrosion '85.

8. F. Mansfeld, M.W. Kendig and S. Tsai, "Evaluation of Corrosion Behavior of Coated Metals with AC Impedance," Corrosion 38, 478 (1982).

9. F. Mansfeld and M.W. Kendig, "Electrochemical Impedance Spectroscopy of Protective Coatings," Werkstoffe und Korrosion 36, 473 (1985).

10. F. Mansfeld and M.W. Kendig, "Evaluation of Protective Coatings with Impedance Measurements," 9th Int. Cong. on Metallic Corrosion, Toronto, Canada,1984, Vol. 3-74.

11. F. Mansfeld and M.W. Kendig, "Electrochemical Impedance Spectroscopy of Perfective Coatings," Proc. Symp. "Electrochemical Techniques in Corrosion Research," Toulouse, France, July 1985.

12. F. Mansfeld, S.L. Jeanjaquet and M.W. Kendig, "An Electrochemical Impedance Spectroscopy Study of Reactions at the Metal/Coating Interface," submitted to Corr. Sci.

13. M. Kendig and H. Leidheiser Jr., J. Electrochem. Soc., 123, 982 (1976).

14. D.M. Brasher and A.H. Kingsbury, J.Appl. Chem 4, 62 (1954).

15. R.E. Touhsaent, and H. Leidheiser, Jr., Corrosion 28,435 (1972).

16. J. E. O. Mayne, Brit. Corr. J., 5,106 (1970).

17. M. Kendig, A.T. Allen and F. Mansfeld, "Optimized Collection and Analysis of Impedance Data," J. Electrochem. Soc. 131, 935 (1984).

18. M. Kendig, E.M. Meyer, G. Lindberg and F. Mansfeld, Corr. Sci. 23, 1007 (1983).

19. H. Isaacs and M. Kendig, Corrosion 36(6), 269 (1980).

20. J. Standish and H. Leidheiser, Jr. Corosion 36(8), 390 (1980).

21. T. Rugeri and T. Beck, "Application of Electrochemical Engineering Methods and Theory to Solving Corrosion and Adhesion Problems with Organic Coatings," Interim Summary, Contract No. N62299-82-C-0281, Naval Air Development Center, Warminster, PA, Report No. NADC-84107-60 (1984), and references therein.

22. H. Hansmann, Ind. Eng. Chem. Prod. R&D, 24, 252 (1985).

23. M.S. Balera, T.A. Strivers and D.E.A. Williams-Wynn, J. Oil and Colour Chemists Assoc. (5), 133 (1984).

24. M.S. Balera, T.A. Strivers and D.E.A. Williams-Wynn, ibid, 143 (1984).

25. H. Hansmann, H.G. Mosle, Adhesion 28, 18-21 and 24-26 (1982).

26. J.S. Rooun and R.d. Rawlings, J. Mater. Sci. 17, 1745 (1982).

27. H.G. Mosle, B. Wellenkotter, Z. Werkstofftech. 9, 265 (1978).

28. T. Szauer and A. Brandt,JOCCA, 1981(1), 13(1981).

29. J.E. Castle and J.F. Watts, I&EC Product R&D, 24, 361 (1985).

30. R.A. Dickie, in "Adhesion Aspects of Polymeric Coatings," 339-343, K.L. Mittal, ed., Plenum, New York (1983).

31. H. Leidheiser, W. Wang and L. Igtoft, Prog. Org. Coatings, 11, 19 (1983).

32. J. Lumsden and P. Stocker, J. Electrochem. Soc. (to be published).

33. M. Kendig and T.A. Fadner, Ind. and Eng. Chem. Fundamentals 24, 50 (1985).

34. R. Bendure, J. Colloid. & Interfacial Sci. 42, 137 (1973).

35. J.S. Thornton, R.E. Montgomery, J.F. Curtier, "Failure Rate Model for Cathodic Delamination of Protective Coatings," Texas Research Institute, NRL Memorandum Report 5584, Contract No. N00014-83-C-2258 (1985).

7.0 APPENDIX

Definitions and Symbols:

ACM = atmospheric corrosion monitor

ACRM = atmospheric corrosion rate monitor

A_d = delaminated area

AD = alkaline derusting

AE = acoustic emission

C_d = double layer capacitance

C_c = coating capacitance

corr = corrosion rating (ASTM D510)

d = coating thickness

del = delamination rating (ASTM D510)

E_{corr} = corrosion potential

ε_d = delamination efficiency = Q/A_d

EIS = electrochemical impedance spectroscopy

ϵ = relative dielectric constant

ϵ_o = dielectric constant of free space $8.85\ (10)^{-14}$ F/cm

Ex = epoxy

F = fourier transform operator

F^{-1} = inverse fourier transform operator

f = $\omega/2\pi$

HA = hot alkaline pretreatment

HNO_3 = nitric acid pretreatment

I_g = galvanic current

inh. HCl = inhibited HCl pretreatment

ω = angular frequency (rad/s)

P + D = polished and degreased

ρ = volume resistivity of electrolyte

Q = cathodic charge passed during the cathodic disbonding test

R = resistance parameters for a delaminated region

P_1 = acoustic pulse from the coating/metal interface

$R_{dc} = \lim_{\omega \to 0} |Z|$

P_0 = acoustic reflection from the coating-water interface

R_p = polarization resistance

R_{po} = pore resistance

R_Ω = ohmic resistance

SCE = saturated calomel electrode

SrChro = Strontium chromate

t_{corr} = exposure time

θ = area fraction where corrosion occurs

V_{eff} = effective volume of delamination

Z = complex impedance

Z' = in-phase impedance (real component)

Z" = out-of-phase impedance (complex component)

Z_σ = impedance proportional to $(j\omega)^{1/2}$.

$|Z| = \sqrt{(Z'')^2 + (Z')^2}$

Z_i = interfacial impedance

ZnPhos = Zn phosphate pigment

ZnBaP = Zn barium phosphate